



HAL
open science

Ion and Water Transport in Ion-Exchange Membranes for Power Generation Systems: Guidelines for Modeling

Semyon Mareev, Andrey Gorobchenko, Dimitri Ivanov, Denis Anokhin, Victor Nikonenko

► To cite this version:

Semyon Mareev, Andrey Gorobchenko, Dimitri Ivanov, Denis Anokhin, Victor Nikonenko. Ion and Water Transport in Ion-Exchange Membranes for Power Generation Systems: Guidelines for Modeling. International Journal of Molecular Sciences, 2023, 24 (1), pp.34. 10.3390/ijms24010034 . hal-04284624

HAL Id: hal-04284624

<https://hal.science/hal-04284624v1>

Submitted on 14 Nov 2023

HAL is a multi-disciplinary open access archive for the deposit and dissemination of scientific research documents, whether they are published or not. The documents may come from teaching and research institutions in France or abroad, or from public or private research centers.

L'archive ouverte pluridisciplinaire **HAL**, est destinée au dépôt et à la diffusion de documents scientifiques de niveau recherche, publiés ou non, émanant des établissements d'enseignement et de recherche français ou étrangers, des laboratoires publics ou privés.



1 Review

2 Ion and water transport in Ion-Exchange Membranes for power 3 generation systems: Guidelines for Modeling

4 Semyon Mareev ^{1,2}, Andrey Gorobchenko ^{1,2}, Dimitri Ivanov ^{2,3,4}, Denis Anokhin ^{2,4,5}
5 and Victor Nikonenko ^{1,2,*}

6
7 ¹ Membrane Institute, Kuban State University, 350040 Krasnodar, Russia

8 ² Faculty of Fundamental Physical and Chemical Engineering, Lomonosov Moscow State University, 119991 Moscow, Russia

9 ³ Institut de Sciences des Matériaux de Mulhouse-IS2M, CNRS UMR 7361, Jean Starcky, 15,

10 F-68057 Mulhouse, France

11 ⁴ Center for Genetics and Life Science, Sirius University of Science and Technology, 1 Olympic Ave, 354340 Sochi, Russia

12 ⁵ Institute of Chemical Physics Problems of RAS, Acad. Semenov Av., 1, 142432 Chernogolovka, Russia

13 * Correspondence: v_nikonenko@mail.ru; Tel.: +7-918-41-45-816

14 **Abstract:** Artificial ion-exchange and other charged membranes, like as biomembranes, are
15 self-organizing nanomaterials built from macromolecules. The interactions of fragments of mac-
16 romolecules results in phase separation and formation of ion-conducting channels. The properties
17 conditioned by the structure of charged membrane determine their application in separation pro-
18 cesses (water treatment, electrolyte concentration, food industry and other), energy (reverse
19 electro dialysis, fuel cells and other), chlore-alkali production and other. The purpose of this review
20 if to provide guidelines for modeling the transport of ions and water in charged membranes, as
21 well as to describe the latest advances in these field with a focus on power generation systems. We
22 briefly describe the main structural elements of charged membranes, which determine their ion
23 and water transport characteristics. The main governing equations and the most commonly used
24 theories and assumptions are presented and analyzed. Known models are classified; they are de-
25 scribed based on the information about the equations and assumptions given in previous sections.
26 The main attention is paid to the models, which have the greatest impact and are most frequently
27 used in the literature. Among them, we focus on recent models developed for proton-exchange
28 membranes used in fuel cells and for membranes applied in reverse electro dialysis.

29 **Keywords:** charged ion-exchange membranes; mathematical modelling; energy production and
30 storage; ion and water transport; structure-property models; transport equations; conductivity;
31 permeability; permselectivity

33 Table of contents

34 1. Introduction

35 2. Structure of IEMs

36 2.1. Clusters and channels

37 2.2. Functional properties and their relation to the nanostructure

38 3. Basics of modelling of ion and water transport in ion-exchange membranes

39 3.1. Conservation equations

40 3.1.1. Material conservation

41 3.1.2. Navier-Stokes equation

42 3.1.3. Charge conservation law. Poisson equation

43 3.2. Irreversible thermodynamics

44	3.2.1. Onsager phenomenological equations
45	3.2.2. Kedem-Katchalsky equations
46	3.2.3. Nernst-Planck equation
47	3.3. Chemical reactions
48	3.4. Donnan equilibrium relation
49	3.5. Donnan-Manning equilibrium relation
50	3.5.1. Manning's condensation theory
51	3.5.2. Condensation theory applied to IEMs. Donnan-Manning's theory
52	4. Modeling of ion and water transport in IEMs
53	4.1. "Solution-diffusion" models
54	4.1.1. Teorell-Meyer-Sievers (TMS) model
55	4.1.2. Multiphase models
56	Microheterogeneous model
57	Three-wire model
58	Cell model
59	4.2. "Pore-flow" models
60	5. Current state of modeling of ion and water transport in membrane energy generation systems
61	5.1. PEMFC models
62	5.2. RED models
63	6. Conclusions
64	Author Contributions
65	Funding
66	Conflicts of Interest
67	Nomenclature
68	

69

70

1. Introduction

Ion exchange membranes (IEMs) are widely used in water treatment and energy storage/generation systems. Water treatment, desalination and concentration of solutions, ion separation and some other applications are carried out using electrodialysis (ED) [1–4]. As for energy storage and generation, proton-exchange membrane (PEM) electrolysis, reverse electrodialysis (RED), redox flow batteries (RFB), fuel cells (FC) and some other membrane processes are applied [5–13] (Figure 1). In ED (Figure 1a), feed solution components are transferred through alternating cation-exchange (CEM) and anion-exchange membranes (AEM) under the action of an external electric field [1–4]. As a result of this process, the feed solution is concentrated in some compartments (concentration compartments) and desalinated in others (desalination compartments). This also allows to consider ED as a process associated with the energy storage. Such features of ED make it an attractive technology for application in various fields [7]: water desalination (sea water, well water, brackish water, etc.); wastewater treatment (industrial, agricultural, municipal wastes); food industry (wine, dairy, production of juice drinks, etc.); medicine (purification of amino acids, desalination of pharmaceutical intermediates, recovery of blood plasma proteins, etc.); electronic industry (purification of water for electronics processing); production of ultrapure water and many other areas. In RED (Figure 1b) no external electric field is applied, and alternating CEM and AEM separate the feed concentrated (e. g. sea water) and the feed dilute (e. g. river water) solutions. Species diffusion through a membrane causes an ionic fluxes from a concentrated solution to a dilute one, and the energy released during this process generates electricity [14]. It should be noted that in Figure 1b, as an example, the counter-current operation of the RED is demonstrated (sea and river water in the corresponding compartments moves in opposite directions). However, from a practical viewpoint, the co-current mode (co-directional movement of sea and river water in the respective compartments) is preferable and al-

95

96 lows for greater productivity [15]. Power generation is an application of RED, but there
97 are some specific applications [16]: RED, designed to produce hydrogen and store energy
98 in batteries; RED for wastewater treatment using electricity in situ; various integrations
99 of RED with other desalination technologies. By analogy with ED, PEM electrolysis
100 (Figure 1c) is associated with energy storage [10], and FC (Figure 1d) with its production
101 RED [17,18], similar to RED. In PEM electrolysis, water molecules are fed into the anode
102 catalyst layer, where they are oxidized to oxygen and protons, i.e., an oxygen evolution
103 reaction (OER) takes place:



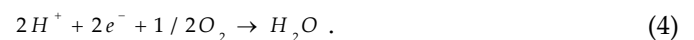
104 The resulting oxygen is removed from the device, and the protons are transferred by
105 an electric field through the PEM to the cathode catalyst layer, where they are reduced to
106 hydrogen, i.e., a hydrogen evolution reaction (HER) takes place:



107 In FC with PEM, the opposite happens: hydrogen is fed into the anode catalyst layer,
108 where it is oxidized to protons – hydrogen oxidation reaction (HOR):

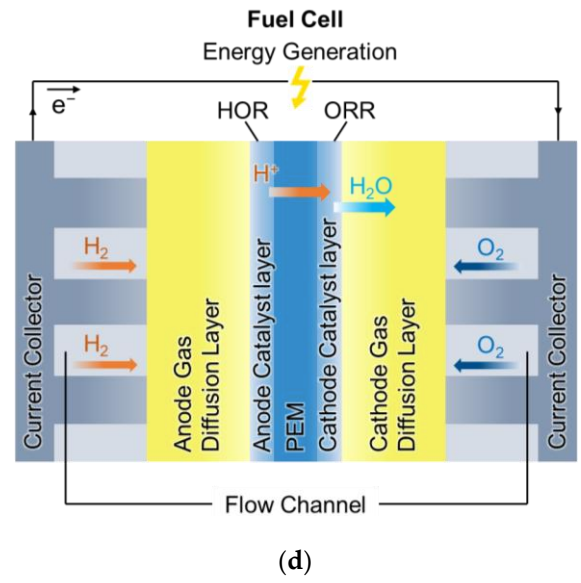
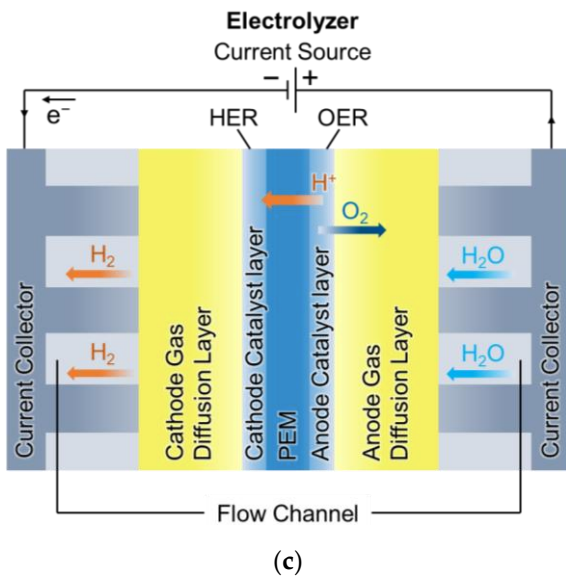
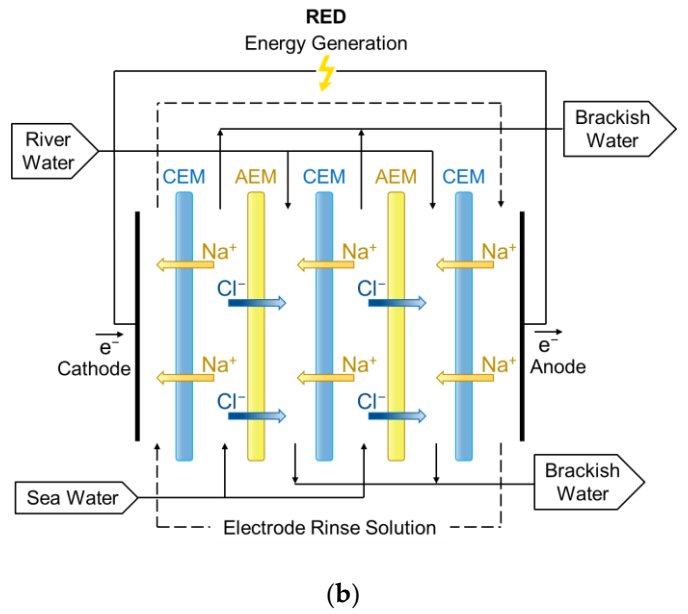
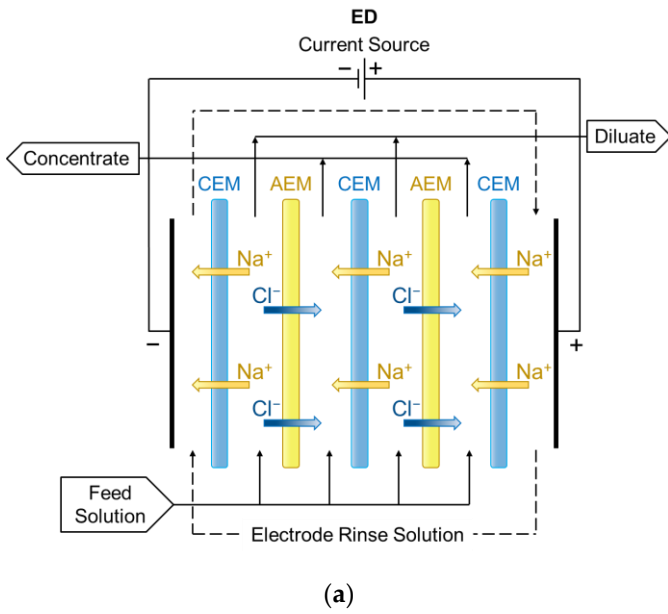


109 As a result of this reaction, heat and a direct electric current are generated. The re-
110 sulting protons are transferred through the PEM to the cathode catalyst layer, where
111 oxygen is also supplied. As a result, an oxygen reduction reaction (ORR) takes place in
112 the cathode layer with the water formation:



113 As for RFB, their application is related to both generation and storage of energy.
114 Aqueous RFB (Figure 1e) is a sandwiched structure consisting of positive and negative
115 porous carbon electrodes separated by an ion-exchange membrane. The external reser-
116 voirs contain electrolytes with dissolved active species that circulate through the porous
117 electrodes. Electrochemical reactions take place on the electrodes to store or release elec-
118 tricity. The energy storage tanks are separated from the power pack, therefore, the stored
119 energy can be scaled [17].

120 The use of IEMs in these applications is due to their ability to enhance or impede
121 species transfer not only because of the size of the species, but also because of their
122 charge.



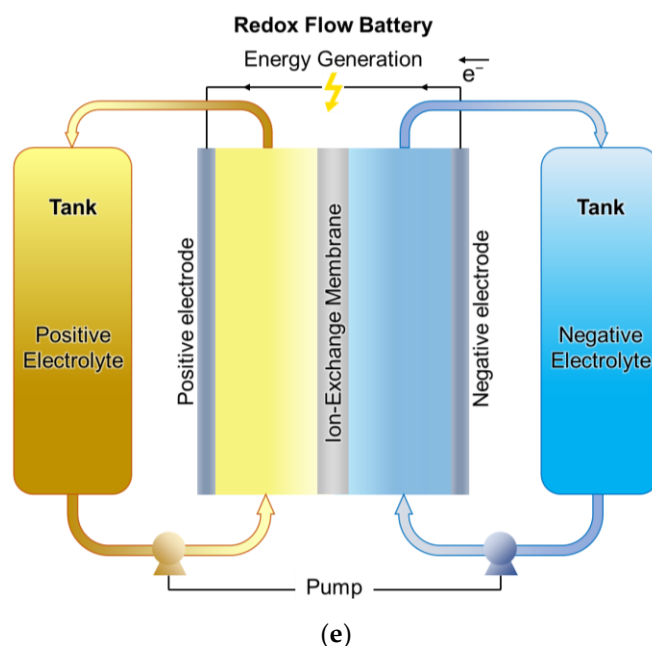


Figure 1. Scheme and principle of work of the main membrane devices related to energy production and storage: conventional electro dialysis (a), reverse electro dialysis (b), PEM electrolyzer (c), fuel cell (d) and redox flow battery (e).

Synthetic ion exchange membranes (IEMs) are polymeric materials whose structure is based on aliphatic, aromatic or perfluorinated residues containing functional groups ($-\text{SO}_3^-$, $-\text{NH}_3^+$ and others). These functional groups are fixed due to a strong chemical bond with the polymer matrix, and the presence of a charge in such a group allows it to participate in exchange reactions with ions from an external solution (Figure 2).

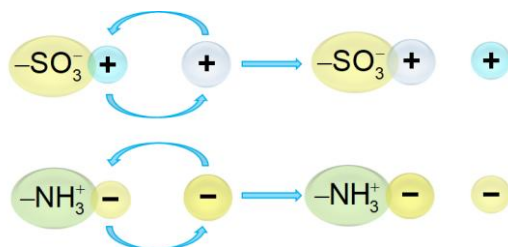


Figure 2. Schematic representation of exchange reactions on fixed membrane groups.

Depending on the sign of the charge of the functional groups fixed to their matrix, membranes are divided into cation-exchange (negative fixed charge) and anion-exchange (positive fixed charge). A detailed description of the structure and types of polymer chain architecture of various cation and anion exchange membranes was reviewed by Ran et al. [19].

According to the structural feature and method of production, membranes are traditionally divided into homogeneous and heterogeneous. Homogeneous membranes are usually produced by copolymerization of monomers. There are two types of such IEMs: single-phase (Nafion, DuPont Co., Wilmington, California, USA; MF-4SK, Plastpolimer, St. Petersburg, Russia, and others) represent a continuous layer of ion exchange material (homogeneous at the micrometer scale) with more or less evenly distributed fixed groups; two-phase (Neosepta AMX, CMX, Astom, Tokyo, Japan; CJMCD, CJMAED, Hefei ChemJoy Polymer Materials, Hefei, China; and others), the structure of which, along with a sulfonated polymer, may include an inert binder and reinforcing fibers [20,21]. Heterogeneous membranes are produced by mixing microgranules (about 5–50

148 μm) of an ion exchange resin with an inert binder (MK-40, MA-40, Shchekinoazot, Rus-
149 sia; Ralex CMH, AMH, MEGA a.s., Czech Republic, and others) [21]. This IEMs may be
150 reinforced with meshes or fabrics made of various polymers (polyester, capron, lavsan,
151 polyvinyl chloride, and others) to achieve high mechanical strength. Such a structure
152 leads to significant differences in physicochemical properties of membrane bulk and
153 surface on micrometer scale: there are both electrically conductive and non-conductive
154 areas corresponding to the phase of the ion exchanger and the inert binder, respectively;
155 the presence of a reinforcing fabric contributes to the development of geometric hetero-
156 geneity (waviness) of the surface. This kind of heterogeneity may contribute to the de-
157 velopment of electroconvection in electromembrane systems [22,23].

158 It should be noted that despite the presence of two phases in the structure of the
159 material, Neosepta, CJMCEd, CJMAED and other similar membranes are still tradition-
160 ally called homogeneous [3,7]. However, "homogeneous" membranes, strictly speaking,
161 are inhomogeneous on the 10-100 nm scale. When swollen in an aqueous solution, they
162 contain hydrophilic pores/channels enclosed in a hydrophobic matrix. These
163 pores/channels allow the transport of ions and water across the membrane [24].

164 The characteristics of the IEM are determined by the requirements of the process in
165 which they are applied [9]. There are membranes of several special grades, which are
166 used in different applications. In electrodialysis water desalination, alternating cati-
167 on-exchange and anion-exchange membranes (CEM and AEM) are used. Cations pass
168 through the cation-exchange membrane, and anions, respectively, through the ani-
169 on-exchange membrane. Thus, ED requires membranes that provide counterion/coion
170 selectivity [25]. There are many applications where the permselectivity for a specific ion
171 is needed. For example, the separation of monovalent and multivalent ions of the same
172 sign of charge (such as Na^+ and Ca^{2+}) is required for water softening. This separation is
173 achieved with the use of special-grade membranes, monovalent-ion-selective mem-
174 branes, which are used in a process called selectrodialysis [26]. In the electrodialysis
175 production of alkalis and acids, another special-grade membranes, bipolar membranes,
176 are used. Their important property is an increased catalytic activity for the water disso-
177 ciation reaction [27]. In vanadium redox flow batteries [12], IEMs are utilized that allow
178 catholyte and anolyte solutions to exchange charge balancing species (e.g. protons for
179 CEM and sulfate/bisulfate for AEM) but not active redox vanadium ions. In pro-
180 ton-exchange membranes used in fuel cells and electrolysis, in addition to ions, it is im-
181 portant to control the transfer of water and/or neutral solutes [9,28].

182 With such diverse requirements for IEMs, the challenge for researchers is to improve
183 understanding of the fundamental properties of membranes responsible for various de-
184 sirable or undesirable effects. The purpose of this article is to help researchers solve this
185 problem of better understanding through mathematical modeling and simulation. The
186 paper discusses the relationships between membrane structure and their properties,
187 gives basic equations and well-established models, their classification. With that, new
188 approaches to the description of transport phenomena in charged membranes are re-
189 viewed. The main attention is given to the models related to energy generation applica-
190 tions. Related phenomena such as chemical reactions (water splitting, acid dissociation,
191 etc.) are also considered.

192 2. Structure of IEMs

193 2.1. Clusters and channels

194 IEMs are self-assembling nanostructured materials composed of macromolecules
195 [29]. The structure and hence the properties of biological membranes and IEMs have
196 some similarities [30]. The main components of the structure of biological membranes are
197 amphiphilic compounds having both hydrophilic and hydrophobic components (Figure
198 3). They consist of a phosphate 'head' (circles in Figure 3b) and a lipid 'tail' (lines) that
199 are, respectively, compatible and incompatible with water.

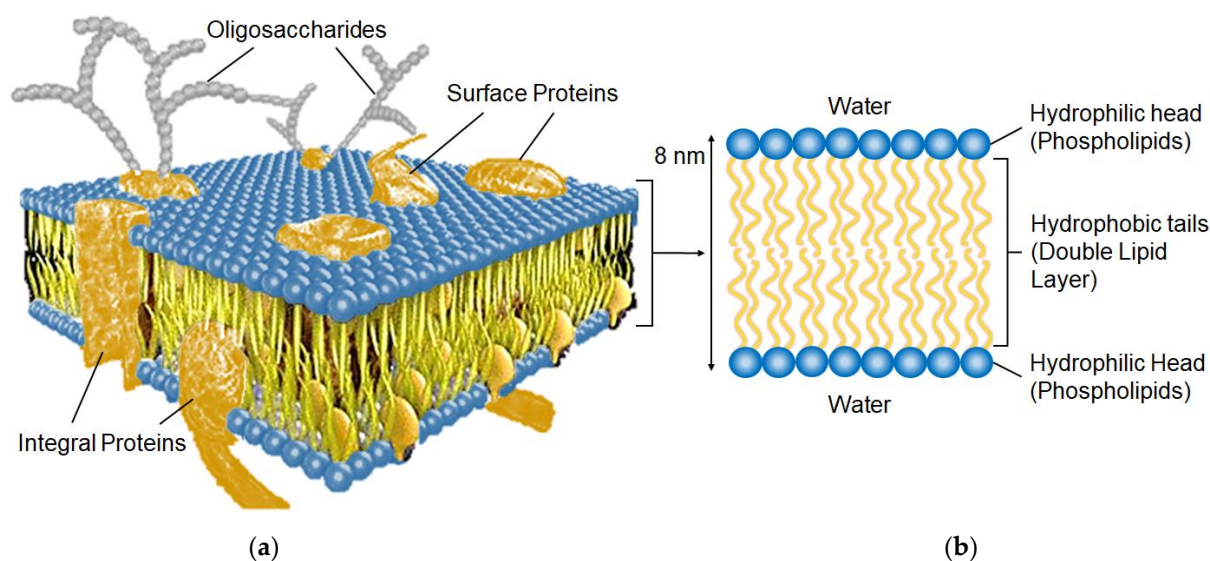
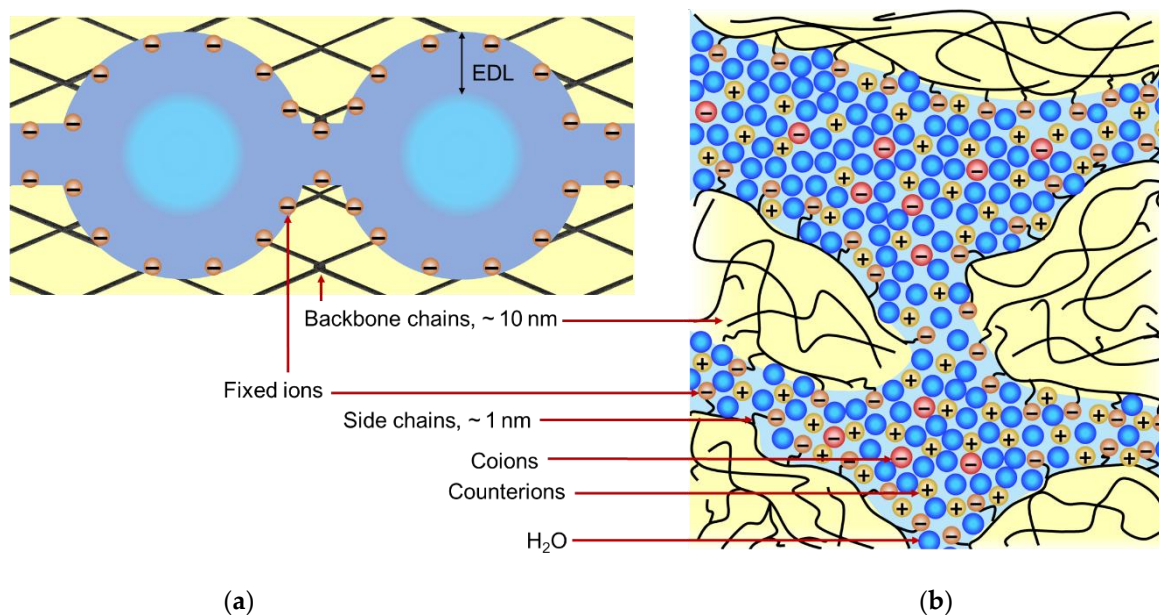


Figure 3. Schematic representation of a biological membrane (a) and lipid bilayer (b).

The main structural element of the functional part of IEMs is a hydrophobic base, consisting of hydrocarbon (such as in Neosepta membranes, Astom) or perfluorinated (such as in a Nafion®, Dupont) chains. The charged functional groups make up the hydrophilic part of the IEM. Due to the flexibility of polymer chains, this combination ensures self-organization in the membrane bulk [31]. The polymer chains form the matrix of the membrane, while the functional groups are assembled into clusters, the size of which is on the order of several nanometers. In an aqueous solution, the hydrophilic functional groups became hydrated and the membrane swells. The size of the clusters increases, conducting channels appear between them, and they form a percolation system when a certain water content is reached [32]. Therefore, hydrophobic components contribute to the morphological stability of the membrane, and hydrophilic components create a system of conducting channels. The degree of swelling depends on the concentration of the external solution: with an increase in the concentration of the solution, the water content in the IEM decreases [33]. If the membrane contains weakly basic functional groups, such as secondary and tertiary amino groups, there is a dependence of the water content on the pH of the external solution.[34,35].

The cluster and channel model, first proposed by Gierke in [36], describes the main features of the behavior and adequately explains the transport properties of Nafion® membranes [24]. The main idea of the existence of relatively large agglomerates/clusters of functional groups (several nanometers or more), which are connected by narrower channels (about 1 nm in diameter) (Figure 4) can be also applied to most other IEMs. Kreuer developed a more detailed representation of the two-dimensional structure of Nafion® [37], which generally corresponds to the Gierke model. Clusters, channels, some structural defects, gaps between ion-exchange resin particles, binder and tissue form a system of pores in IEM, the size of which varies from a few nm to 1-2 microns [38–40].



(a)

(b)

Figure 4. Schematic representation of Nafion® structure, proposed by Gierke (a) [36] and Kreuer (b) [37]. An electrical double layer (EDL) is formed at the charged pore wall, and an electrically neutral solution is present in the center of the pore.

There is an analogy of the structure of polymer side chains with a fixed functional group (Figure 5a) and phospholipid molecules of biomembranes (Figure 3b): both contain a hydrophilic ‘head’ and a hydrophobic ‘tail’.

Figure 5b shows that structuration of a membrane of the kind of Nafion® begins even in dry state: functional $-\text{SO}_3\text{H}$ groups attract each other and form clusters because they are dipoles. The flexibility of polymer chains allows this to be done. With an increase in the membrane water content, hydrated clusters first form, then intercluster channels appear, and percolation occurs (Figure 5c). If the backbone polymer chains are not intertwined enough, with sufficient water content, the polymer can split into individual chains and dissolve.

The solution that fills the clusters, where fixed functional groups are concentrated, mainly contains counterions formed as a result of the dissociation of functional groups. The counterions in thermal motion are attracted to fixed charged groups, thus forming an electrical double layer (EDL) separating fixed ions and electrically neutral solution. The latter can be present in the center of the cluster, if the EDL thickness is smaller than the cluster radius (Figure 4a). The central part of the pore contains a small number of coions carrying a charge of the same sign as the fixed ions. Coions are repelled from the pore walls by electrostatic forces; this effect is called Donnan exclusion [33] and first described in his paper in 1911 [41]. The distribution of ions inside the EDL is described by the Gouy-Chapman theory, which takes into account both electrostatic and thermal interactions. Figure 6a schematically shows the distribution of ions near the pore wall, represented as a charged plane. The concentration of counterions in the pore solution increases, and the concentration of coions decreases with a decrease in the ratio of the pore radius to the Debye length (Figure 6a). The latter characterizes the EDL thickness. Therefore, the smaller the pore radius, the higher the selectivity of the membrane (and the higher the resistance of the membrane). If the pore radius is greater than the Debye length, an electrically neutral solution is located in the center of the pore.

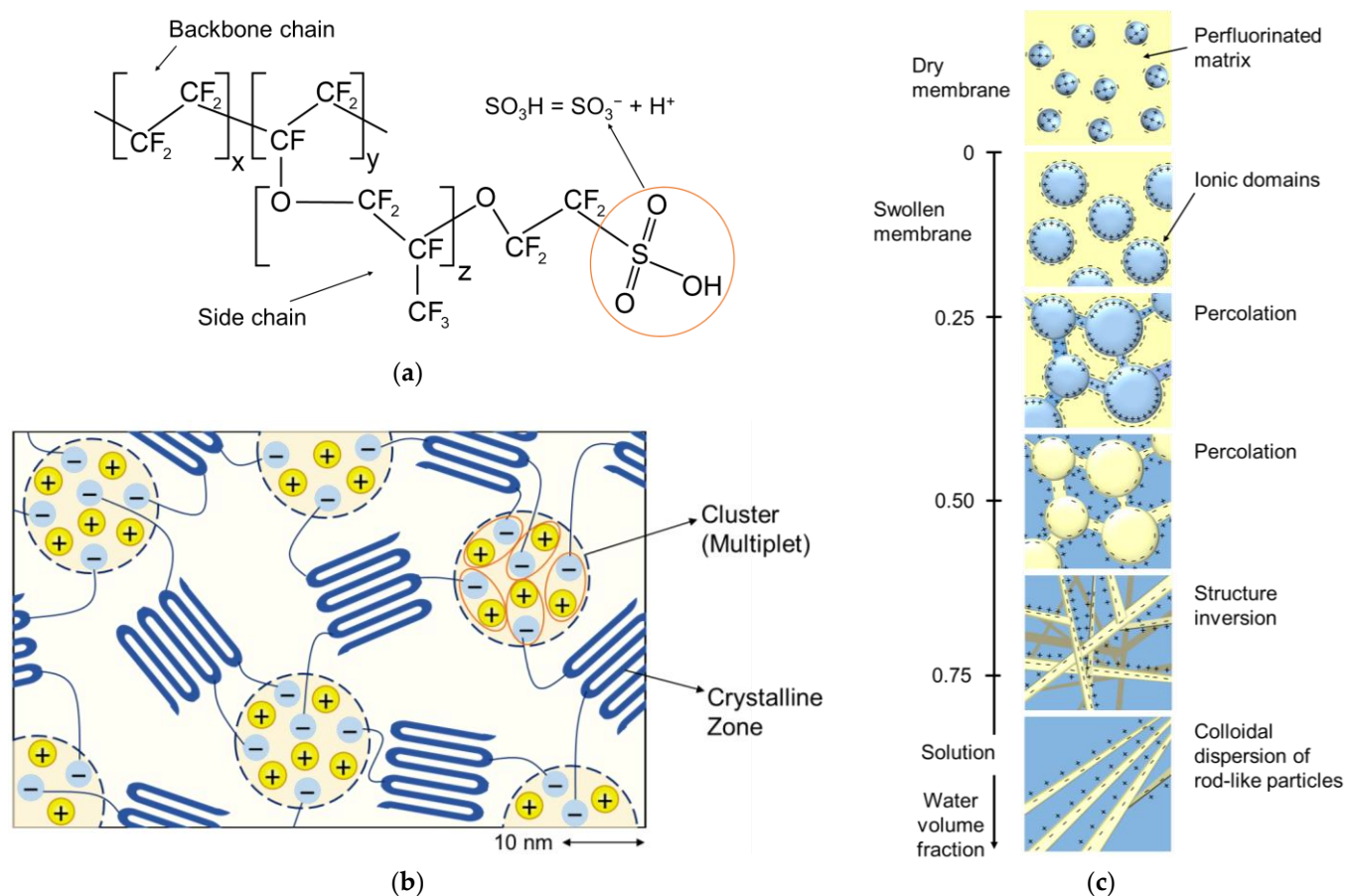


Figure 5. A perfluorinated sulfonated polymer (supra)molecule (a); Formation of nanoclusters in dry state of a perfluorinated sulfonic-acid polymer (b) (redrawn from [42]); Evolution of the nanostructure of such a polymer during hydration (c) (redrawn from [32]).

Water molecules that are close to functional groups are structured and largely lose their mobility [24,30]. As a result, the relative permittivity ϵ decreases as the solution approaches the functional groups. The permittivity of the Nafion membrane was studied in detail by Paddison et al. [43]. It is shown that with increasing water content, ϵ increases linearly, starting from the value corresponding to the dry polymer ($\epsilon = 2.1$ for polytetrafluorethylen (PTFE)) to the value referred to the pore solution of the hydrated polymer ($\epsilon = 20$ for Nafion® 117) [44] (Figure 6b). The mobility of counterions concentrated near the functional groups is very low, mainly due to the strong electrostatic interaction [24]. The side chains also contribute to their low mobility, cluttering up the space [45]. Due to the finite size of hydrated counterions, their concentration decreases when the distance from the fixed group becomes less than about 0.5 nm. When approaching the center of the pores, the concentration of counterions also decreases in accordance with the Gouy-Chapman ion distribution law in the EDL (Figure 6a).

Water molecules located in the center of sufficiently large pores behave similarly to molecules in a free solution and ϵ also approaches the value of 81, corresponding to an electrically neutral solution [46]. The Grotthuss shuttling dominates vehicular diffusion (solvation diffusion): the proton hops from one H_3O^+ (or H_5O_2^+ or even greater) complex to the neighboring one, instead of moving in the aqueous environment, transferring in the hydration shell [46].

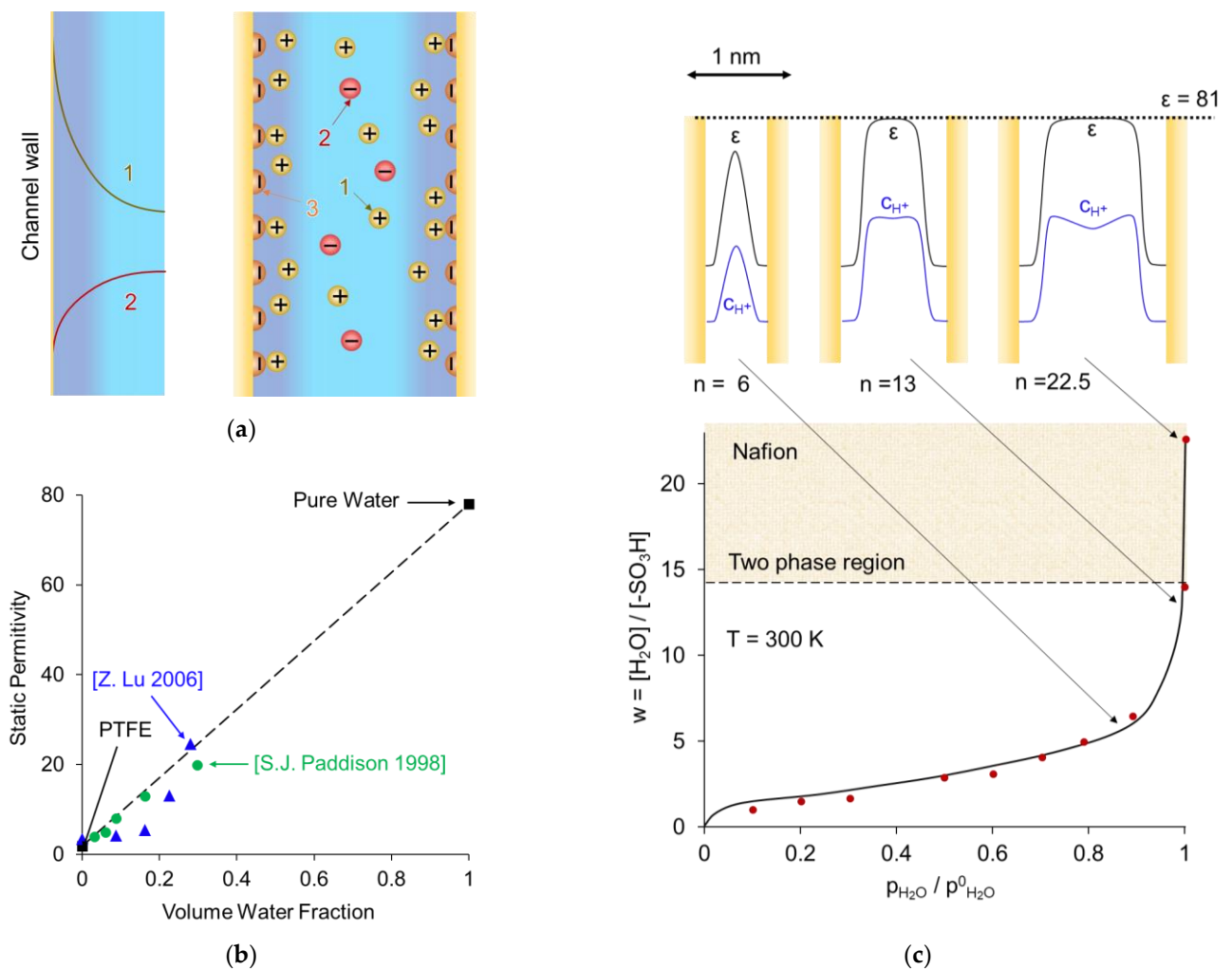


Figure 6. (a) Distribution of counterions (1) and coions (2) within a pore near a charged wall with fixed functional groups (3). Reproduced with permission from [47]. (b) Static permittivity of Nafion® 117 measured by by Paddison et al. [44] and Lu [48], plotted as a function of the volume fraction of water sorbed in the polymer. (c) Hydration isotherm (water content, w , as a function of relative water vapor pressure) for Nafion 117, and the distribution of the dielectric constant and proton concentration across the hydrated hydrophilic pores for three different values of n (top). A hydrated counterion is shown near the pore wall. Adapted from [24].

Electronic structure calculations [49] show that in perfluorinated membranes (such as Nafion®) 2-3 water molecules per sulfonic acid group (w) are needed for proton dissociation. The dissociated proton is separated from the sulfonate anion when 6 water molecules are added to the membrane. According to Kreuer et al. [24], only at $w > 14$ there is a two-phase system, where free water is clearly distinguishable in the pore (Figure 6c).

A generalized representation of the structure of an IEM is shown in Figure 7. It is a fragment that includes hydrophobic domains of the matrix, micropores (where EDLs overlap) and mesopores (where EDLs do not overlap but occupy a significant part of the pore). This fragment is typical for a homogeneous IEM, which usually do not contain macropores. Heterogeneous membranes, in addition to micro- and mesopores, also contain macropores, which can be spaces between the particles of the ion exchange resin and the reinforcing binder and fabric.

The counterion must overcome the potential barrier when moving from one functional group to another [50]. The value of this barrier depends on the energy of electrostatic and chemical interactions between the hydrated counterion and the functional

278
279
280
281
282
283
284

285
286
287
288
289
290
291
292
293
294
295
296
297
298
299
300

group and on the energy required to move polymer chains to form a sufficiently large ion transport channel or cluster in the membrane matrix. The average distance between two adjacent functional group depends on the exchange capacity and membrane morphology. For conventional membrane materials, this distance is in the range of 0.5–1.0 nm [30], in particular for perfluorosulfonic membrane Nafion, it is about 0.8 nm [24,30].

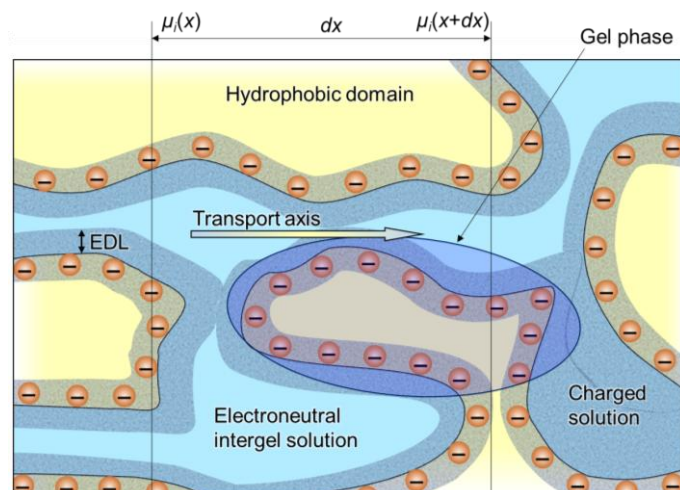


Figure 7. Schematic representation of the IEM structure with its main elements: fixed ions (shown as circles with “-”), EDL formed at the internal interfaces, and electroneutral solution in the center zone of inter-gel spaces. The gel phase includes the polymer matrix bearing the fixed ions and the EDL. Redrawn from [51].

2.2. Functional properties and their relation to the nanostructure

The main characteristics of IEMs, such as permselectivity and conductivity, primarily depend on the ratio of the volumes of the central and near-wall parts of the liquid in the pores. A large fraction of the electroneutral central part, which is typical for big pores, reduces the permselectivity. With an increase in the pore radius, the concentrations of coions and counterions converge, therefore, the contribution of coions to the electric charge transfer increases. Reducing the number and/or radius of the pores leads to a decrease in conductivity [12,37]. By increasing the length of the backbone and side chains, it is possible to reduce the number and size of hydrophilic pores by increasing the hydrophobic component of IEM.

The membrane conductivity increases with increasing water content [32]. At low water content, which can occur in a PEM of fuel cells due to water crossover [52], an increase in water content leads to a sharp increase in the percolation degree (see Figure 5c) causing an exponential growth in conductivity. At elevated water content, the higher w , the larger the pore size, which reduces the tortuosity of the inner membrane morphology, resulting in higher ion mobility.

3. Basics of modelling of ion and water transport in ion-exchange membranes

The mathematical description of ion and water transport in membranes is reduced to several basic approaches [53–55], which include the balance and transport of charge and matter. In the following, we will briefly review the basic equations, present them in expanded and concise form, and discuss important aspects that will help formulate transfer problems in IEMs.

3.1. Conservation equations

3.1.1. Material conservation

Conservation equations form the main part of the fundamental basis for the mathematical description of mass transfer. Let us consider an elementary volume $\Delta V = \Delta x \Delta y \Delta z$

(Figure 8). The change in the amount of some substance in this volume over time t will be due to two possible reasons. The first reason is the inequality of the incoming and outgoing fluxes of the substance (J_{sub}^{in} and J_{sub}^{out} respectively). The second reason is the generation or decay of this substance inside the volume. Thus, the rate of change in the amount of a substance in an elementary volume, will be determined by the formula [56]:

$$\left(\begin{array}{c} \text{Substance amount} \\ \text{change rate} \end{array} \right) = \left(\sum J_{sub}^{in} - \sum J_{sub}^{out} \right) + \left(\begin{array}{c} \text{Substance} \\ \text{generation rate} \end{array} \right) - \left(\begin{array}{c} \text{Substance} \\ \text{decay rate} \end{array} \right). \quad (5)$$

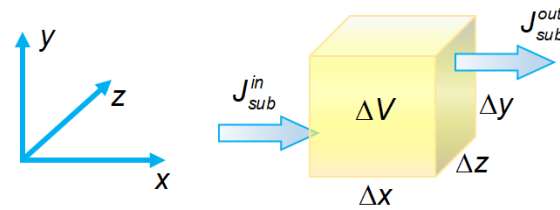


Figure 8. An elementary volume in three-dimensional space, incoming and outgoing fluxes of a substance.

In the mathematical description of the transport of species i (an ion or a molecule) in membrane systems, Equation (5) can be reduced to the following form [54]:

$$p^m \frac{\partial c_i}{\partial t} = -(\nabla \cdot \mathbf{j}_i) + p^m R_i, \quad (6)$$

here p^m is the pore volume fraction in the membrane; c_i (in mol/m³ pore solution) and \mathbf{j}_i (in mol/(m²s) membrane area) are the concentration and the flux density of species i , respectively; R_i (in mol/(m³s) pore solution) is the generation rate of species i in a chemical reaction; t is the time.

3.1.2. Navier-Stokes equation

The Navier-Stokes equation is derived from the momentum conservation equation. This equation is based on Newton's second law of motion when considering all major surface and body forces acting on a unit fluid element. When a force is applied to this element, momentum is generated. Body forces, \mathbf{F} , are applied to the entire volume: the gravitational force is equal to $\rho g \Delta V$, electric body force is equal to $\rho_e \mathbf{E} \Delta V$, where ρ and ρ_e are the density and space charge density of the fluid, respectively; ΔV is the volume of the element; g is gravitational acceleration, and \mathbf{E} is electric field intensity. Surface forces act on the surface of the body: pressure (p), friction force or internal stress (usually are taken into account using kinematic, ν , or dynamic viscosity, $\mu = \rho \nu$). The momentum conservation equation for a Newtonian fluid is written as follows:

$$\frac{\partial \rho \mathbf{v}}{\partial t} = -\mathbf{v} \cdot \nabla \rho \mathbf{v} - \nabla p + \mu \nabla^2 \mathbf{v} + \mathbf{F}. \quad (7)$$

The term on the left-hand side of the Equation (7) characterizes the rate of momentum accumulation per unit volume over time. On the right side, the first term describes the change in the convective component of the momentum flux entering and leaving the elementary volume, the second and third terms characterize the effect of the surface forces, the pressure and viscous forces and the last term characterizes the effect of external body forces. In the case of IEMs, the gravity is often irrelevant and ignored.

Equation (7) is usually used in the models of fuel cells, where the gas phase is taken into account [28]. When a Newtonian incompressible fluid is considered, Equation (7) is reduced to:

$$\frac{\partial \mathbf{v}}{\partial t} = -(\mathbf{v} \cdot \nabla) \mathbf{v} - \frac{1}{\rho} \nabla p + \nu \nabla^2 \mathbf{v} + \frac{1}{\rho} \mathbf{F} . \quad (8)$$

Equation (8) is largely applied when simulating solution flow between membranes in ED, RED and RedOx systems [23]. Sometimes the gravitational and electric body forces are important, which generate gravitational (natural) convection and electroconvection, respectively. As well as, Equation (8) is applied in the membrane pores, where electric body force can generate electroosmotic fluid transfer.

It should be noted that in the case of porous materials, where the gravity forces could be neglected, the empirical Darcy law is used instead the Navier-Stokes equation [57]:

$$\mathbf{v} = - \frac{k_p}{\mu} \nabla p , \quad (9)$$

here k_p is the hydraulic permeability of the porous medium.

3.1.3. Charge conservation law. Poisson equation

The Poisson equation relates the distribution of electric field with the distribution of space charge density:

$$\frac{\rho_e}{\epsilon \epsilon_0} = \nabla \cdot \mathbf{E} = -\nabla^2 \phi , \quad (10)$$

where ϵ_0 and ϵ are vacuum and relative permittivity, respectively; E is the electric field strength; ϕ is the electric potential. This equation is important for modelling ion and water transport in membrane charged pores as well as when considering EDL in depleted solution near membrane surface. The Poisson equation is based on Coulomb's law of electrostatics and its generalization, Gauss's flux theorem [58]

The charge conservation equation is an extension of the material conservation Equation (6). Multiplying it by the charge of species i , z_i , and the Faraday's constant, F , and summing over all species and noting that all reactions are charge balanced yields:

$$p^m \frac{\partial}{\partial t} F \sum_i z_i c_i = -\nabla F \sum_i z_i j_i , \quad (11)$$

here the volumetric charge density, ρ_e , and the Faradaic current density, i_F , can be defined by Equations (12) and (13), respectively

$$\rho_e = F \sum_i z_i c_i \quad (12)$$

and

$$i_F = F \sum_i z_i j_i . \quad (13)$$

Combination of the Poisson's (10) and charge conservation (11) equations gives the following equation for the current density [59,60]:

$$i = F \sum_i z_i j_i - \epsilon \epsilon_0 \frac{\partial \nabla \phi}{\partial t} = i_F - \epsilon \epsilon_0 \frac{\partial \nabla \phi}{\partial t} . \quad (14)$$

The second term on the right-hand side of Equation (14) is the displacement current, which occurs due to very fast processes (lasting less than milliseconds), e.g. high fre-

quency part of the electrochemical impedance spectra [61]. In some cases, the contribution of the EDL charging/discharging process to the total resistance (or impedance) of the system is negligibly small compared to the contribution of other processes, thus the second term in (14) may be neglected. The Faradaic current density, i_f , does not change with a distance (in the case of 1D geometry), while the total current density can change: a part of charges forming the current may be consumed, for example, for charging EDL.

Equation (14) should be applied to a continuous phase, which can be a solution in a membrane pore or outside the membrane, or a membrane itself considered as a homogeneous solution.

In some cases, the local electroneutrality (LEN) assumption may be applied:

$$\sum_i z_i c_i = 0 . \quad (15)$$

This assumption can be applied to solution or membrane bulk except interfacial space charge regions (EDLs) [51]. Deviation from electroneutrality should be taken into account, when describing transients and impedance spectra at small time scales or at high frequencies, when the double layer is charging and discharging, as well as when modeling at length scales about the Debye length (on the order of nanometers) near the membrane surface. For these cases, Poisson's equation allows providing a correct description of the distribution and space charge density and electric potential/field strength [62].

The use of Equation (15) does not mean that the Laplace equation ($\nabla^2 \phi = 0$) can be used to find the distribution of potential. The latter formally follows from Poisson's equation when $\rho_e = 0$ is substituted into Equation (10). Let us rewrite Equation (10) in the form:

$$C_+ - C_- = \theta \frac{dE}{dX}, \quad 0 \leq X \leq 1, \quad (16)$$

$$\text{where } \theta = \frac{\epsilon \epsilon_0 R T}{F^2 c_s \delta^2}, \quad X = \frac{x}{\delta}, \quad E = \frac{E \delta F}{R T}, \quad \text{and } C_i = \frac{|z_i| c_i}{|z_A| c_A}$$

are dimensionless permittivity, x coordinate, electric field strength and equivalent concentration of ion i , respectively; δ is the diffusion layer thickness; c_s is the molar concentration of salt in the electrolyte solution; R is the gas constant; T is temperature. The subscripts "+" and "-" correspond to the cation and anion, respectively; the subscript "A" corresponds to the coion.

The θ coefficient at the derivative in the right-hand side of Equation (16) is quite small. Therefore, the value of $\nabla^2 \phi$ (equal to $-\partial E / \partial x$ in a 1D case) may not necessarily be reduced to 0, to consider the value of $\sum_i z_i c_i$ to be approximately zero. Thus, Equation (15) can be applied out of the interfacial regions where j and E vary very rapidly with distance causing a large value of $\nabla^2 \phi$. To find j and/or E in the regions where the LEN assumption is applied, Equation (15) should be solved together with the Nernst-Planck equations written for all mobile ions. This equation system can be considered as a simplification of the Nernst-Planck-Poisson (NPP) equation system [54]. The NPP equation system can be applied everywhere in membrane system. The limitations are related with the size of the considered region, which cannot be smaller than the size of atom/molecule [63].

Substitution of Equations (15) in (11) yields the following equation, showing that in the electroneutrality region, the divergence of the current density is zero (the current density does not change with a distance in the 1D geometry case):

$$\nabla^r i = 0 . \quad (17)$$

3.2. Irreversible thermodynamics

Modelling ion and water transport in a membrane on the basis of the irreversible thermodynamics (the phenomenological approach) allows establishing general relationships between fluxes and driving forces that are valid for membranes of any type. This approach does not require an explicit description of the relationship between the membrane properties and its structure. On the one hand, this greatly simplifies the mathematical problem; on the other hand, important relations remain unknown. The peculiarities of ion and water transport in a particular membrane under study can be taken into account using phenomenological coefficients, which makes it possible to describe the membrane behavior under certain external conditions (concentrations, electric potential difference, solution flow rate *etc.*). To obtain quantitative relationships, it is necessary that the properties of the membrane be previously characterized. As a rule, such a description is sufficient for studying the patterns of development of various effects in electromembrane systems (e. g. concentration polarization and coupled transport phenomena, such as electroosmosis), predicting energy consumption and current efficiency, and also analyzing the applicability of membranes in specific applications. It should be noted that the equations used in the framework of the phenomenological approach may include phenomenological coefficients that directly or indirectly reflect the structural features of the membrane. For example, such coefficients can be evaluated via tortuosity factor, τ , used to take into account the fact that ion transport in the membrane is slower than in solution due to its dense structure [64–66]; membrane porosity, p^m , can be accounted also to express the fact that ions and water can only pass through the pores of the membrane [28,67,68].

3.2.1. Onsager phenomenological equations

In a state of equilibrium, the electrochemical potential, μ_i , of any mobile species i is the same at every point of the membrane material. When the gradients of the electrochemical potential are not equal to zero, fluxes of species i appear in the system. Linear relationships between thermodynamic forces $\overset{r}{F}_i = -\nabla \mu_i$ and the resulting fluxes $\overset{r}{j}_i$ can be described by the Onsager equation:

$$\overset{r}{j}_i = -\sum_j L_{ij} \nabla \mu_j, \quad (18)$$

here L_{ij} are the phenomenological conductivity coefficients. L_{ij} depend on the material properties, species concentration, temperature, and pressure. Note that generally the flux of species i ($\overset{r}{j}_i$) in Equation (18) depends not only on the thermodynamic force applied to that species ($\overset{r}{F}_i$) but also on all forces acting on other species.

The electrochemical potential μ_i in Equation (18) can be represented as a function of activity a_i of species i , electric potential ϕ and pressure p in the virtual solution (an electroneutral solution that is in local equilibrium with a small membrane volume corresponding to the x coordinate [69]):

$$\mu_i = \mu_i^0 + RT \ln a_i + z_i F \phi + \bar{V}_i p, \quad (19)$$

where μ_i^0 and \bar{V}_i are standard electrochemical potential and partial molar volume of species i , respectively.

Onsager's reciprocity theorem (1931) suggests that the matrix composed of the phenomenological coefficients is symmetric [53]:

$$L_{ij} = L_{ji}. \quad (20)$$

This relation makes it possible to reduce the number of independent phenomenological coefficients. For example, if three different species (counterion, coion, and solvent) are present in a membrane or solution, then the number of independent coefficients is 6.

Along with the Onsager equation (18), the relationship between the fluxes and forces can be expressed using other systems of equations (Spiegler, Stefan-Maxwell, Kedem-Kachalsky, and some others) [70–72]). Generally, these systems are mathematically equivalent, which allows moving from one system of equations to another by simple transformations of variables; at least it is possible in the case of Onsager and Kedem-Katchalsky equation systems [73].

3.2.2. Kedem-Katchalsky equations

The Kedem-Kachalsky equation system [70] is of great interest for the practical description of the ions and water transport through the membranes. In differential form, these equations are written as follows [73]:

$$j_v^r = -L_p (\nabla p - \sigma RT c_s v_{\pm} \nabla \ln a_{\pm}) + \beta i^r = -L_p (\nabla p - \sigma \nabla \pi) + \beta i^r, \quad (21)$$

$$j_i^r = -P \nabla c_i + \frac{it_i}{z_i F} - c_i L_p (1 - \sigma) \nabla p, \quad (22)$$

$$\nabla \phi = -\frac{i^r}{\kappa} - \frac{RT}{F} \left(\frac{t_+}{z_+} \nabla \ln a_+ + \frac{t_-}{z_-} \nabla \ln a_- - \beta c_s v_{\pm} F \nabla \ln a_{\pm} \right) - \beta \nabla p, \quad (23)$$

where j_v^r is the volumetric flux density; L_p , β and P are the hydraulic, electroosmotic and diffusion permeability coefficients respectively; π is the osmotic pressure; σ is the Staverman reflection coefficient (if $\sigma = 1$ then the membrane completely reflects the solute carried by the convective flow through the membrane; $\sigma = 0$ corresponds to zero solute reflection); c_s and c_i are the molar concentrations of salt and ion i , respectively, in the virtual solution of the membrane; $v_{\pm} = v_+ + v_-$ is stoichiometric number; a_{\pm} is the average ionic activity of the electrolyte; t_i is the transport number of species i (equal to the fraction of electric current carried by ion i at zero concentration and pressure gradients); κ is the electrical conductivity.

The fluxes described by Equations (21)–(23) are functions of 3 thermodynamic forces acting in the membrane system: mechanical, caused by the hydrostatic pressure gradient ∇p ; electrical due to electrical potential gradient, $\nabla \phi$; chemical, expressed through the gradient of osmotic pressure or solute activity, coupled by the following relation [70]:

$$\nabla \pi = RT c_s v_{\pm} \nabla \ln a_{\pm}. \quad (24)$$

Transport coefficients L_p , β , P , t_i , κ and σ in the Kedem-Katchalsky equations are commonly used to characterize the transport properties of a membrane [14,74,75], they are called practical coefficients. Due to this, Equations (21)–(23) form the basis for the characterization of membranes and membrane processes [38]. Experimental measurement of such transport coefficients is carried out, as a rule, when only one driving force acts in the system. For example, to evaluate the diffusion permeability coefficient P , it is necessary to carry out measurements at $\nabla p = i^r = 0$ [76–79].

3.2.3. Nernst-Planck equation

The classical Nernst-Planck equation can be considered as a special reduction of the Onsager equation. If the cross phenomenological coefficients in Equation (18) are neglected and Darcy's law (9) (establishing a linear relationship between the fluid flow velocity, v^r , and pressure gradient) is applied, the extended Nernst-Planck equation with convective term can be obtained [54]:

$$j_i^r = -p^m D_i \left(g \nabla c_i + z_i c_i \frac{F}{RT} \nabla \phi \right) + c_i V^r, \quad (25)$$

518 where $D_i = \frac{L_i R T}{c_i}$ is the diffusion coefficient of species i ; $g = 1 + \frac{d \ln \gamma_i}{d \ln c_i}$ is the
 519 activity factor; γ_i is the activity coefficient of species i .

520 In some cases, it is convenient to apply in the membrane the ion transport equation
 521 in the reduced form, which could also be derived from Equation (25) using LEN as-
 522 sumption (15) and Equation (13):

$$j_i^r = -p^m D \nabla c_i + \frac{it_i^r}{z_i F} + c_i V^r. \quad (26)$$

523 3.3. Chemical reactions

524 Accounting for chemical reactions is necessary when considering the transfer of a
 525 weak electrolyte (water, ampholytes, etc.) [80] or a multicomponent solution whose spe-
 526 cies react with functional groups of the membrane or with each other (for example, in
 527 fuel cells) [28]. The protonation and deprotonation of weak acidic or basic functional
 528 groups [67,81,82] is of particular interest, because they are a source or absorber of protons
 529 and hydroxyl ions, but do not move in space and determine the selectivity of the mem-
 530 brane. In the case of BPM, the catalytic water splitting reaction occurs in the bipolar re-
 531 gion [27] and in the membrane bulk.

532 3.4. Donnan equilibrium relation

533 The Donnan model and, in particular, relation (30), obtained in 1911 [41], can be
 534 considered as the first successful attempt to interpret the known experimental results on
 535 electrolyte sorption by a membrane. In this model, an ion-exchange material is consid-
 536 ered as an ideal gel. The Donnan equilibrium between a solution and an ion exchanger is
 537 described by the continuity of electrochemical potential at their interface [33,54,55,83]:

$$RT \ln a_i + z_i F \phi = RT \ln \bar{a}_i + z_i F \bar{\phi}, \quad (27)$$

538 where the value with the overbar refers to the ion-exchanger.

539 The following two relations are derived from Equation (27):
 540 one for the activities

$$(\bar{a}_+^k)^{1/z_+} / (\bar{a}_-^k)^{1/z_-} = (a_+^k)^{1/z_+} / (a_-^k)^{1/z_-}, \quad (28)$$

541 and the other for the electric potential difference between two phases (called the
 542 Donnan potential):

$$\Delta \phi_D = \bar{\phi}^k - \phi^k = -\frac{RT}{z_+ F} \ln \frac{\bar{a}_+^k}{a_+^k} = -\frac{RT}{z_- F} \ln \frac{\bar{a}_-^k}{a_-^k}, \quad (29)$$

543 where k is the left-hand ($k = I$) or right-hand ($k = II$) membrane / solution interface.

544 Taking into account that $a_i = c_i \gamma_i$ and $\bar{a}_i = \bar{c}_i \bar{\gamma}_i$, we find from Equation (29) the
 545 Donnan relation for a binary electrolyte:

$$\frac{(\bar{c}_+)^{1/z_+}}{(\bar{c}_-)^{1/z_-}} = K_D \frac{(c_+)^{1/z_+}}{(c_-)^{1/z_-}}, \quad (30)$$

546 here $K_D = (\gamma_+ / \bar{\gamma}_+)^{1/z_+ - 1/z_-}$ is the Donnan equilibrium coefficient, expressed through
 547 the ratio of mean ionic activity coefficients in the external solution,

548

$\gamma_{\pm} = (\gamma_+^{v_+} \gamma_-^{v_-})^{1/v} = (\gamma_+^{1/z_+} \gamma_-^{-1/z_-})^{(1/z_+ - 1/z_-)^{-1}}$ and in the membrane,

549

$\bar{\gamma}_{\pm} = (\bar{\gamma}_+^{v_+} \bar{\gamma}_-^{v_-})^{1/v} = (\bar{\gamma}_+^{-1/z_+} \bar{\gamma}_-^{-1/z_-})^{(1/z_+ - 1/z_-)^{-1}}$. The electrolyte activity coefficients in aqueous solutions can be taken from the literature [84,85].

550

551

552

553

554

555

556

The Donnan theory cannot quantitatively predict the activity coefficients in the membrane. However, the consideration of only the “free” or “bulk” water in the membrane [86,87] made it possible to achieve quantitative agreement between the theory and experiment of coion sorption.

Another approach is to generalize the Donnan theory by taking into account the Manning condensation theory [88]. This approach is described in the next Section.

557

3.5. Donnan-Manning equilibrium relation

558

3.5.1. Manning's condensation theory

559

560

561

562

563

564

565

566

567

Manning's model [89] is the main theoretical approach in the field of polyelectrolyte solutions since 1970's. The proposed equations have shown their applicability in a wide range of polyelectrolyte solutions [89,90] and are still successfully applied.

Manning's theory of the polyelectrolyte solution is based on the mean field approximation [89] and does not contain adjustable parameters. It takes into account only long-range point-to-line electrostatic forces, which cause “condensation of counterions” around charged polymer chains [89]. The theory is based on a simplified representation of the distribution of fixed charges in a polymer chain. The model is based on the dimensionless parameter, which is the reduced linear charge density of the polymer, ξ ,

$$\xi = \frac{\lambda_B}{b} = \frac{e^2}{4\pi\epsilon_0\epsilon k_B T b} \tag{31}$$

568

The critical value of this parameter is

$$\xi_{\text{crit}} = \frac{1}{|z_Q z_c|} \tag{32}$$

569

570

571

572

573

574

575

576

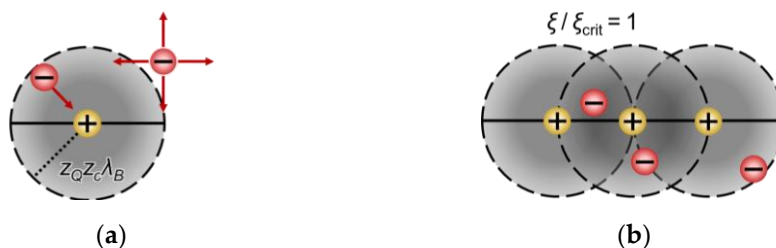
577

578

579

580

here λ_B is the Bjerrum length; b is the distance between two neighboring functional groups; e is the protonic charge; k_B is the Boltzmann constant; z_Q is the charge of functional group; z_c is the charge of counterion. The value of ϵ was left as that of pure water, because Manning's model considers dilute systems. The Bjerrum length represents the distance at which electrostatic forces between two elementary charges are comparable in magnitude to the thermal energy scale [91]. At a distance less than $z_Q z_c \lambda_B$, the energy due to electrostatic attractive force of a functional group (Figure 9a) prevail over the thermal energy. To diffuse away from the polymer chain, counterion has to escape the attractive force of the fixed ions. Two neighbor fixed charges on polyelectrolyte chain, separated by a distance b , may have regions of predominating electrostatic influence (of radius $z_Q z_c \lambda_B$), which are overlapping (Figure 9b and c). The local energy minima created by the overlap resulting in condensation of counterions.



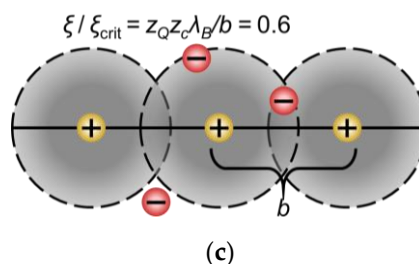


Figure 9. Schematic representation of the attraction of counterions by neighboring functional groups of a polyelectrolyte chain at different ξ/ξ_{crit} . Adapted from [92].

3.5.2. Condensation theory applied to IEMs. Donnan-Manning's theory

It is difficult to measure the average distance between functional groups, b , of IEM. For cross-linked IEM, b can be calculated from the theoretical or experimental ion-exchange capacity and knowledge of the membrane's molecular architecture [93]. Jang et al. [94] considered homogeneous gel membranes (not containing meso and macropores). For example, in the case vinyl polymers, the following equation was proposed:

$$b = 2.5 \text{ \AA} \left(1 + \frac{n_{xl}}{n_{ch}} \right), \quad (33)$$

where n_{xl} is the mole fraction of neutral crosslinker and n_{ch} is the mole fraction of charged monomer; 2.5 Å is the projection length of a repeat unit of vinyl polymers. The functional groups are assumed to be evenly distributed on the polymer backbone.

Authors [95–99] studied laboratory scale IEMs, whose structure was known quite accurately. This made possible to calculate the value of parameter b . In a fairly wide range of electrolyte concentrations, good agreement was found between theoretical and experimental data on coion sorption. It should be noted that for the best agreement, the membranes should be as close to homogeneous as possible. The presence of inhomogeneities leads to the need to apply additional assumptions when determining b .

Determining the parameter b of commercial membranes is also not particularly difficult if the structure of their matrix is known [88,100,101]. However, in some cases, exact determination of b is difficult, then ξ is treated as an adjustable parameter [102,103]. Even in this case interesting observations may be made. Thus, the Neosepta IEMs of the latest generation (CSE and ASE) have larger values of ξ than the previous generation of these membranes (CMX and AMX), so counterion condensation is more significant in the case of CSE and ASE [104].

In the presence of large inhomogeneities (tenth of nanometers), such as in the case of the Nafion 117 membrane, the size and proportion of hydrophilic and hydrophobic regions (see Fig. 4b) must be taken into account. From the point of view of the Donnan-Manning theory, such an IEM is heterogeneous. The use of various assumptions and/or ξ as an adjustable parameter makes it possible to achieve sufficient agreement between theory and experiment on ion sorption [88,94,105,106]. Block copolymer electrolyte (BCE) phase-separated membranes are considered in [107,108]. These membranes also have inhomogeneities in the structure, but the structure parameters are known. The authors succeeded to predict b based only on the structure parameters of the charged half of the BCE.

In the case of commercial reverse osmosis (RO) membranes, consideration of the concentration of fixed ions in a dense active layer made it possible to determine b (with some assumptions) and predict partition coefficients of RO membranes equilibrated with different chloride solutions (LiCl, NaCl, KCl, RbCl, and CsCl) [109,110].

The estimation of the dielectric constant, ϵ , is also complicated. The polymer can occupy more than half of the total membrane volume. As it was mentioned in Section 2 an average dielectric constants in IEMs may be experimentally determined via microwave dielectric relaxation spectrometry (Figure 6) [43,99,111,112]. ϵ may be calculated using the co-continuous model [88,92]:

$$\epsilon = \epsilon_p (1 - \phi_w) + \epsilon_w \phi_w, \quad (34)$$

here, ϕ_w is the membrane water volume fraction, ϵ_p and ϵ_w are the polymer and water dielectric constants, respectively.

4. Modeling of ion and water transport in IEMs

Most of the known mathematical models describing ion and water transport in charged membranes can be classified according to the scheme shown in Figure 10. All models are conditionally divided in two types, which differ in the approach to describing the structure-property relationship. In the first approach, used in the so called “solution-diffusion” models, the membrane material is considered as a quasi-homogeneous (macroscopically homogeneous) medium [113]. The components of the external solution are dissolved (sorbed) in this medium and can be transported there under the action of concentration, electric potential and pressure gradients. In “pore-flow” models, only one pore is considered. The transport of species here occurs under the action of the same driving forces as in the “solution-diffusion” models. The difference is that these forces are applied only in an aqueous solution phase filling the pore. The “pore-flow” models are also called the “capillary” models (because they are based on the models previously developed to describe ion and water transport in capillaries), and the “space charge” models (since it is essential to take into account the deviation from LEN in EDL formed at charged pore walls). The main governing equations relating species fluxes to driving forces (the Onsager, Kedem-Katchalsky or Nernst-Planck equations) are applied in both “solution-diffusion” and “pore-flow” models [114].

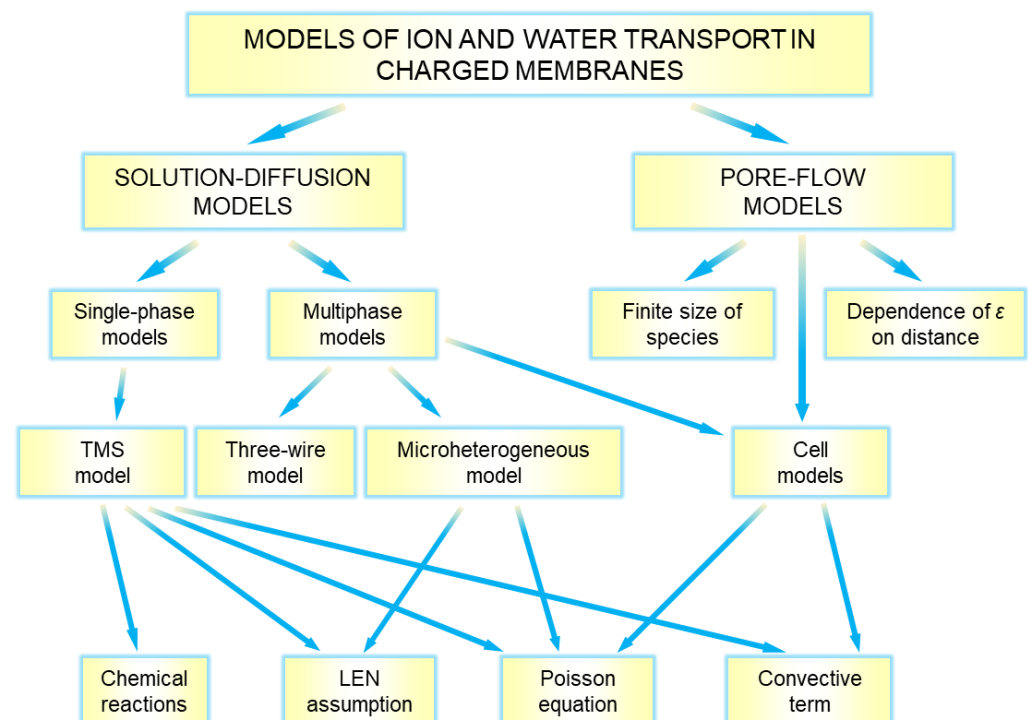


Figure 10. Classification of mathematical models used for describing ion and water transport in charged membranes.

648 “Solution-diffusion” models have been developed for membranes considered as a
 649 single-phase medium or a multiphase medium. In the first case, the
 650 Teorell-Meyer-Sievers (TMS) model is most often used. In the second case, the effective
 651 medium approach [115] is applied. When formulating mathematical problems for some
 652 specific membranes/cases, various conditions/assumptions may be used. This may be the
 653 LEN assumption or the use of Poisson's equation in “solution-diffusion” models. As-
 654 sumptions of infinitesimal or finite species sizes are used in “pore flow” models, while the
 655 use of Poisson's equation is almost always necessary because of the existence of a space
 656 charge in charged pores. Below we will consider in more detail the models that form the
 657 scheme in Figure 10.

658 4.1. “Solution-diffusion” models

659 4.1.1. Teorell-Meyer-Sievers (TMS) model

660 The first successfully applied model for revealing the main properties of charged
 661 membranes was a model proposed independently by Teorell [116] and Meyer and
 662 Sievers [117], in the 1930s, called the TMS model. It serves as the basis for the mathe-
 663 matical description of ion transport in IEMs when the “solution-diffusion” approach is
 664 used.

665 The TMS model is based on the Nernst-Planck equation (25). The membrane is con-
 666 sidered as a single homogeneous phase (charged gel), or in other words, an aqueous so-
 667 lution of matrix polymer chains together with mobile ions and functional groups. The
 668 underlying model includes the assumption of LEN (15) in the membrane, an equation
 669 expressing electric current as the sum of individual ion flux densities (13), and the
 670 Donnan equilibrium relation (35) at the left-hand (I) and right-hand (II) interfaces used as
 671 the boundary conditions:

$$\frac{(\bar{c}_+^k)^{1/z_+}}{(\bar{c}_-^k)^{1/z_-}} = K_D \frac{(c_+^k)^{1/z_+}}{(c_-^k)^{1/z_-}}, \quad k = \text{I, II}, \quad (35)$$

672 here \bar{c}_i^k and c_i^k are the concentrations of ion i at interface k , from the side of the
 673 membrane and solution, respectively [118].

674 Equation (29) for calculating the potential drop across the solution/membrane in-
 675 terfaces is applied as well [119].

676 Instead of LEN assumption (15) and Donnan equilibrium (35) at membrane bound-
 677 aries, the Poisson equation (10) can be used [120–122]. In this case the activity coefficients
 678 of each species are involved; in principle, they can be determined from the data in the
 679 literature [84,85] or evaluated using an appropriate theory such as Donnan-Manning [93]
 680 or others.

681 The TMS models gives an adequate qualitative description of such fundamental
 682 membrane properties as electric conductivity, transport number and membrane potential
 683 [123]. When two kinds of counterions, 1 and 2, are present in the membrane, the
 684 Nernst-Planck equation together with Equations (29) and (35) allow description of
 685 counterion competitive transfer. For more information on the TMS model, see References
 686 [124,125]. The paper [126] gives a description of the main features of this model and an-
 687 alyzes the area of its applicability.

688 Modeling of ion and water transport in systems with bipolar membranes (BPM) is
 689 mainly carried out using the TMS model [67,127,128]. This is due to the fact that the
 690 processes in the interphase layer between the cation-exchange and anion-exchange lay-
 691 ers, where the maximum electric field strength and the catalyst are located [129], are of
 692 the greatest interest, and the description of the processes of ion and water transport [130]
 693 in the membranes themselves should be, first of all, qualitative. The processes of energy
 694 accumulation and production [131–133] using BPM are also well described and predicted
 695 using the TMS theory. Recent paper [134] reveal that in anion exchange layer of BPMs the
 696 charge is carried mainly by bisulphate and sulphate ions instead of hydroxyls, produced

697 inside BPM. The developed models make it possible to describe the current-voltage
698 characteristics [64,67,135,136], the electrochemical impedance spectra [137] of BPM and
699 asymmetric BPM, the performance of ED devices (using a 2D model [138]), and to ex-
700 plain the selectivity of IEMs with a modified surface in ternary electrolyte solutions
701 [64,65,139,140]. Some software packages (e.g. COMSOL Multiphysics) include modules
702 based on the TMS model and are used in modeling of such processes [64].

703 Using this simple approach, it is possible to explain the deviation of the IEM behav-
704 ior from the classical one in solutions of weak electrolytes (such as phosphate or tar-
705 trate salts) and explain some feature of this behavior compared to that in strong electro-
706 lyte solutions: the appearance of a second limiting current [141], increased diffusion
707 permeability [68] or unusual concentration dependence of membrane conductivity [142].
708 Models based on TMS shed light on the transient characteristics of IEMs [120] and pro-
709 vide an explanation for scaling formation on surface in solutions with multivalence ions
710 [143], and are still an indispensable theoretical tool in the field of RED [144–147] and fuel
711 cells [17,28,52]. It is applicable also in the environmental analysis systems based on the
712 dialysis membranes [148]. In [149,150] authors used the same assumption as the TMS
713 model, but apply the extended Nernst-Planck equation, which contains the convective
714 term that is important when considering the application of IEMs in chlor-alkali electrol-
715 ysis.

716 There are models considering the membrane as a single phase (charged gel), in
717 which the concentration of fixed charges and/or diffusion coefficients continuously
718 change along the normal coordinate [151,152]. Generally, these models show that a het-
719 erogeneity in the fixed charge distribution leads to an increase of permselectivity in
720 comparison with a membrane wearing homogeneously distributed fixed charges of the
721 same average concentration. The explanation is that the permselectivity is controlled by
722 the layer having the highest local concentration of fixed charge, while the layers with low
723 fixed charge concentrations have a minor impact on the global membrane behavior.

724 The further development of TMS model proceed in several ways. One of them is to
725 apply other transport equations such as Stephen-Maxwell [28] and Kedem-Katchalsky
726 [70] instead of Nernst-Planck; as well the Poisson equation is used instead of the LEN
727 assumption. But the basic principle of representing the membrane structure remains the
728 same: the membrane is considered as a single gel phase. Another approach takes into
729 account inhomogeneities in the membrane structure, which can be at different levels,
730 from a few nanometers to microns. In the following subsections, we will discuss the
731 models dealing with pores and clusters, as well as hydrophobic regions, which are re-
732 vealed by experimental investigations.

733 4.1.2. Multiphase models

734 In multiphase models a membrane, in accordance with the effective medium ap-
735 proach [115], is represented as a quasi-homogeneous system comprising two (or several)
736 phases, the transport properties of which are functions of the properties of the corre-
737 sponding phase [153,154]. This system may be considered as an array of capillary pores
738 [155], a cluster-channel network [156], or as a uniformly distributed porous grains [157].

739 Microheterogeneous model

740 Earlier, in Section 2, we described that charged membranes are porous materials.
741 The structure of these materials generally includes micro-, meso-, and macropores. To dis-
742 tinguish between these types of pores, one can use the ratio of the pore radius r to several
743 characteristics, such as the EDL length, λ , or length of action of adsorption forces [158].
744 Usually, micropores are considered as the pores for which $r < \lambda$ (approximately, $r < 1$ nm);
745 if $r > \lambda$, but r and λ are in the same order, then we are dealing with a mesopore; the con-
746 dition $r \gg \lambda$ ($r > 50$ nm) is characteristic for macropores. Mesopores and macropores
747 contain an electrically neutral solution in their central part. Such a solution can be con-
748 sidered as a separate phase, and its properties (ion and water diffusion coefficients,

permittivity) are very close to those of an external free solution equilibrated with the membrane [24].

Based on the foregoing, the first phase can be distinguished in the IEM structure: an electrically neutral solution in meso- and macropores. Then the remaining volume can be attributed to the second phase. This second phase is the “gel phase” [153], which includes a hydrated polymer matrix with fixed charged groups, whose charge is compensated by the charge of mobile ions. The gel phase can be considered as a microporous medium not containing electroneutral solution (Figure 7).

It is important to note that in reality there is no distinct boundary between the intergel electroneutral solution and the EDL at the internal pore walls. Nevertheless, the conditional separation of the membrane material into different phases makes it possible to simplify the mathematical description. The main idea of such a model approach is to assign certain physicochemical properties to each phase. Then the properties of each individual phase are functionally related to the entire membrane properties (effective medium approach [115]).

Consider a macroscopic volume in the form of a layer of thickness dx (Figure 7). This layer should be sufficiently large to be “representative” and contain all membrane phases. At the same time, it should be small enough to be considered elementary when applying the transport equations in differential form, such as the Onsager equation (18). Detailed changes in concentrations and potential within dx are not considered, and the values of these parameters in phase elements are averaged; it is assumed that the phases in the dx layer are in equilibrium with each other. When describing ion and water transport, the problem is to obtain the effective transfer coefficient L_i , which characterizes the membrane layer of thickness dx as a function of L_i^k coefficients (characterizing the individual phases k), and the structural-geometric parameters characterizing the shape and mutual arrangement of the phases.

First elements of the microheterogeneous model were formulated by Gnusin et al. [159] when developing the so called “principle of generalized conductivity”, which is an analog of effective medium theory [115]. The main elements of this model and its experimental verification are described in References [153,160]. Later on, some modifications of this model [35,161–163] and numerous applications are presented in References [14,35,161–175]. The application of the microheterogeneous model allows, along with the electrical conductivity of the membrane [165–168,173–175], to determine electrolyte diffusion permeability [14,21], permselectivity (ion transport numbers) [14,21,169,170,176], electrolyte sorption [177–179] and some other properties [14,21,172,180]. It is possible to quantitatively describe the concentration dependences of the mentioned membrane characteristics based on a single set of structural and kinetic parameters [14,21,172].

Within the framework of the microheterogeneous model, the transport equation is written in the form, reduced from the Onsager equation (18):

$$j_i^r = - \sum_j L_{ij} \nabla \mu_i \quad (18)$$

The effective membrane conductance coefficient L_i is then expressed as follows [153]:

$$L_i = \left[f_1 (L_i^g)^\alpha + f_2 (L_i^s)^\alpha \right]^{1/\alpha}, \quad (36)$$

where L_i^g refers to the gel phase, and L_i^s to the intergel electroneutral solution; f_1 and f_2 are the volume fractions of the corresponding phases: $f_1 = V_g/V_m$, $f_2 = V_s/V_m$, $f_1+f_2=1$ (where V_g , V_s and V_m are the volumes of gel, intergel solution and the membrane, respectively); α is the structural parameter depending on the position of the phases with respect to the transport axis: when the phases are parallel to this axis, $\alpha = 1$; when they are in serial disposition, $\alpha = -1$; in other cases $-1 < \alpha < 1$.

The mathematical description of the ion transport in the gel phase contains all the assumptions made in the TMS model (see Section 4.1.1). The properties of the intergel solution are the same as those of the equilibrium bathing solution. The Nernst-Planck equation (Equation 25 without convective term) is used, and the condition of local electrical neutrality (Equation 15) is assumed. L_i^s and L_i^g are expressed as functions of the ion diffusion coefficients, D_i^s and D_i^g , and the concentrations, c_i^s and c_i^g , in the corresponding phases [153]:

$$L_i^s = D_i^s c_i^s / RT, \quad L_i^g = D_i^g c_i^g / RT. \quad (37)$$

Concentrations c_i^s and c_i^g are linked by the Donnan relations (Equation 30), the local equilibrium being assumed between both phases.

As a rule, IEMs have a rather high concentration of fixed ions (\bar{Q}), close to 1 mol/L swollen membrane or higher. Therefore, in the case of dilute solutions, the concentration of coions in the gel phase is negligible compared to \bar{Q} . When assuming $\bar{c}_- \ll \bar{Q}$ and $\bar{c}_+ \approx \bar{Q}$, Equation (30) can be simplified. In the case of a symmetrical electrolyte ($z_+ = -z_- = z$) one gets [51]:

$$\bar{c}_A = \frac{K_D^z}{Q} c_A^2, \quad \bar{c}_c = \bar{Q} + \bar{c}_A, \quad (38)$$

where subscripts "c" and "A" are used for the counterion and coion, respectively; c_A is the coion concentration in the inter-gel solution.

Since ions are present in both phases, the partition coefficient, K_s , involving the coion concentration in the membrane, c_A^* , can be found using Equation (38) [153]:

$$K_s = \frac{c_A^*}{c_A} = f_1 \frac{K_D}{Q^g} c_A + f_2. \quad (39)$$

The first and second terms on the right-hand side of Equation (39) correspond to the contribution of the gel phase and the inter-gel solution, respectively. Q^g and K_D are the ion-exchange capacity of the gel phase and the Donnan coefficient, respectively. Despite the fact that the intergel phase volume fraction in IEM is quite small (less than 0.1 in homogeneous membranes and about 0.2 in heterogeneous ones), electrolyte is predominantly sorbed by this phase (especially in dilute solutions).

Equation (39) describes the linear dependence between K_s and the external solution concentration. At a low electrolyte concentration, K_s is close to f_2 , i.e., its value is approximately 0.1 (or lower) for homogeneous membranes and about 0.2 for heterogeneous ones [51].

In the case of a binary electrolyte, the microheterogeneous model expressed by Equations (36)-(39), includes six basic input parameters: two static, K_D and Q^g (thermodynamics coefficients); two structural, f_1 and α ; and two kinetic ones (D_1^s and D_A^s , diffusion coefficients in the gel phase). When these parameters are known, L_i coefficients can be calculated. Membrane transport characteristics (conductivity, κ , ion transport numbers, t_i , and diffusion permeability, P) are calculated using equations relating the Onsager and Kedem-Kachalsky conductance coefficients:

$$\kappa = (z_+^2 L_+ + z_-^2 L_-) F^2, \quad (40)$$

$$t_i = \frac{z_i^2 L_i}{z_+^2 L_+ + z_-^2 L_-} = \frac{z_i^2 L_i F^2}{\kappa}, \quad i = +, -, \quad (41)$$

$$P = \frac{(z_+ L_+ t_- + |z_-| L_- t_+) RT}{c} = \frac{2RT\kappa t_+ t_-}{F^2 c}, \quad (42)$$

where $c = |z_i|c_i$ is the equivalent electrolyte concentration in the solution in equilibrium with the membrane.

It is important to note that Equations (40)-(42) are applicable both in the case where the membrane is in equilibrium with an external solution and in the presence of a concentration gradient across the membrane (zero or non-zero current). When there is a concentration gradient, Equations (40)-(42) are applied locally [51].

The input parameters of the microheterogeneous model (the six parameters listed above) are found from the experimentally obtained membrane exchange capacity and concentration dependences of electrical conductivity, and diffusion permeability. For example, the volume fraction of the gel phase (or intergel solution) can be approximately found from the concentration dependence of the membrane conductivity, κ [14,21,153,171,172,181]:

$$\kappa = (\kappa^g)^{f_1} (\kappa^s)^{f_2}. \quad (43)$$

Equation (43) is obtained as a limiting case of Equations (36) and (40) at $\alpha \rightarrow 0$.

At low electrolyte concentrations (usually < 1 M), the gel conductivity, κ^g , is almost independent of the electrolyte concentration due to the weak coion sorption by this phase. In this case, the dependence $\lg\kappa - \lg\kappa^g$, according to Equation (43), is linear with a slope factor f_2 . According to numerical calculations, Equation (43) is hold near the "isoconductance point" (where $\kappa = \kappa^g = \kappa^s$), if $|\alpha| \leq 0.2$.

A detailed algorithm for determining the remaining parameters of the microheterogeneous model is described in Reference [181].

Various modifications of the microheterogeneous model are also known [35,161–163].

Porozhnyy et al. [161] proposed a mathematical description of the effect of charged nanoparticles on the membrane transport properties. In addition to the gel phase and the electrically neutral solution, the presence of nanoparticles was considered (Figure 11). The core of the nanoparticle is impermeable to ions and water, but the EDL formed around it contributes to a significant increase in the counterion concentration in the pore solution. The fraction of the charged solution in membrane pores increases and the fraction of electroneutral solution decreases. As a consequence, the presence of charged nanoparticles causes an increase in the conductivity and a decrease in the diffusion permeability of the membrane [161]. According to Equation (42), these changes in κ and P result in an improvement of the membrane permselectivity with respect to counterions (an increase in the counterion transport number).

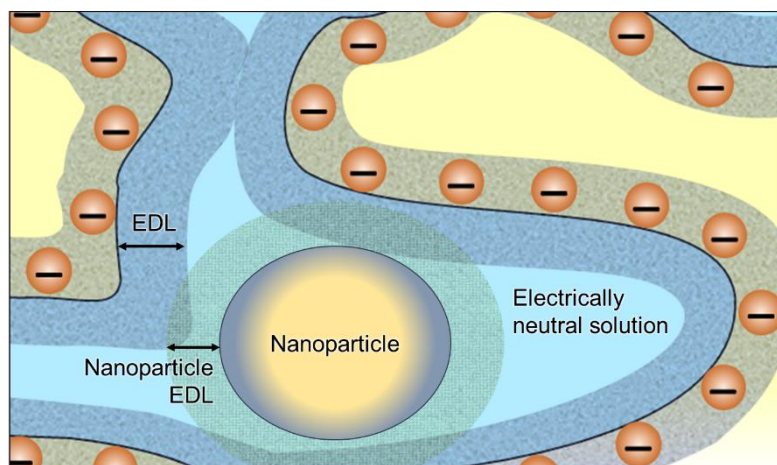


Figure 11. Schematic representation of a fragment of a mesoporous IEM containing a charged nanoparticle surrounded by an EDL. Redrawn from [161].

Nichka et al. [162] proposed a modification of the microheterogeneous model that takes into account the changes in the contribution of the EDL at the internal boundaries of the gel phase, which occur with external concentration changes. This modification assumes that the EDL thickness at the pore wall increases with the dilution of the external solution inversely proportional to \sqrt{c} . As a result, the membrane conductivity decreases with solution dilution less rapidly compared to the basic version [153]. This trend agrees with experimental data [162].

Kozmai et al. [35] found the ion diffusion coefficients in the membrane gel phase, \bar{D}_i , and the volume fraction of the intergel one, f_2 , as functions of the membrane water content (the higher water content, the higher \bar{D}_i and f_2). The approach proposed in [35] made it possible to more correctly describe the transport characteristics of MA-40 and MA-41 membranes depending on the concentration and pH of the external solution. In this description, it was taken into account that the membrane water content decreases when the external concentration increases and when there is a loss in the exchange capacity. The latter is due to deprotonation of weakly basic fixed groups with increasing pH.

In another work of the same scientific group [163], the microheterogeneous model was supplemented to describe changes in the structure of the CJMA-7 anion-exchange membrane transport properties (Hefei Chemjoy Polymer Materials Co. Ltd., China) due to various modifications. The model [163] takes into account the presence of a perfluorosulfonated ionomer modifying film on the substrate membrane surface and partial filling of macropores with this modifier.

Three-wire model

Another approach was developed in middle 1950s by Willie and Southwick [182]. The model described the system “ion-exchange resin granules/electrolyte solution” [183,184]. Later this idea was applied to ion-exchange membranes [185,186]. The model represents the system under study in the form of three parallel conducting layers [182,184] (Figure 12). The first layer consists of electrolyte solution and ion-exchange gel arranged in series. It represents the passage of ions through the conductive spheres and the solution between them. The second layer is a pure ion-exchange gel. It describes gel phases (ion-exchange granules in original work), which touch each other to form conducting paths. The third layer is the pure electrolyte solution. This component represents the conductance through the solution-filled regions (macropores in a heterogeneous membrane).

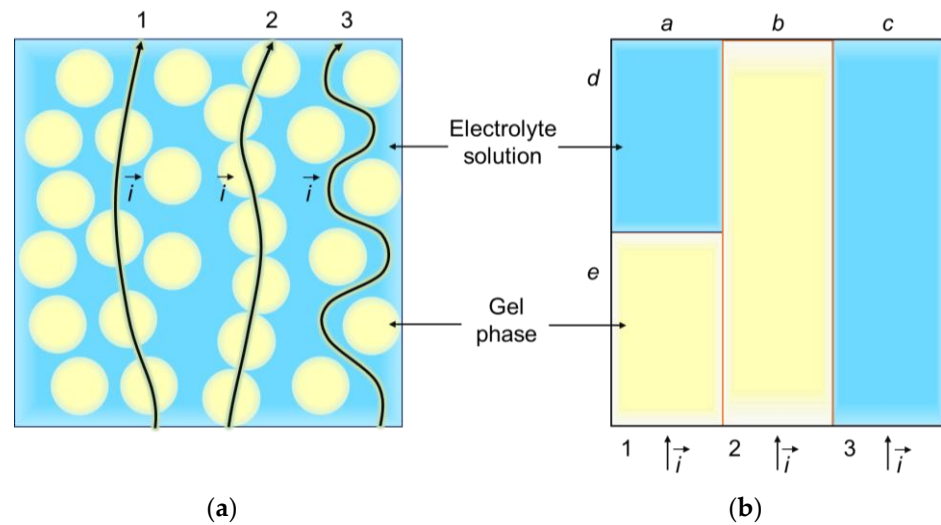


Figure 12. Schematic representation of three pathways of ions and electrical current in two phase system (a) and three-wire model (b).

The resulting conductivity of the IEM κ_m is a function of the electrical conductivity of the gel phase κ_s and geometrical parameters a , b , c , d , and e of the model (Figure 12):

$$\kappa = a\kappa^s / (e + d\kappa^s) + b\kappa^s + c. \quad (44)$$

There are two relations between the geometrical parameters: $a+b+c = 1$ and $d+e = 1$. Thus, the number of independent fitting parameters can be reduced to 3. Although the model has been proposed for a long time, it continues to be effectively used [154,169,187].

Cell model

Filippov et al. [188–190] described the ion and water transport in IEMs using the so-called «cell method», proposed by Happel and Brenner [191]. The method is quite efficient for description of concentrated disperse systems. In the case of IEMs, cell models take into account the size and some transport properties (such as conductivity, hydraulic and diffusion permeability) of grains or fibers forming the system, as well as their packing patterns [192,193]. The macropores are formed between the grains (e.g., of an ion exchanger) packed into array and the micro- and mesopores concentrated in the grains themselves, are taken into account. Figure 13 shows an example of a membrane structure in the framework of cell models [194]. An IEM is presented as a periodic array of identical charged porous spheres (or cylinders) of radius a enclosed by liquid spherical (or coaxial) shells of external radius b instead of randomly distributed ion exchange clusters of different sizes. The sphere-to-cell (or cylinder-to-cell) volume ratio is equal to its total fraction in the disperse system.

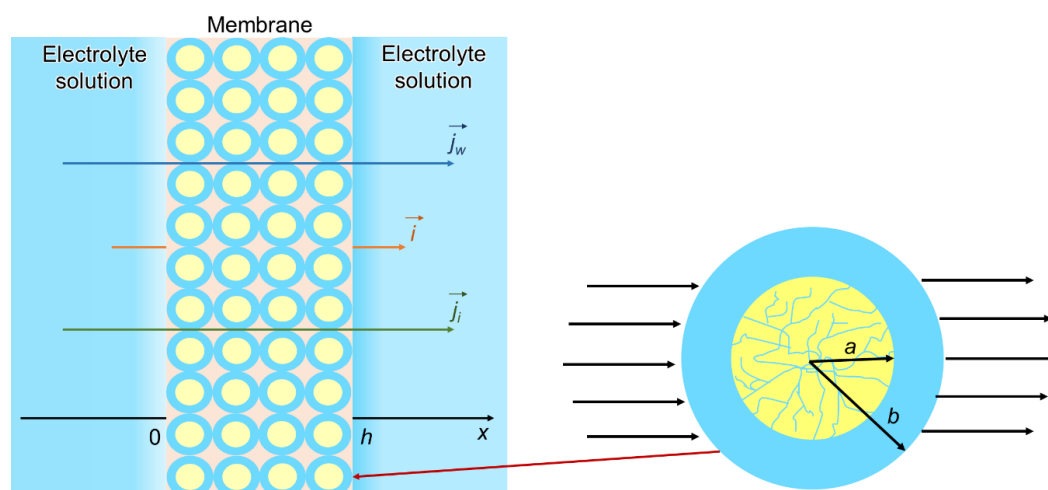


Figure 13. Schematic representation of a cell model, described by Vasin et al. [194].

The mathematical formulation of the problem in the case of modeling membrane electric and hydraulic permeability has been presented in References [157,193,195]. The extended Stokes equation (8) taking into account the spatial electric force describes a “creeping flow” (small Reynolds number) in the outer region of the sphere ($a < r < b$), and the Brinkman vector differential equation [196] with the spatial electric force describes the fluid transport in the inner region ($0 \leq r < a$). The Nernst–Planck equation with the convective term (25) coupled with the Poisson equation (10) are used for description the ion flux density [193]. The mutual influence of adjacent particles is taken into account by establishing certain boundary conditions on their surfaces. An exact algebraic equation for the estimation of membrane hydrodynamic permeability was derived [157,193]. The correctness of the theoretical results was confirmed by their satisfactory agreement with the experimental data on the electrical conductivity and electroosmotic permeability of the MF-4SC cation-exchange membrane in various 1:1 electrolyte solutions [197]. In [198] the analytical expressions for conductivity, limiting current density and diffusion permeability for bi-layer IEMs were also in good agreement with the experimental data for membranes modified by polyaniline decorated clay nanotubes.

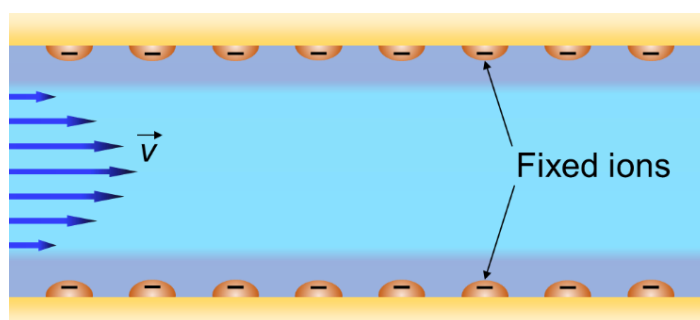
Cell method allows one to take into account different features of membranes. In [199] the action of surface forces on the walls of the micro- and mesopores is taken into account by stress jump at the fluid–porous interface. The authors [199] also considered the deformation of the shape of grains or fibers in the swollen state (deviation from the ideal spherical or cylindrical shape) to describe mass transfer through polymer membranes. In [200], the effect of an external magnetic field on the filtration of an electrolyte solution was considered. In [157], mathematical modeling of the electrobaromembrane process made it possible to confirm the conclusion made in previous experimental and theoretical studies [201,202]: the selectivity to equally charged ions may be achieved due to the difference in their mobility by certain combination of potential and pressure difference applied to the membrane.

4.2. “Pore-flow” models

The “pore-flow” models describe the ion and water transport in a membrane pore [113,203], which is considered as a conducting channel (usually tubular). This approach originates from the description of ion and water transport inside microcapillaries with charged walls [114,204]. These models make it possible to describe such electrokinetic phenomena as the current-induced transfer of a liquid relative to a charged solid surface or the transfer of charged solid particles in a liquid [205,206]. The main role in these phenomena is played by the EDL at the charged surfaces.

958 This kind of models is often called “space-charge models” [207–211] in the literature.
959 The ion and water transport are described by Nernst-Planck-Poisson-Navier-Stokes
960 equations system. The pore size and wall charge density are the main parameters [212]
961 characterizing the system.

962 The basic version of a space-charge model deals with a tubular pore (schematically
963 shown in Figure 14) with surface charge on the walls. The model is based on the extended
964 Nernst-Planck equation containing the convective term, Equation (25), written in 2D or
965 3D geometry with axis symmetry. The diffusion coefficients are usually assumed to be
966 the same as in free solution. The cross-sectional distribution of local concentration is well
967 described by the Poisson-Boltzmann equation. The fluid flow is described by the
968 Navier-Stokes equation (8) with electrical body force term [201]. The letter is provided by
969 the tangential electric field applied to the space charge in the EDL. The walls are usually
970 considered as uniformly charged. The impact of a non-uniform distribution of the pore
971 wall charge on nanofiltration (NF) performance has been investigated by the group of
972 Szymczyk in References [208,213,214]. In addition to NF, the condition of non-uniform
973 pore wall charge distribution is used to describe the transport of ions and water in
974 nanochannels in various other applications [215–219]. The potential at the pore walls also
975 may be controlled using specially designed membranes [220,221] by applying an external
976 voltage source. This makes it possible to switch the ionic selectivity of membranes so that
977 a membrane can be cation-exchange at one applied voltage, and anion-exchange at an-
978 other voltage [222,223].



979 **Figure 14.** Schematic representation of solution flow in a tubular pore with charged walls; an EDL
980 at the wall is shown in a darker shade. Redrawn from [47].
981

982 A simplification of pore-flow model is possible in the case of the pores that are thin
983 relative to the Debye length. The concentration profiles change only slightly across thin
984 pores, as well as the potential [224]. This simplification is known as “fine capillary pore
985 model” or “uniform potential model”. It also may be considered as an extended version
986 of the TMS model [146], which takes into account the fluid flow.

987 Different versions of “pore-flow” models account for different effects at the inter-
988 phases: the dependence of the dielectric constant on the distance from the pore wall [225],
989 finite sizes of ions, ion hydration effects [226], adsorption of diluted species [207,227] and
990 other [228,229]. These effects have a significant impact on the streaming potential [230],
991 diffusion permeability [208] and permselectivity [231], pore conductivity [204,232] and
992 some other properties, which can be computed using such models. These models are
993 very useful for describing the ion and fluid transport in and around nanometer-sized
994 objects with at least one characteristic dimension below 100 nm [233]. Bazant et al.
995 [206,234] paid attention to the steric effects near a non-permeable wall at high voltages
996 taking into account that solvated counter-ions are crowded there.

997 Cwirko and Carbonell [235] and later on Szymczyk et al. [236] have calculated using
998 space-charge models the macroscopic Onsager’s L_i coefficients for a Nafion membrane as
999 functions of the membrane nanostructure parameters (which are the pore radius, pore
1000 wall charge density and the tortuosity factor). Their comparison with the experimental
1001 coefficients determined by Narebska et al. [237] has shown a rather good agreement.

Thus, it becomes possible to bridge the gap between two different approaches, i. e. the microscopic model description and the “solution-diffusion” models applied together with irreversible thermodynamics.

The “pore-flow” models can be applied not only to tubular pore, but also to pores with other geometries. Moreover, Balannec et al. studied how geometry of a pore affects its permselectivity [214]. They found that hourglass-shaped nanopores in nanofiltration membranes improve their salt rejection. The explanation of this effect is that the filtration and desalination properties of hourglass-shaped nanopores are based on two different phenomena: the exclusion of coions in the thinnest region of the pore, and the magnitude of the pressure-induced electric field driving ions through nanopores. This interesting conclusion about the role of the shape of nanopores was proved experimentally [238,239].

5. Current state of modeling of ion and water transport in membrane energy generation systems

The previous section presents the main approaches to the mathematical description of ion and water transport across membranes. However, the question “Which of these approaches are applicable or most often used in the case of membrane energy generation processes?” remained open. In this section, we analyze the current state of modeling in this field and consider in more detail examples of the description of ion and water transport in the RED and proton-exchange membrane fuel cells (PEMFC). It is important to note right away that for such processes, the “solution-diffusion” models are mainly used. This is not to say that “pore-flow” models are not applicable to such cases. However, modeling the distribution of ions in EDL is an over-complication given the fact that in the case of RED and PEMFC, convective transport in free solution within the membrane pores is not dominant. However, “solution-diffusion” microstructural models are increasingly being used in energy generation processes.

5.1. PEMFC models

In recent decades, hundreds of papers have been published on the simulation of PEMFC, which have been considered and structured by many comprehensive reviews [28,52,240–244].

The membrane in PEMFC acts as a barrier to gas transfer, preventing mixing of H₂ and O₂ and electronic conduction between the anode and cathode electrodes, but acting as an ionic conductor, transporting H⁺ protons in the form of hydronium ions H₃O⁺ or H₅O₂⁺. As described in Section 2, in the presence of water, a cluster-channel system is formed in the membrane volume, which provides ionic conductivity. The proton conductivity depends on the size of clusters and especially on the channels. The latter is a strong function of water content. Therefore, the models describing the functioning of PEMFCs usually take into account the dependence of membrane properties on the water content and describe water transfer simultaneously with proton transfer.

Vapor equilibrated (VE) or liquid equilibrated (LE) conditions influence the water and proton transfer in the membrane and the interfacial resistance. PEMFCs are mostly operated under VE conditions at both electrodes, and PEM water electrolyzers for water splitting are mostly operated under LE [245]. Therefore, the PEM water content is rather low when the membrane is used in fuel cells, while it is high when operating in water electrolyzers. The humidity of PEM also determines the operating temperature of the PEMFC itself [246]: when the membrane dehydrates, its ionic resistance increases, which leads to an increase in its temperature and the temperature of the entire device. The water content in PEMs depends on the supply of water vapor from the supplied air to the cathode channel and on the transport of water formed in the porous electrode, where reaction (4) takes place. Ionic conductivity of the membrane depends on the percolation effect (described in Section 2), which depends on the water content of the membrane. Thus, water transport limits the performance of the fuel cell. Great attention is paid to

1053 water management, that is optimization of water transport and water content in PEMFC
1054 [247].

1055 In recent works on PEMFC models [247–255], a membrane is considered as a ho-
1056 mogeneous phase, in which water transport occurs. The water flux through the mem-
1057 brane is described phenomenologically as the sum of two terms: a Fickian diffusion and
1058 an electroosmotic drag. Ion transport is taken into account through ionic conductivity
1059 (which is a strong function of water content and temperature) and current density.

1060 In Section 2, we also considered two mechanisms of proton transport in a PEM: the
1061 vehicle mechanism, in which protons are carried in the form of hydronium ions, H_3O^+ or
1062 $H_5O_2^+$; and the hopping (Grotthuss) mechanism, which is rather characteristic of bulk
1063 liquid water. Membranes at low hydration do not contain fluid domains with extensive
1064 hydrogen bond networks, the Grotthuss mechanism is suppressed, and the vehicle
1065 mechanism is considered to be dominant [24,105]. Running the hopping mechanism at
1066 higher water content, especially in LE conditions, increases the conductivity as the water
1067 content increases.

1068 In the field of fuel cell modeling, the most common approaches are those developed
1069 by Springer, Zawodzinski and Gottesfeld [256] (hereafter the “Springer model”) and by
1070 Weber and Newman [257].

1071 The widely used Springer model accounts for electroosmotic drag and water diffu-
1072 sion in the membrane in an essentially empirical manner. It considers a PEM under VE
1073 conditions only. The water content (in H_2O / SO_3^-), λ_{eq} , in a Nafion 1100 PEM at the in-
1074 terface with the electrode as a function of water vapor activity outside the membrane, a_w
1075 , was presented as an empirical polynomial relation [256]:

$$\lambda_{eq} = 0.043 + 17.81a_w - 39.85a_w^2 + 36.0a_w^3, \text{ at } 0 \leq a_w \leq 1. \quad (45)$$

1076 An equilibrium is assumed between the water vapor outside the membrane and the
1077 water content inside the membrane at the interface. The water vapor activity is calculated
1078 as $a_w = \chi_w P / P_{sat}$, where χ_w and P are the mole fraction of water in the gas and the pressure at
1079 the electrode/membrane interface, respectively; P_{sat} is the saturation pressure of water.

1080 In the literature the isotherm measured by Zawodzinski et al. [258] and expressed by
1081 Equation (45) is commonly used in modelling of PEMFC [52,247,249,254,259] and PEM
1082 electrolyzers [245]. Nafion 1100 is the most popular PEM, for which empirical sorption
1083 isotherms have been established experimentally [105].

1084 The Springer model also includes the water diffusion coefficient measured by
1085 Zawodzinski et al. using nuclear magnetic resonance method [258]. From a thermody-
1086 namic point of view, taking into account the pressure drop inside the membrane is most
1087 likely useful only under LE conditions [256,257]. The models that take into account the
1088 pressure gradient become relevant only in the LE mode, when free liquid water is present
1089 in the PEM [257].

1090 The main difference between the Springer model and the Weber–Newman model
1091 [257] is that the latter takes into account an additional effect. The Springer model ac-
1092 counts for water diffusion and water electroosmotic drag (when an electric current of
1093 protons induces water transport), the ionic transport is assumed depending only on
1094 membrane water content. The Weber–Newman model also considers another cross ef-
1095 fect: water flux can induce streaming current of protons. The latter effect is especially
1096 important under LE conditions.

1097 The earlier models [256,257] have become widespread and have been supplemented
1098 with various empirical dependencies that refine water content, diffusivity, and ionic
1099 conductivity. The heat management is also quite important [247]. Machine learning pro-
1100 cesses are actively used on experimental data and calculation results using 3D models
1101 [241,260]. The developed approaches to describing the processes of proton and water
1102 transfer in a PEM, considered as ideally homogeneous, are sometimes even sufficient for
1103 practical purposes of operating fuel cells. From the point of view of the classification

given in Section 4, the assumption of the isotropy of membrane properties makes it possible to attribute the above models to the “solution-diffusion” approach, namely, to the TMS model. At the same time, the fact that the ion and water transport through PEM considered using the relationship of process parameters, rather than being directly simulated, makes these models very different from TMS. The use of empirical and semi-empirical dependences of water content, diffusivity, and ionic conductivity makes it possible to achieve a relatively good qualitative and quantitative description of the transfer process in a membrane. However, this is not always sufficient for a detailed study of the mechanism of ion and water transport through membranes. Moreover, these models depend too much on experiment. The development of PEMFC models that more explicitly take into account the relationship between the membrane structure and its properties can partially or completely solve these problems.

5.2. RED models

When describing the RED, the main attention is paid to ion transport, while water transport is generally not important in this process. This is due to the fact that the main driving force is the concentration gradient of counterions, which weakly depends on the electroosmotic and osmotic water transport. In addition, these two contributions to water transport in the case of RED are counter-directional.

Veerman et al. [15] were among the first to take into account the features of transport phenomena in IEMs when modeling the RED process. Ionic fluxes in the membrane were described by the Nernst-Planck equation (25) in the approximation of a linear concentration distribution; the variation of ion concentration in the solution diffusion layers were not taken into account. The use of species conservation equations together with the fluxes found using the Nernst-Planck equations allowed calculation of the ion concentration distribution along the length of the membranes in chambers with sea water and river water flowing between a cation-exchange and an anion-exchange membranes. Along with the salt flux, j_{salt} (Equation 46), the water flux, j_{water} (Equation 47), due to osmosis of water from the river water compartment to the sea water compartment was also considered:

$$j_{salt}(y) = \frac{i(y)}{F} + \frac{2D}{d}(c^S(y) - c^R(y)), \quad (46)$$

$$j_{water}(y) = -\frac{2D_{water}}{d}(c^S(y) - c^R(y)) \frac{M_{water}}{\rho_{water}}, \quad (47)$$

where y is the tangential coordinate; i is the current density; d is the membrane thickness; D and D_{water} are the electrolyte and water diffusion coefficients, respectively; c^S and c^R are electrolyte concentrations in sea and river water, respectively; M_{water} and ρ_{water} are the water molar mass and density, respectively.

The model made it possible to calculate the generated average power density, $\overline{P_d}$ (Equation 48).

$$\overline{P_d} = \frac{\int_0^L \left(\frac{1}{2} i^2(y) R_{cell}(y) \right) dy}{L}, \quad (48)$$

where L is the length of RED cell; factor 1/2 is due to the double membrane area (CEM and AEM) in a cell; $R_{cell}(y) = R^S(y) + R^R(y) + R^{AEM} + R^{CEM}$ is the area resistance of RED cell, which depends on the area resistance of the river, R^S , and sea water, R^R , compartments and the resistance of the cation-, R^{CEM} , and anion-exchange, R^{AEM} , membranes. It was assumed that the values of R^{CEM} and R^{AEM} are constant.

1144 The obtained value of $\overline{p_d}$ was close to the experimentally determined value of 1
 1145 W/m² when using an apparatus equipped with Fumasep FKD cation exchange mem-
 1146 branes and Fumasep FAD anion exchange membranes (Fumatech, Germany). This result
 1147 was obtained when the solution residence time in RED stack chambers was minimal. The
 1148 main conclusion in relation to the performance of the process was that the IEMs should
 1149 be as thin as possible and have small resistance.

1150 Within the framework of the classification in Section 4, it can be said that the ap-
 1151 proach proposed by [15] is close to the “solution-diffusion” approach (TMS model). Sim-
 1152 ilar modeling approaches were used to evaluate the maximum power density of RED
 1153 systems based on Fumasep membranes FAS-50 and FKS-50 [261,262] and Fujifilm CEM
 1154 and AEM membranes (Fujifilm, Netherlands) [263]. It is shown that the power density
 1155 increases significantly with an increase in the concentration of the sea water solution and
 1156 the Reynolds number.

1157 Tedesco et al [145] took into account the distribution of concentration not only along
 1158 the length of each chamber in the RED stack, but also along their width. The membrane
 1159 was considered as a gel phase (the TMS model). Ion transport was described using the
 1160 Nernst-Planck equation (25) under the LEN assumption (15). Water transport was not
 1161 taken into account due to the fact that it is small due to the counteracting action of os-
 1162 mosis and electroosmosis. This approach made it possible to take into account the con-
 1163 tribution of coion transfer and show that the power density decreases with non-ideality
 1164 of the membrane. Gurreri et al. presented a similar model [264] but with a membrane
 1165 having a profiled surface. They found an elevated flux of coions, which was due to high
 1166 concentration of these ions in the membrane caused by their strong concentration in the
 1167 external solution (seawater).

1168 Moya [265–267] presented a one-dimensional TMS model that takes into account the
 1169 two-dimensionality of the RED system using the diffusion layer thickness, δ , which was
 1170 calculated using the Leveque equation [268]:

$$\delta = \frac{h}{1.47} \left(\frac{h^2 v_0}{LD} \right)^{-1/3}, \quad (49)$$

1171 where h is the intermembrane channel width; v_0 is the average flow rate in the
 1172 intermembrane channel.

1173 The model makes it possible to investigate the efficiency of the RED process in the
 1174 presence of doubly charged counterions in electrolyte solutions. It has been shown that
 1175 the selectivity of membranes decreases as the flux of coions increases due to a decrease in
 1176 the Donnan exclusion of coions from the IEM. The diffusion coefficient of doubly charged
 1177 counterions in the membrane is much less than that of singly charged ones, which leads
 1178 to an additional increase in the resistance of the system. Thus, the efficiency of the RED
 1179 process decreases in the presence of doubly charged ions in electrolyte solutions.

1180 As a continuation of their work, Tedesco et al [146] took into account the transport of
 1181 water through the IEM. To do this, they used the Stefan-Maxwell equation [54]:

$$-\nabla \mu_i = RT \sum_j f_{i-j} (v_i - v_j), \quad (50)$$

1182 where f_{i-j} is the friction factor between ion i and phase j (which can be the water, the
 1183 membrane matrix, or another ion); v_i and v_j are velocities of i and j .

1184 The fluid flow through the membrane was considered as a function of osmotic and
 1185 hydrostatic pressure gradients, the fluid friction against the membrane matrix was taken
 1186 into account. It was shown that water transport through the membrane affects the de-
 1187 crease in the efficiency of the RED process, and its contribution to this decrease is com-
 1188 parable to the contribution of the coion flux through the membrane. The thickness of the
 1189 membrane (in the range from 20 to 100 μm) did not significantly affect the maximum

power density [269], which was about 1 W/m² for the system under study. A similar maximum power density was also obtained by La Cerva et al. [270]. These authors have also shown that membrane profiling allows increasing gross power density, but reduces net power density due to the loss in the solution pumping.

Davydov et al. [14] were the first to use the microheterogeneous model [153] (see Section 4.1) to estimate the power density of RED. This made it possible to take into account the electrical conductivity and diffusion permeability of the applied membranes over a wide range of concentrations. Despite the fact that the model used was relatively simple and did not take into account the channel geometry and solution flow parameters, the authors have achieved relatively good agreement between the calculated and experimental power density.

Fan et al [271] applied the Donnan-Manning theory [88] to describe ion sorption in the IEM during the RED process without fitting parameters. Diffusion coefficients were calculated using the Mackie and Meares model [272] taking into account the Manning condensation theory. Two tradeoffs are considered in the paper: higher seawater salinity reduces IEM selectivity, but membrane resistance also decreases; higher water sorption of IEM increases ion diffusivity in its volume, i.e. reduces resistance, but also reduces selectivity due to dilution of fixed charges. Jin et al [273] The authors also applied Donnan-Manning and Mackie and Meares theory, which made it possible to get rid of fitting parameters even in the 2D model, such as ion diffusivity in IEM, resistance and permselectivity coefficients.

There are also other works on modeling the RED process, however, the main attention there was paid to the influence of hydrodynamic conditions [274–280]. The membrane in these publications was considered as ideally selective [277,278], as an ohmic resistance [274–276,279,281] or its effect was taken into account through the boundary condition [280,282].

6. Conclusions

The review shows that although a relatively small number of governing equations are used in modelling of ion and water transport in charged membranes, the number of different models is quite large. Models of two main types differ by the general approach how to consider the membrane structure: as an integral quasi-homogeneous material (“diffusion-solution” models) or as a heterogeneous material consisting of an array of pores and hydrophobic domains containing these pores (“pore-flow” models). Further, in each approach there are numerous variations where certain simplifications and assumptions are applied, different effects are taken into account. There are rather general models, such as the Teorell-Meyer-Sievers model, and models tailored to describe a particular phenomenon that is important in describing a specific process. An example of models of the second kind are the semi-empirical models of Weber-Newman developed for describing ion and water transport in PEMs used in a fuel cell. This model takes into account the specific effect of current-induced water streaming flow on the ion (proton) mobility, while in other applications of IEMS this effect is not significant.

We believe that a consistent presentation of the basics of mathematical modeling of transport phenomena in charged membranes, as well as examples of specific mathematical descriptions will be useful both for beginners and experts in this field of knowledge.

Author Contributions: Writing—original draft preparation, S.M.; computations – A.G.; writing—review and editing – V.N., D.I. and D.A.; funding acquisition – D.I.

Funding: The authors acknowledge financial support from the Ministry of Science and Higher Education of the Russian Federation within State Contract 075-15-2022-1117 from June 30, 2022.

Conflicts of Interest: The authors declare no conflict of interest. The funders had no role in the design of the study; in the collection, analyses, or interpretation of data; in the writing of the manuscript, or in the decision to publish the results.

Nomenclature

Abbreviations

1242	AEM	anion-exchange membrane
1243	BCE	block copolymer electrolyte
1244	BPM	bipolar membranes
1245	CEM	cation-exchange membrane
1246	DBL	diffusion boundary layer
1247	ED	electrodialysis
1248	EDL	electrical double layer
1249	FC	fuel cell
1250	HER	hydrogen evolution reaction
1251	HOR	hydrogen oxidation reaction
1252	IEM	ion-exchange membrane
1253	LE	liquid equilibrated
1254	LEN	local electroneutrality
1255	NF	nanofiltration
1256	NPP	Nernst-Planck-Poisson
1257	OER	oxygen evolution reaction
1258	ORR	oxygen reduction reaction
1259	PEM	proton-exchange membrane
1260	PEMFC	proton exchange membrane fuel cells
1261	PTFE	polytetrafluorethylene
1262	RED	reverse electrodialysis
1263	RFB	redox flow batteries
1264	RO	reverse osmosis
1265	TMS	Teorell-Meyer-Sievers (model)
1266	VE	vapor equilibrated

Symbols

1268	a_i	activity of species i
1269	a_w	water vapor activity b distance between two neighboring functional groups
1270	c_i	molar concentration of species i
1271	c_s	molar salt concentration
1272	d	membrane thickness
1273	D	electrolyte diffusion coefficient
1274	D_i	diffusion coefficient of species i
1275	E	electric field intensity
1276	e	protonic charge
1277	F	Faraday's constant
1278	F	body force
1279	F_m	morphological factor
1280	f_1	gel phase volume fraction
1281	f_2	intergel electroneutral solution volume fraction
1282	f_{i-j}	friction factor between ion i and phase j
1283	g	gravitational acceleration
1284	g	activity factor
1285	h	channel width
1286	i_r	electric current density
1287	i_F	Faradaic current density
1288	j_i	flux density of species i
1289	J_{sub}	substance flux
1290	j_v	volumetric flux density
1291		

1292	k_B	Boltzmann constant
1293	K_D	Donnan equilibrium coefficient
1294	k_p	porous medium hydraulic permeability
1295	K_s	partition coefficient
1296	L	channel length
1297	L_{ij}	phenomenological conductivity coefficient
1298	L_p	hydraulic permeability coefficient
1299	M_{water}	water molar mass
1300	n_{ch}	charged monomer mole fraction
1301	n_{xl}	neutral crosslinker mole fraction
1302	P	diffusion permeability coefficient
1303	p	pressure
1304	p^m	membrane pore volume fraction
1305	$\overline{P_d}$	average power density,
1306	P_{sat}	saturation pressure of water
1307	\overline{Q}	concentration fixed ions
1308	q	space charge
1309	R	gas constant
1310	R_{cell}	area cell resistance
1311	R_i	generation rate of species i in a chemical reaction
1312	T	temperature
1313	t	time
1314	t_i	transport number of species i
1315	v_0	is the average flow rate
1316	\overline{v}	substance movement velocity
1317	V	volume
1318	\overline{V}	fluid flow velocity
1319	\overline{V}_i	partial molar volume
1320	w	membrane water content
1321	x_w	mole fraction of water in the gas
1322	z_i	charge number of species i
1323	z_Q	charge of functional group

Greek Symbols

1324		
1325	α	structural parameter depending on the position of the phases with respect to
1326		the transport axis
1327	β	electroosmotic permeability coefficient
1328	γ_i	activity coefficient of species i
1329	δ	diffusion layer thickness
1330	ε	relative permittivity
1331	ε_0	vacuum permittivity
1332	ε_p	polymer dielectric constant
1333	ε_w	water dielectric constant
1334	κ	electrical conductivity
1335	λ_B	Bjerrum length
1336	λ_{eq}	water content (in H ₂ O / SO ₃ ⁻)
1337	μ	dynamic viscosity
1338	μ_i	electrochemical potential of species i
1339	μ_i^0	standard electrochemical potential of species i
1340	ν	kinematic viscosity
1341	ν_{\pm}	stoichiometric number
1342	ξ	reduced linear charge density

1343	ξ_{crit}	critical reduced linear charge density
1344	π	osmotic pressure
1345	ρ	density
1346	ρ_e	volumetric charge density
1347	σ	Staverman reflection coefficient
1348	ϕ	electric potential
1349	φ_w	membrane water volume fraction
1350	Δ	difference in a quantity
1351	∇	gradient operator
1352	<i>Indices</i>	
1353	–	anion
1354	+	cation
1355	A	coion
1356	c	counterion
1357	g	superscript denoting that the quantity relates to the gel phase
1358	i	species
1359	s	superscript denoting that the quantity relates to the interstitial solution
1360	w	water

1361 References

- 1362 1. Werber, J.R.; Osuji, C.O.; Elimelech, M. Materials for next-generation desalination and water purification membranes. *Nat. Rev. Mater.* **2016**, *1*, 16018, doi:10.1038/natrevmats.2016.18.
- 1364 2. Mauter, M.S.; Zucker, I.; Perreault, F.; Werber, J.R.; Kim, J.-H.; Elimelech, M. The role of nanotechnology in tackling global water challenges. *Nat. Sustain.* **2018**, *1*, 166–175, doi:10.1038/s41893-018-0046-8.
- 1366 3. Al-Amshawee, S.; Yunus, M.Y.B.M.; Azoddein, A.A.M.; Hassell, D.G.; Dakhil, I.H.; Hasan, H.A. Electrodialysis desalination for water and wastewater: A review. *Chem. Eng. J.* **2020**, *380*, 122231, doi:10.1016/j.cej.2019.122231.
- 1368 4. Gurreri, L.; Tamburini, A.; Cipollina, A.; Micale, G. Electrodialysis Applications in Wastewater Treatment for Environmental Protection and Resources Recovery: A Systematic Review on Progress and Perspectives. *Membranes (Basel)*. **2020**, *10*, 146, doi:10.3390/membranes10070146.
- 1371 5. Alkhadra, M.A.; Su, X.; Suss, M.E.; Tian, H.; Guyes, E.N.; Shocron, A.N.; Conforti, K.M.; de Souza, J.P.; Kim, N.; Tedesco, M.; et al. Electrochemical Methods for Water Purification, Ion Separations, and Energy Conversion. *Chem. Rev.* **2022**, *122*, 13547–13635, doi:10.1021/acs.chemrev.1c00396.
- 1374 6. Apel, P.Y.; Bobreshova, O. V.; Volkov, A. V.; Volkov, V. V.; Nikonenko, V. V.; Stenina, I.A.; Filippov, A.N.; Yampolskii, Y.P.; Yaroslavtsev, A.B. Prospects of Membrane Science Development. *Membr. Membr. Technol.* **2019**, *1*, 45–63, doi:10.1134/S2517751619020021.
- 1377 7. Bazinet, L.; Geoffroy, T.R. Electrodialytic Processes: Market Overview, Membrane Phenomena, Recent Developments and Sustainable Strategies. *Membranes (Basel)*. **2020**, *10*, 221, doi:10.3390/membranes10090221.
- 1379 8. Du, L.; Prabhakaran, V.; Xie, X.; Park, S.; Wang, Y.; Shao, Y. Low-PGM and PGM-Free Catalysts for Proton Exchange Membrane Fuel Cells: Stability Challenges and Material Solutions. *Adv. Mater.* **2021**, *33*, 1908232, doi:10.1002/adma.201908232.
- 1382 9. Luo, T.; Abdu, S.; Wessling, M. Selectivity of ion exchange membranes: A review. *J. Memb. Sci.* **2018**, *555*, 429–454, doi:10.1016/j.memsci.2018.03.051.
- 1384 10. Falcão, D.S.; Pinto, A.M.F.R. A review on PEM electrolyzer modelling: Guidelines for beginners. *J. Clean. Prod.* **2020**, *261*, 121184, doi:10.1016/j.jclepro.2020.121184.
- 1386 11. Jiang, S.; Sun, H.; Wang, H.; Ladewig, B.P.; Yao, Z. A comprehensive review on the synthesis and applications of ion

- 1387 exchange membranes. *Chemosphere* **2021**, *282*, 130817, doi:10.1016/j.chemosphere.2021.130817.
- 1388 12. Xiong, P.; Zhang, L.; Chen, Y.; Peng, S.; Yu, G. A Chemistry and Microstructure Perspective on Ion-Conducting Membranes
1389 for Redox Flow Batteries. *Angew. Chemie Int. Ed.* **2021**, *60*, 24770–24798, doi:10.1002/anie.202105619.
- 1390 13. Logan, B.E.; Elimelech, M. Membrane-based processes for sustainable power generation using water. *Nature* **2012**, *488*,
1391 313–319, doi:10.1038/nature11477.
- 1392 14. Davydov, D.; Nosova, E.; Loza, S.; Achoh, A.; Korzhov, A.; Sharafan, M.; Melnikov, S. Use of the Microheterogeneous
1393 Model to Assess the Applicability of Ion-Exchange Membranes in the Process of Generating Electricity from a
1394 Concentration Gradient. *Membranes (Basel)*. **2021**, *11*, 406, doi:10.3390/membranes11060406.
- 1395 15. Veerman, J.; Saakes, M.; Metz, S.J.; Harmsen, G.J. Reverse electrodialysis: A validated process model for design and
1396 optimization. *Chem. Eng. J.* **2011**, *166*, 256–268, doi:10.1016/j.cej.2010.10.071.
- 1397 16. Tian, H.; Wang, Y.; Pei, Y.; Crittenden, J.C. Unique applications and improvements of reverse electrodialysis: A review and
1398 outlook. *Appl. Energy* **2020**, *262*, 114482, doi:10.1016/j.apenergy.2019.114482.
- 1399 17. Xu, A.; Shyy, W.; Zhao, T. Lattice Boltzmann modeling of transport phenomena in fuel cells and flow batteries. *Acta Mech.*
1400 *Sin.* **2017**, *33*, 555–574, doi:10.1007/s10409-017-0667-6.
- 1401 18. Vichard, L.; Steiner, N.Y.; Zerhouni, N.; Hissel, D. Hybrid fuel cell system degradation modeling methods: A
1402 comprehensive review. *J. Power Sources* **2021**, *506*, 230071, doi:10.1016/j.jpowsour.2021.230071.
- 1403 19. Ran, J.; Wu, L.; He, Y.; Yang, Z.; Wang, Y.; Jiang, C.; Ge, L.; Bakangura, E.; Xu, T. Ion exchange membranes: New
1404 developments and applications. *J. Memb. Sci.* **2017**, *522*, 267–291, doi:10.1016/j.memsci.2016.09.033.
- 1405 20. Mizutani, Y. Structure of ion exchange membranes. *J. Memb. Sci.* **1990**, *49*, 121–144, doi:10.1016/S0376-7388(00)80784-X.
- 1406 21. Sarapulova; Shkorkina; Mareev; Pismenskaya; Kononenko; Larchet; Dammak; Nikonenko Transport Characteristics of
1407 Fujifilm Ion-Exchange Membranes as Compared to Homogeneous Membranes AMX and CMX and to Heterogeneous
1408 Membranes MK-40 and MA-41. *Membranes (Basel)*. **2019**, *9*, 84, doi:10.3390/membranes9070084.
- 1409 22. Nikonenko, V. V.; Mareev, S.A.; Pis'menskaya, N.D.; Uzdenova, A.M.; Kovalenko, A. V.; Urtenov, M.K.; Pourcelly, G.
1410 Effect of electroconvection and its use in intensifying the mass transfer in electrodialysis (Review). *Russ. J. Electrochem.* **2017**,
1411 *53*, 1122–1144, doi:10.1134/S1023193517090099.
- 1412 23. Mani, A.; Wang, K.M. Electroconvection Near Electrochemical Interfaces: Experiments, Modeling, and Computation. *Annu.*
1413 *Rev. Fluid Mech.* **2020**, *52*, 509–529, doi:10.1146/annurev-fluid-010719-060358.
- 1414 24. Kreuer, K.-D.; Paddison, S.J.; Spohr, E.; Schuster, M. Transport in Proton Conductors for Fuel-Cell Applications:
1415 Simulations, Elementary Reactions, and Phenomenology. *Chem. Rev.* **2004**, *104*, 4637–4678, doi:10.1021/cr020715f.
- 1416 25. Giorno, L.; Drioli, E.; Strathmann, H. Permselectivity of Ion-Exchange Membranes. **2016**, 1490–1493,
1417 doi:10.1007/978-3-662-44324-8_1435.
- 1418 26. Zhang, Y.; Paepen, S.; Pinoy, L.; Meesschaert, B.; Van der Bruggen, B. Electrodialysis: Fractionation of divalent ions from
1419 monovalent ions in a novel electrodialysis stack. *Sep. Purif. Technol.* **2012**, *88*, 191–201, doi:10.1016/j.seppur.2011.12.017.
- 1420 27. Pärnamäe, R.; Mareev, S.; Nikonenko, V.; Melnikov, S.; Sheldeshov, N.; Zabolotskii, V.; Hamelers, H.V.M.; Tedesco, M.
1421 Bipolar membranes: A review on principles, latest developments, and applications. *J. Memb. Sci.* **2021**, *617*, 118538.
- 1422 28. Weber, A.Z.; Borup, R.L.; Darling, R.M.; Das, P.K.; Dursch, T.J.; Gu, W.; Harvey, D.; Kusoglu, A.; Litster, S.; Mench, M.M.;
1423 et al. A Critical Review of Modeling Transport Phenomena in Polymer-Electrolyte Fuel Cells. *J. Electrochem. Soc.* **2014**, *161*,
1424 F1254–F1299, doi:10.1149/2.0751412jes.
- 1425 29. van Rijn, P.; Tutus, M.; Kathrein, C.; Zhu, L.; Wessling, M.; Schwaneberg, U.; Böker, A. Challenges and advances in the
1426 field of self-assembled membranes. *Chem. Soc. Rev.* **2013**, *42*, 6578, doi:10.1039/c3cs60125k.
- 1427 30. Timashev, S.F. *Physical chemistry of membrane processes*; Ellis Horwood Ltd: New York, 1991; ISBN 9780136629825.
- 1428 31. Mauritz, K.A.; Moore, R.B. State of Understanding of Nafion. *Chem. Rev.* **2004**, *104*, 4535–4586, doi:10.1021/cr0207123.

- 1429 32. Gebel, G. Structural evolution of water swollen perfluorosulfonated ionomers from dry membrane to solution. *Polymer*
1430 (*Guldf.*) **2000**, *41*, 5829–5838, doi:10.1016/S0032-3861(99)00770-3.
- 1431 33. Helfferich, F.G. *Ion exchange*; McGraw-Hil.; Dover Publications: New York, 1995; Vol. 138; ISBN 0486687848.
- 1432 34. Drozdov, A.D.; deClaville Christiansen, J. The effects of pH and ionic strength on equilibrium swelling of polyampholyte
1433 gels. *Int. J. Solids Struct.* **2017**, *110–111*, 192–208, doi:10.1016/j.ijsolstr.2017.01.028.
- 1434 35. Kozmai, A.E.; Nikonenko, V.V.; Zyryanova, S.; Pismenskaya, N.D.; Dammak, L.; Baklouti, L. Modelling of anion-exchange
1435 membrane transport properties with taking into account the change in exchange capacity and swelling when varying
1436 bathing solution concentration and pH. *J. Memb. Sci.* **2019**, *590*, 117291, doi:10.1016/j.memsci.2019.117291.
- 1437 36. Zvaigzne, M.A.; Martynov, I.L.; Samokhvalov, P.S.; Nabiev, I.R. Fabrication of composite materials from semiconductor
1438 quantum dots and organic polymers for optoelectronics and biomedicine: role of surface ligands. *Russ. Chem. Bull.* **2016**, *65*,
1439 2568–2577, doi:10.1007/s11172-016-1620-8.
- 1440 37. Kreuer, K.D. On the development of proton conducting polymer membranes for hydrogen and methanol fuel cells. *J. Memb.*
1441 *Sci.* **2001**, *185*, 29–39, doi:10.1016/S0376-7388(00)00632-3.
- 1442 38. Berezina, N.P.; Kononenko, N.A.; Dyomina, O.A.; Gnusin, N.P. Characterization of ion-exchange membrane materials:
1443 Properties vs structure. *Adv. Colloid Interface Sci.* **2008**, *139*, 3–28, doi:10.1016/j.cis.2008.01.002.
- 1444 39. Kononenko, N.; Nikonenko, V.; Grande, D.; Larchet, C.; Dammak, L.; Fomenko, M.; Volkovich, Y. Porous structure of ion
1445 exchange membranes investigated by various techniques. *Adv. Colloid Interface Sci.* **2017**, *246*, 196–216,
1446 doi:10.1016/j.cis.2017.05.007.
- 1447 40. Svoboda, M.; Beneš, J.; Vobecká, L.; Slouka, Z. Swelling induced structural changes of a heterogeneous cation-exchange
1448 membrane analyzed by micro-computed tomography. *J. Memb. Sci.* **2017**, *525*, 195–201, doi:10.1016/j.memsci.2016.10.046.
- 1449 41. Donnan, F.G. The theory of membrane equilibrium and membrane potential in the presence of a non-dialyzable electrolyte.
1450 A contribution to physical-chemical physiology. *Zeitschrift für Elektrochemie und Angew. Phys. Chemie* **1911**, *17*, 572–581.
- 1451 42. Shiryaeva, I.M.; Victorov, A.I. Equilibrium of ion-exchange polymeric membrane with aqueous salt solution and its
1452 thermodynamic modeling. *Fluid Phase Equilib.* **2001**, *180*, 115–138, doi:10.1016/S0378-3812(00)00516-1.
- 1453 43. Paddison, S.J.; Bender, G.; Kreuer, K.D.; Nicoloso, N.; Zawodzinski, T.A. The microwave region of the dielectric spectrum
1454 of hydrated Nafion® and other sulfonated membranes. *J. New Mater. Electrochem. Syst.* **2000**, *3*, 291–300.
- 1455 44. Paddison, S.J.; Reagor, D.W.; Zawodzinski Jr, T.A. High frequency dielectric studies of hydrated Nafion®. *J. Electroanal.*
1456 *Chem.* **1998**, *459*, 91–97, doi:10.1016/S0022-0728(98)00321-0.
- 1457 45. Haubold, H.-G.; Vad, T.; Jungbluth, H.; Hiller, P. Nano structure of NAFION: a SAXS study. *Electrochim. Acta* **2001**, *46*,
1458 1559–1563, doi:10.1016/S0013-4686(00)00753-2.
- 1459 46. Kornyshev, A.A.; Kuznetsov, A.M.; Spohr, E.; Ulstrup, J. Kinetics of Proton Transport in Water. *J. Phys. Chem. B* **2003**, *107*,
1460 3351–3366, doi:10.1021/jp020857d.
- 1461 47. Nikonenko, V. V.; Yaroslavtsev, A.B.; Pourcelly, G. Ion Transfer in and Through Charged Membranes: Structure, Properties,
1462 and Theory. In *Ionic Interactions in Natural and Synthetic Macromolecules*; John Wiley & Sons, Inc.: Hoboken, NJ, USA, 2012;
1463 pp. 267–335 ISBN 9780470529270.
- 1464 48. Lu, Z. State of water in perfluorosulfonic acid membranes. **2005**, 67–68.
- 1465 49. Paddison, S.J. Proton Conduction Mechanisms at Low Degrees of Hydration in Sulfonic Acid-Based Polymer Electrolyte
1466 Membranes. *Annu. Rev. Mater. Res.* **2003**, *33*, 289–319, doi:10.1146/annurev.matsci.33.022702.155102.
- 1467 50. Zhou, X.; Wang, Z.; Epsztein, R.; Zhan, C.; Li, W.; Fortner, J.D.; Pham, T.A.; Kim, J.-H.; Elimelech, M. Intrapore energy
1468 barriers govern ion transport and selectivity of desalination membranes. *Sci. Adv.* **2020**, *6*, 1–10, doi:10.1126/sciadv.abd9045.
- 1469 51. Larchet, C.; Nouri, S.; Auclair, B.; Dammak, L.; Nikonenko, V. Application of chronopotentiometry to determine the
1470 thickness of diffusion layer adjacent to an ion-exchange membrane under natural convection. *Adv. Colloid Interface Sci.* **2008**,

- 1471 139, 45–61, doi:10.1016/j.cis.2008.01.007.
- 1472 52. Dickinson, E.J.F.; Smith, G. Modelling the Proton-Conductive Membrane in Practical Polymer Electrolyte Membrane Fuel
1473 Cell (PEMFC) Simulation: A Review. *Membranes (Basel)*. **2020**, *10*, 310, doi:10.3390/membranes10110310.
- 1474 53. Tanaka, Y. *Ion exchange membranes: fundamentals and applications*; Volume 12.; Elsevier Science: Amsterdam, The
1475 Netherlands, 2015; ISBN 9780444633194.
- 1476 54. Newman, J.S.; Balsara, N.P. *Electrochemical Systems*; 4th ed.; Wiley-Blackwell, 2021; ISBN 9781119514602.
- 1477 55. Nikonenko, V.; Nebavsky, A.; Mareev, S.; Kovalenko, A.; Urtenov, M.; Pourcelly, G.; Nikonenko, V.; Nebavsky, A.; Mareev,
1478 S.; Kovalenko, A.; et al. Modelling of ion transport in electromembrane systems: Impacts of membrane bulk and surface
1479 heterogeneity. *Appl. Sci.* **2018**, *9*, 25, doi:10.3390/app9010025.
- 1480 56. Soetaert, K.; Herman, P.M.J. *A practical guide to ecological modelling: Using R as a simulation platform*; Soetaert, K., Herman,
1481 P.M.J., Eds.; Springer Netherlands: Dordrecht, 2009; ISBN 9781402086236.
- 1482 57. Bear, J. Dynamics of Fluids in Porous Media (Dover Civil and Mechanical Engineering). *Publ. 1972 Repr. 1988 New York NY*
1483 *by Dover* **1972**, 784.
- 1484 58. Liu, J.-L. Poisson's equation in electrostatics. *Unpubl. Work* **2010**.
- 1485 59. Cohen, H.; Cooley, J.W. The Numerical Solution of the Time-Dependent Nernst-Planck Equations. *Biophys. J.* **1965**, *5*,
1486 145–162, doi:10.1016/S0006-3495(65)86707-8.
- 1487 60. Uzdanova, A.; Kovalenko, A.; Urtenov, M.; Nikonenko, V. 1D Mathematical Modelling of Non-Stationary Ion Transfer in
1488 the Diffusion Layer Adjacent to an Ion-Exchange Membrane in Galvanostatic Mode. *Membranes (Basel)*. **2018**, *8*, 84,
1489 doi:10.3390/membranes8030084.
- 1490 61. Moya, A.A. Electrochemical Impedance of Ion-Exchange Membranes in Ternary Solutions with Two Counterions. *J. Phys.*
1491 *Chem. C* **2014**, *118*, 2539–2553, doi:10.1021/jp4108238.
- 1492 62. Yaroshchuk, A.; Zhu, Y.; Bondarenko, M.; Bruening, M.L. Deviations from Electroneutrality in Membrane Barrier Layers: A
1493 Possible Mechanism Underlying High Salt Rejections. *Langmuir* **2016**, *32*, 2644–2658, doi:10.1021/acs.langmuir.5b04588.
- 1494 63. Kilic, M.S.; Bazant, M.Z.; Ajdari, A. Steric effects in the dynamics of electrolytes at large applied voltages. II. Modified
1495 Poisson-Nernst-Planck equations. *Phys. Rev. E* **2007**, *75*, 021503, doi:10.1103/PhysRevE.75.021503.
- 1496 64. Golubenko, D.V.; Yaroslavtsev, A.B. Effect of current density, concentration of ternary electrolyte and type of cations on the
1497 monovalent ion selectivity of surface-sulfonated graft anion-exchange membranes: modelling and experiment. *J. Memb. Sci.*
1498 **2021**, *635*, 119466, doi:10.1016/j.memsci.2021.119466.
- 1499 65. Gorobchenko, A.; Mareev, S.; Nikonenko, V. Mathematical Modeling of Monovalent Permselectivity of a Bilayer
1500 Ion-Exchange Membrane as a Function of Current Density. *Int. J. Mol. Sci.* **2022**, *23*, 4711, doi:10.3390/ijms23094711.
- 1501 66. Honarparvar, S.; Reible, D. Modeling multicomponent ion transport to investigate selective ion removal in electrodialysis.
1502 *Environ. Sci. Ecotechnology* **2020**, *1*, 100007, doi:10.1016/j.ese.2019.100007.
- 1503 67. Mareev, S.A.; Evdochenko, E.; Wessling, M.; Kozaderova, O.A.; Niftaliev, S.I.; Pismenskaya, N.D.; Nikonenko, V. V. A
1504 comprehensive mathematical model of water splitting in bipolar membranes: Impact of the spatial distribution of fixed
1505 charges and catalyst at bipolar junction. *J. Memb. Sci.* **2020**, *603*, 118010, doi:10.1016/j.memsci.2020.118010.
- 1506 68. Skolotneva, E.; Tsygurina, K.; Mareev, S.; Melnikova, E.; Pismenskaya, N.; Nikonenko, V. High Diffusion Permeability of
1507 Anion-Exchange Membranes for Ammonium Chloride: Experiment and Modeling. *Int. J. Mol. Sci.* **2022**, *23*, 5782,
1508 doi:10.3390/ijms23105782.
- 1509 69. Yaroshchuk, A.; Bruening, M.L.; Zholkovskiy, E. Modelling nanofiltration of electrolyte solutions. *Adv. Colloid Interface Sci.*
1510 **2019**, *268*, 39–63.
- 1511 70. Kedem, O.; Katchalsky, A. Permeability of composite membranes. Part 1.—Electric current, volume flow and flow of solute
1512 through membranes. *Trans. Faraday Soc.* **1963**, *59*, 1918–1930, doi:10.1039/TF9635901918.

- 1513 71. Meares, P. Coupling of ion and water fluxes in synthetic membranes*. *J. Memb. Sci.* **1981**, *8*, 295–307,
1514 doi:10.1016/S0376-7388(00)82317-0.
- 1515 72. Koter, S.; Kujawski, W.; Koter, I. Importance of the cross-effects in the transport through ion-exchange membranes. *J. Memb.*
1516 *Sci.* **2007**, *297*, 226–235, doi:10.1016/j.memsci.2007.03.047.
- 1517 73. Auclair, B.; Nikonenko, V.; Larchet, C.; Métayer, M.; Dammak, L. Correlation between transport parameters of
1518 ion-exchange membranes. *J. Memb. Sci.* **2002**, *195*, 89–102, doi:10.1016/S0376-7388(01)00556-7.
- 1519 74. Sarapulova, V.; Pismenskaya, N.; Butylskii, D.; Titorova, V.; Wang, Y.; Xu, T.; Zhang, Y.; Nikonenko, V. Transport and
1520 Electrochemical Characteristics of CJMCEd Homogeneous Cation Exchange Membranes in Sodium Chloride, Calcium
1521 Chloride, and Sodium Sulfate Solutions. *Membranes (Basel)*. **2020**, *10*, 165, doi:10.3390/membranes10080165.
- 1522 75. Rubinstein, I.; Schur, A.; Zaltzman, B. Artifact of “Breakthrough” osmosis: comment on the local
1523 Spiegler-Kedem-Katchalsky equations with constant coefficients. *Sci. Rep.* **2021**, *11*, 5051, doi:10.1038/s41598-021-83404-9.
- 1524 76. Jarzyńska, M.; Saryga, E.; Kluza, F.; Spiess, W.E.L.; Góral, D. Diffusion Characteristics in Ethyl Alcohol and Glucose
1525 Solutions Using Kedem-Katchalsky Equations. *Chem. Eng. Technol.* **2020**, *43*, 248–252, doi:10.1002/ceat.201900416.
- 1526 77. Kujawski, W.; Yaroshchuk, A.; Zholkovskiy, E.; Koter, I.; Koter, S. Analysis of Membrane Transport Equations for Reverse
1527 Electrodialysis (RED) Using Irreversible Thermodynamics. *Int. J. Mol. Sci.* **2020**, *21*, 6325, doi:10.3390/ijms21176325.
- 1528 78. Hidalgo, A.M.; León, G.; Gómez, M.; Murcia, M.D.; Gómez, E.; Macario, J.A. Removal of different dye solutions: A
1529 comparison study using a polyamide nf membrane. *Membranes (Basel)*. **2020**, *10*, 1–16, doi:10.3390/membranes10120408.
- 1530 79. De Jaegher, B.; De Schepper, W.; Verliefde, A.; Nopens, I. A model-based analysis of electrodialysis fouling during pulsed
1531 electric field operation. *J. Memb. Sci.* **2022**, *642*, 119975, doi:10.1016/j.memsci.2021.119975.
- 1532 80. Rybalkina, O.A.; Sharafan, M.V.; Nikonenko, V.V.; Pismenskaya, N.D. Two mechanisms of H⁺/OH⁻ ion generation in
1533 anion-exchange membrane systems with polybasic acid salt solutions. *J. Memb. Sci.* **2022**, *651*, 120449,
1534 doi:10.1016/j.memsci.2022.120449.
- 1535 81. Kimani, E.M.; Pranić, M.; Porada, S.; Kemperman, A.J.B.; Ryzhkov, I.I.; van der Meer, W.G.J.; Biesheuvel, P.M. The
1536 influence of feedwater pH on membrane charge ionization and ion rejection by reverse osmosis: An experimental and
1537 theoretical study. *J. Memb. Sci.* **2022**, *660*, 120800, doi:10.1016/j.memsci.2022.120800.
- 1538 82. Zhang, L.; Biesheuvel, P.M.; Ryzhkov, I.I. Theory of Ion and Water Transport in Electron-Conducting Membrane Pores
1539 with p H-Dependent Chemical Charge. *Phys. Rev. Appl.* **2019**, *12*, 014039, doi:10.1103/PhysRevApplied.12.014039.
- 1540 83. Chen, G. Donnan equilibrium revisited: Coupling between ion concentrations, osmotic pressure, and donnan potential. *J.*
1541 *Micromechanics Mol. Phys.* **2022**, *07*, 127–134, doi:10.1142/S2424913021420145.
- 1542 84. Robinson, R.A.; Stokes, R.H. *Electrolyte solutions. 2nd ed.*; Butterworths: London, UK, 2002; ISBN 0-486-42225-9.
- 1543 85. Miller, D.G. Application of Irreversible Thermodynamics to Electrolyte Solutions. I. Determination of Ionic Transport
1544 Coefficients l_{ij} for Isothermal Vector Transport Processes in Binary Electrolyte Systems 1,2. *J. Phys. Chem.* **1966**, *70*,
1545 2639–2659, doi:10.1021/j100880a033.
- 1546 86. Münchinger, A.; Kreuer, K.-D. Selective ion transport through hydrated cation and anion exchange membranes I. The effect
1547 of specific interactions. *J. Memb. Sci.* **2019**, *592*, 117372, doi:10.1016/j.memsci.2019.117372.
- 1548 87. Tran, T.; Lin, C.; Chaurasia, S.; Lin, H. Elucidating the relationship between states of water and ion transport properties in
1549 hydrated polymers. *J. Memb. Sci.* **2019**, *574*, 299–308, doi:10.1016/j.memsci.2018.12.059.
- 1550 88. Kamcev, J.; Galizia, M.; Benedetti, F.M.; Jang, E.-S.; Paul, D.R.; Freeman, B.D.; Manning, G.S. Partitioning of mobile ions
1551 between ion exchange polymers and aqueous salt solutions: importance of counter-ion condensation. *Phys. Chem. Chem.*
1552 *Phys.* **2016**, *18*, 6021–6031, doi:10.1039/C5CP06747B.
- 1553 89. Manning, G.S. Limiting Laws and Counterion Condensation in Polyelectrolyte Solutions I. Colligative Properties. *J. Chem.*
1554 *Phys.* **1969**, *51*, 924–933, doi:10.1063/1.1672157.

- 1555 90. Manning, G.S. Polyelectrolytes. *Annu. Rev. Phys. Chem.* **1972**, *23*, 117–140, doi:10.1146/annurev.pc.23.100172.001001.
- 1556 91. Bockris, J.O.; Reddy, A.K.N. *Modern Electrochemistry, 2nd Edition*; Springer, 1998; ISBN 0306455552.
- 1557 92. Kitto, D.; Kamcev, J. Manning condensation in ion exchange membranes: A review on ion partitioning and diffusion
1558 models. *J. Polym. Sci.* **2022**, *60*, 2929–2973, doi:10.1002/pol.20210810.
- 1559 93. Kamcev, J.; Paul, D.R.; Freeman, B.D. Ion Activity Coefficients in Ion Exchange Polymers: Applicability of Manning’s
1560 Counterion Condensation Theory. *Macromolecules* **2015**, *48*, 8011–8024, doi:10.1021/acs.macromol.5b01654.
- 1561 94. Jang, E.-S.; Kamcev, J.; Kobayashi, K.; Yan, N.; Sujanani, R.; Talley, S.J.; Moore, R.B.; Paul, D.R.; Freeman, B.D. Effect of
1562 Water Content on Sodium Chloride Sorption in Cross-Linked Cation Exchange Membranes. *Macromolecules* **2019**, *52*,
1563 2569–2579, doi:10.1021/acs.macromol.8b02550.
- 1564 95. Yu, Y.; Yan, N.; Freeman, B.D.; Chen, C. Mobile ion partitioning in ion exchange membranes immersed in saline solutions. *J.*
1565 *Memb. Sci.* **2021**, *620*, 118760, doi:10.1016/j.memsci.2020.118760.
- 1566 96. Yan, N.; Paul, D.R.; Freeman, B.D. Water and ion sorption in a series of cross-linked AMPS/PEGDA hydrogel membranes.
1567 *Polymer (Guildf)*. **2018**, *146*, 196–208, doi:10.1016/j.polymer.2018.05.021.
- 1568 97. Ji, Y.; Luo, H.; Geise, G.M. Specific co-ion sorption and diffusion properties influence membrane permselectivity. *J. Memb.*
1569 *Sci.* **2018**, *563*, 492–504, doi:10.1016/j.memsci.2018.06.010.
- 1570 98. Chang, K.; Luo, H.; Geise, G.M. Water content, relative permittivity, and ion sorption properties of polymers for membrane
1571 desalination. *J. Memb. Sci.* **2019**, *574*, 24–32, doi:10.1016/j.memsci.2018.12.048.
- 1572 99. Chang, K.; Luo, H.; Bannon, S.M.; Lin, S.Y.; Agata, W.-A.S.; Geise, G.M. Methoxy groups increase water and decrease salt
1573 permeability properties of sulfonated polysulfone desalination membranes. *J. Memb. Sci.* **2021**, *630*, 119298,
1574 doi:10.1016/j.memsci.2021.119298.
- 1575 100. Galizia, M.; Paul, D.R.; Freeman, B.D. Co-ion specific effect on sodium halides sorption and transport in a cross-linked
1576 poly(p-styrene sulfonate-co-divinylbenzene) for membrane applications. *J. Memb. Sci.* **2020**, *612*, 118410,
1577 doi:10.1016/j.memsci.2020.118410.
- 1578 101. Galizia, M.; Manning, G.S.; Paul, D.R.; Freeman, B.D. Ion partitioning between brines and ion exchange polymers. *Polymer*
1579 *(Guildf)*. **2019**, *165*, 91–100, doi:10.1016/j.polymer.2019.01.026.
- 1580 102. Chen, G.Q.; Wei, K.; Hassanvand, A.; Freeman, B.D.; Kentish, S.E. Single and binary ion sorption equilibria of monovalent
1581 and divalent ions in commercial ion exchange membranes. *Water Res.* **2020**, *175*, 115681, doi:10.1016/j.watres.2020.115681.
- 1582 103. Kingsbury, R.S.; Zhu, S.; Flotron, S.; Coronell, O. Microstructure Determines Water and Salt Permeation in Commercial
1583 Ion-Exchange Membranes. *ACS Appl. Mater. Interfaces* **2018**, *10*, 39745–39756, doi:10.1021/acsami.8b14494.
- 1584 104. Wang, Q.; Chen, G.Q.; Kentish, S.E. Sorption and diffusion of organic acid ions in anion exchange membranes: Acetate and
1585 lactate ions as a case study. *J. Memb. Sci.* **2020**, *614*, 118534, doi:10.1016/j.memsci.2020.118534.
- 1586 105. Kusoglu, A.; Weber, A.Z. New Insights into Perfluorinated Sulfonic-Acid Ionomers. *Chem. Rev.* **2017**, *117*, 987–1104,
1587 doi:10.1021/acs.chemrev.6b00159.
- 1588 106. Sujanani, R.; Katz, L.E.; Paul, D.R.; Freeman, B.D. Aqueous ion partitioning in Nafion: Applicability of Manning’s
1589 counter-ion condensation theory. *J. Memb. Sci.* **2021**, *638*, 119687, doi:10.1016/j.memsci.2021.119687.
- 1590 107. Ramos-Garcés, M. V.; Li, K.; Lei, Q.; Bhattacharya, D.; Kole, S.; Zhang, Q.; Strzalka, J.; Angelopoulou, P.P.; Sakellariou, G.;
1591 Kumar, R.; et al. Understanding the ionic activity and conductivity value differences between random copolymer
1592 electrolytes and block copolymer electrolytes of the same chemistry. *RSC Adv.* **2021**, *11*, 15078–15084,
1593 doi:10.1039/D1RA02519H.
- 1594 108. Lei, Q.; Li, K.; Bhattacharya, D.; Xiao, J.; Kole, S.; Zhang, Q.; Strzalka, J.; Lawrence, J.; Kumar, R.; Arges, C.G. Counterion
1595 condensation or lack of solvation? Understanding the activity of ions in thin film block copolymer electrolytes. *J. Mater.*
1596 *Chem. A* **2020**, *8*, 15962–15975, doi:10.1039/D0TA04266H.

- 1597 109. Ritt, C.L.; Werber, J.R.; Wang, M.; Yang, Z.; Zhao, Y.; Kulik, H.J.; Elimelech, M. Ionization behavior of nanoporous
1598 polyamide membranes. *Proc. Natl. Acad. Sci.* **2020**, *117*, 30191–30200, doi:10.1073/pnas.2008421117.
- 1599 110. Wang, J.; Kingsbury, R.S.; Perry, L.A.; Coronell, O. Partitioning of Alkali Metal Salts and Boric Acid from Aqueous Phase
1600 into the Polyamide Active Layers of Reverse Osmosis Membranes. *Environ. Sci. Technol.* **2017**, *51*, 2295–2303,
1601 doi:10.1021/acs.est.6b04323.
- 1602 111. Chang, K.; Luo, H.; Geise, G.M. Influence of Salt Concentration on Hydrated Polymer Relative Permittivity and State of
1603 Water Properties. *Macromolecules* **2021**, *54*, 637–646, doi:10.1021/acs.macromol.0c02188.
- 1604 112. Chang, K.; Geise, G.M. Dielectric Permittivity Properties of Hydrated Polymers: Measurement and Connection to Ion
1605 Transport Properties. *Ind. Eng. Chem. Res.* **2020**, *59*, 5205–5217.
- 1606 113. Baker, R.W. *Membrane Technology and Applications*; 3rd ed.; John Wiley and Sons Ltd, 2012; ISBN 9780470743720.
- 1607 114. Yaroshchuk, A.E.; Dukhin, S.S. Phenomenological theory of reverse osmosis in macroscopically homogeneous membranes
1608 and its specification for the capillary space-charge model. *J. Memb. Sci.* **1993**, *79*, 133–158, doi:10.1016/0376-7388(93)85113-B.
- 1609 115. Choy, T.C. *Effective Medium Theory: Principles and Applications*; Oxford University Press: Oxford, 2015; ISBN 0198518927.
- 1610 116. Teorell, T. An Attempt to Formulate a Quantitative Theory of Membrane Permeability. *Proc. Soc. Exp. Biol. Med.* **1935**, *33*,
1611 282–285, doi:10.3181/00379727-33-8339C.
- 1612 117. Meyer, K.H.; Sievers, J.F. La perméabilité des membranes I. Théorie de la perméabilité ionique. *Helv. Chim. Acta* **1936**, *19*,
1613 649–664, doi:10.1002/hlca.19360190199.
- 1614 118. Verbrugge, M.W.; Pintauro, P.N. Transport Models for Ion-Exchange Membranes. In: Springer, Boston, MA, 1989; pp. 1–67.
- 1615 119. Nikonenko, V.; Lebedev, K.; Manzanares, J.A.; Pourcelly, G. Modelling the transport of carbonic acid anions through
1616 anion-exchange membranes. *Electrochim. Acta* **2003**, *48*, 3639–3650, doi:10.1016/S0013-4686(03)00485-7.
- 1617 120. Titorova, V.D.; Mareev, S.A.; Gorobchenko, A.D.; Gil, V.V.; Nikonenko, V.V.; Sabbatovskii, K.G.; Pismenskaya, N.D. Effect
1618 of current-induced coion transfer on the shape of chronopotentiograms of cation-exchange membranes. *J. Memb. Sci.* **2021**,
1619 *624*, 119036, doi:10.1016/j.memsci.2020.119036.
- 1620 121. Rossi, M.; Wallmersperger, T. Thermodynamically consistent three-dimensional electrochemical model for polymeric
1621 membranes. *Electrochim. Acta* **2018**, *283*, 1323–1338, doi:10.1016/j.electacta.2018.06.174.
- 1622 122. Murphy, W.D.; Manzanares, J.A.; Mafe, S.; Reiss, H. A numerical study of the equilibrium and nonequilibrium diffuse
1623 double layer in electrochemical cells. *J. Phys. Chem.* **1992**, *96*, 9983–9991, doi:10.1021/j100203a074.
- 1624 123. Tanaka, Y. Chapter 4 Theory of Teorell, Meyer and Sievers (TMS Theory). *Membr. Sci. Technol.* **2007**, *12*, 59–66,
1625 doi:10.1016/S0927-5193(07)12004-0.
- 1626 124. Tanaka, Y. Ion Exchange Membranes, Volume 12 2nd Edition. In *Fundamentals and Applications*; Elsevier Science, 2015; p.
1627 522 ISBN 9780444633194.
- 1628 125. Wang, X.L.; Tsuru, T.; Nakao, S. ichi; Kimura, S. Electrolyte transport through nanofiltration membranes by the
1629 space-charge model and the comparison with Teorell-Meyer-Sievers model. *J. Memb. Sci.* **1995**, *103*, 117–133,
1630 doi:10.1016/0376-7388(94)00317-R.
- 1631 126. Galama, A.H.; Post, J.W.; Hamelers, H.V.M.; Nikonenko, V. V.; Biesheuvel, P.M. On the origin of the membrane potential
1632 arising across densely charged ion exchange membranes: How well does the teorell-meyer-sievers theory work? *J. Membr.*
1633 *Sci. Res.* **2016**, *2*, 128–140, doi:10.22079/jmsr.2016.20311.
- 1634 127. Yan, Z.; Zhu, L.; Li, Y.C.; Wycisk, R.J.; Pintauro, P.N.; Hickner, M.A.; Mallouk, T.E. The balance of electric field and
1635 interfacial catalysis in promoting water dissociation in bipolar membranes. *Energy Environ. Sci.* **2018**, *11*, 2235–2245,
1636 doi:10.1039/c8ee01192c.
- 1637 128. Vermaas, D.A.; Wiegman, S.; Nagaki, T.; Smith, W.A. Ion transport mechanisms in bipolar membranes for
1638 (photo)electrochemical water splitting. *Sustain. Energy Fuels* **2018**, *2*, 2006–2015, doi:10.1039/c8se00118a.

- 1639 129. Strathmann, H.; Krol, J.; Rapp, H.-J.; Eigenberger, G. Limiting current density and water dissociation in bipolar
1640 membranes. *J. Memb. Sci.* **1997**, *125*, 123–142, doi:10.1016/S0376-7388(96)00185-8.
- 1641 130. Wrubel, J.A.; Chen, Y.; Ma, Z.; Deutsch, T.G. Modeling Water Electrolysis in Bipolar Membranes. *J. Electrochem. Soc.* **2020**,
1642 *167*, 114502, doi:10.1149/1945-7111/ab9ccb.
- 1643 131. Culcasi, A.; Gurreri, L.; Zaffora, A.; Cosenza, A.; Tamburini, A.; Micale, G. On the modelling of an Acid / Base Flow Battery :
1644 An innovative electrical energy storage device based on pH and salinity gradients. *Appl. Energy* **2020**, *277*, 115576,
1645 doi:10.1016/j.apenergy.2020.115576.
- 1646 132. Ortega, A.; Arenas, L.F.; Pijpers, J.J.H.; Vicencio, D.L.; Martínez, J.C.; Rodríguez, F.A.; Rivero, E.P. Modelling water
1647 dissociation, acid-base neutralization and ion transport in bipolar membranes for acid-base flow batteries. *J. Memb. Sci.*
1648 **2022**, *641*, doi:10.1016/j.memsci.2021.119899.
- 1649 133. Yan, Z.; Wycisk, R.J.; Metlay, A.S.; Xiao, L.; Yoon, Y.; Pintauro, P.N.; Mallouk, T.E. High-Voltage Aqueous Redox Flow
1650 Batteries Enabled by Catalyzed Water Dissociation and Acid–Base Neutralization in Bipolar Membranes. *ACS Cent. Sci.*
1651 **2021**, *7*, 1028–1035, doi:10.1021/acscentsci.1c00217.
- 1652 134. Dykstra, J.E.; Heijne, A.; Puig, S.; Biesheuvel, P.M. Electrochimica Acta Theory of transport and recovery in microbial
1653 electrosynthesis of acetate from CO₂. *Electrochim. Acta* **2021**, *379*, 138029, doi:10.1016/j.electacta.2021.138029.
- 1654 135. Bui, J.C.; Corpus, K.R.M.; Bell, A.T.; Weber, A.Z. On the Nature of Field-Enhanced Water Dissociation in Bipolar
1655 Membranes. *J. Phys. Chem. C* **2021**, *125*, 24974–24987, doi:10.1021/acs.jpcc.1c08276.
- 1656 136. Lin, M. Sustainable Energy & Fuels interfacial junction profiles of bipolar membranes at solar flux relevant operating
1657 current densities †. **2021**, 2149–2158, doi:10.1039/d1se00201e.
- 1658 137. Hurwitz, H.D.; Dibiani, R. Experimental and theoretical investigations of steady and transient states in systems of ion
1659 exchange bipolar membranes. *J. Memb. Sci.* **2004**, *228*, 17–43, doi:10.1016/j.memsci.2003.09.009.
- 1660 138. León, T.; López, J.; Torres, R.; Grau, J.; Jofre, L.; Cortina, J.-L. Describing ion transport and water splitting in an
1661 electro dialysis stack with bipolar membranes by a 2-D model: Experimental validation. *J. Memb. Sci.* **2022**, *660*, 120835,
1662 doi:10.1016/j.memsci.2022.120835.
- 1663 139. Achoh, A.R.; Zabolotsky, V.I.; Lebedev, K.A.; Sharafan, M. V; Yaroslavtsev, A.B. Electrochemical Properties and Selectivity
1664 of Bilayer Ion-Exchange Membranes in Ternary Solutions of Strong Electrolytes. *Membr. Membr. Technol.* **2021**, *3*, 52–71,
1665 doi:10.1134/S2517751621010029.
- 1666 140. Zabolotsky, V.I.; Achoh, A.R.; Lebedev, K.A.; Melnikov, S.S. Permselectivity of bilayered ion-exchange membranes in
1667 ternary electrolyte. *J. Memb. Sci.* **2020**, *608*, 118152, doi:10.1016/j.memsci.2020.118152.
- 1668 141. Melnikova, E.D.; Pismenskaya, N.D.; Bazinet, L.; Mikhaylin, S.; Nikonenko, V.V. Effect of ampholyte nature on
1669 current-voltage characteristic of anion-exchange membrane. *Electrochim. Acta* **2018**, *285*, 185–191,
1670 doi:10.1016/j.electacta.2018.07.186.
- 1671 142. Sarapulova, V.; Nevakshenova, E.; Pismenskaya, N.; Dammak, L.; Nikonenko, V. Unusual concentration dependence of
1672 ion-exchange membrane conductivity in ampholyte-containing solutions: Effect of ampholyte nature. *J. Memb. Sci.* **2015**,
1673 *479*, 28–38, doi:10.1016/j.memsci.2015.01.015.
- 1674 143. Titorova, V.D.; Moroz, I.A.; Mareev, S.A.; Pismenskaya, N.D.; Sabbatovskii, K.G.; Wang, Y.; Xu, T.; Nikonenko, V.V. How
1675 bulk and surface properties of sulfonated cation-exchange membranes response to their exposure to electric current during
1676 electro dialysis of a Ca²⁺ containing solution. *J. Memb. Sci.* **2022**, *644*, 120149, doi:10.1016/j.memsci.2021.120149.
- 1677 144. Zhang, W.; Yan, H.; Wang, Q.; Zhao, C. An extended Teorell-Meyer-Sievers theory for membrane potential under
1678 non-isothermal conditions. *J. Memb. Sci.* **2022**, *643*, 120073, doi:10.1016/j.memsci.2021.120073.
- 1679 145. Tedesco, M.; Hamelers, H.V.M.V.M.; Biesheuvel, P.M.M. Nernst-Planck transport theory for (reverse) electro dialysis: I.
1680 Effect of co-ion transport through the membranes. *J. Memb. Sci.* **2016**, *510*, 370–381, doi:10.1016/j.memsci.2016.03.012.

- 1681 146. Tedesco, M.; Hamelers, H.V.M.; Biesheuvel, P.M. Nernst-Planck transport theory for (reverse) electro dialysis: II. Effect of
1682 water transport through ion-exchange membranes. *J. Memb. Sci.* **2017**, *531*, 172–182, doi:10.1016/j.memsci.2017.02.031.
- 1683 147. Gurreri, L.; Filingeri, A.; Ciofalo, M.; Cipollina, A.; Tedesco, M.; Tamburini, A.; Micale, G. Electro dialysis with
1684 asymmetric ally profiled membranes: Influence of profiles geometry on desalination performance and limiting current
1685 phenomena. *Desalination* **2021**, *506*, 115001, doi:10.1016/j.desal.2021.115001.
- 1686 148. Forrest, T.; Höfler, L.; Bakker, E. Dialysis membranes as liquid junction materials: Simplified model based on the phase
1687 boundary potential. *J. Electroanal. Chem.* **2022**, *904*, 115886, doi:10.1016/j.jelechem.2021.115886.
- 1688 149. Fíla, V.; Bouzek, K. *The effect of convection in the external diffusion layer on the results of a mathematical model of multiple ion*
1689 *transport across an ion-selective membrane*; Springer Netherlands, 2008; Vol. 38, pp. 1241–1252;.
- 1690 150. Fíla, V.; Bouzek, K. *A mathematical model of multiple ion transport across an ion-selective membrane under current load conditions*;
1691 Kluwer Academic Publishers, 2003; Vol. 33, pp. 675–684;.
- 1692 151. Sokirko, A. V.; Manzanara, J.A.; Pellicer, J. The Permselectivity of Membrane Systems with an Inhomogeneous
1693 Distribution of Fixed Charge Groups. *J. Colloid Interface Sci.* **1994**, *168*, 32–39, doi:10.1006/JCIS.1994.1390.
- 1694 152. Moya, A.A.; Moleón, J.A. Study of the electrical properties of bi-layer ion-exchange membrane systems. *J. Electroanal. Chem.*
1695 **2010**, *647*, 53–59, doi:10.1016/j.jelechem.2010.05.011.
- 1696 153. Zabolotsky, V.I.; Nikonenko, V.V. Effect of structural membrane inhomogeneity on transport properties. *J. Memb. Sci.* **1993**,
1697 *79*, 181–198, doi:10.1016/0376-7388(93)85115-D.
- 1698 154. Berezina, N.P.; Gnusin, N.P.; Demina, O.A.; Annikova, L.A. Effect of polyaniline on the current passing through structural
1699 fragments of ion-exchange sulfonic-cationite resins and membranes. *Russ. J. Electrochem.* **2009**, *45*, 1226–1233,
1700 doi:10.1134/S1023193509110020.
- 1701 155. Mafé, S.; Manzanara, J.A.; Pellicer, J. On the introduction of the pore wall charge in the space-charge model for
1702 microporous membranes. *J. Memb. Sci.* **1990**, *51*, 161–168, doi:10.1016/S0376-7388(00)80899-6.
- 1703 156. Hsu, W.Y.; Gierke, T.D. Ion transport and clustering in nafion perfluorinated membranes. *J. Memb. Sci.* **1983**, *13*, 307–326,
1704 doi:10.1016/S0376-7388(00)81563-X.
- 1705 157. Filippov, A.N. A Cell Model of an Ion-Exchange Membrane. Capillary-Osmosis and Reverse-Osmosis Coefficients. *Colloid J.*
1706 **2022**, *84*, 332–343, doi:10.1134/S1061933X2203005X.
- 1707 158. Dubinin, M.M. Surface and Porosity of Adsorbents. *Russ. Chem. Rev.* **1982**, *51*, 605–611,
1708 doi:10.1070/RC1982v051n07ABEH002876.
- 1709 159. Gnusin, N.P.; Zabolotsky, V.I.; Nikonenko, V. V.; Meshechkov, A.I. Development of the generalized conductance principle
1710 to the description of transfer phenomena in disperse systems under the acting of different forces. *Russ. J. Phys. Chem* **1980**,
1711 *54*, 1518–1522.
- 1712 160. Gnusin, N.P.; Berezina, N.P.; Kononenko, N.A.; Dyomina, O.A. Transport structural parameters to characterize ion
1713 exchange membranes. *J. Memb. Sci.* **2004**, *243*, 301–310, doi:10.1016/j.memsci.2004.06.033.
- 1714 161. Porozhnyy, M.; Huguet, P.; Cretin, M.; Safronova, E.; Nikonenko, V. Mathematical modeling of transport properties of
1715 proton-exchange membranes containing immobilized nanoparticles. *Int. J. Hydrogen Energy* **2016**, *41*, 15605–15614,
1716 doi:10.1016/j.ijhydene.2016.06.057.
- 1717 162. Nichka, V.S.; Mareev, S.A.; Porozhnyy, M. V.; Shkirskaya, S.A.; Safronova, E.Y.; Pismenskaya, N.D.; Nikonenko, V. V.
1718 Modified Microheterogeneous Model for Describing Electrical Conductivity of Membranes in Dilute Electrolyte Solutions.
1719 *Membr. Membr. Technol.* **2019**, *1*, 190–199, doi:10.1134/S2517751619030028.
- 1720 163. Kozmai, A.; Pismenskaya, N.; Nikonenko, V. Mathematical Description of the Increase in Selectivity of an Anion-Exchange
1721 Membrane Due to Its Modification with a Perfluorosulfonated Ionomer. *Int. J. Mol. Sci.* **2022**, *23*, 2238,
1722 doi:10.3390/IJMS23042238/S1.

- 1723 164. Manohar, M.; Thakur, A.K.; Pandey, R.P.; Shahi, V.K. Efficient and stable anion exchange membrane: Tuned membrane
1724 permeability and charge density for molecular/ionic separation. *J. Memb. Sci.* **2015**, *496*, 250–258,
1725 doi:10.1016/j.memsci.2015.08.051.
- 1726 165. Niftaliev, S.I.; Kozaderova, O.A.; Kim, K.B. Electroconductance of heterogeneous ion-exchange membranes in aqueous salt
1727 solutions. *J. Electroanal. Chem.* **2017**, *794*, 58–63, doi:10.1016/j.jelechem.2017.03.046.
- 1728 166. Sedkaoui, Y.; Szymczyk, A.; Lounici, H.; Arous, O. A new lateral method for characterizing the electrical conductivity of
1729 ion-exchange membranes. *J. Memb. Sci.* **2016**, *507*, 34–42, doi:10.1016/j.memsci.2016.02.003.
- 1730 167. Tong, X.; Zhang, B.; Fan, Y.; Chen, Y. Mechanism Exploration of Ion Transport in Nanocomposite Cation Exchange
1731 Membranes. *ACS Appl. Mater. Interfaces* **2017**, *9*, 13491–13499, doi:10.1021/acsami.7b01541.
- 1732 168. Kudashova, D.S.; Kononenko, N.A.; Brovkina, M.A.; Falina, I. V. A Study of the Degradation of a Perfluorinated Membrane
1733 during Operation in a Proton-Exchange Membrane Fuel Cell. *Membr. Membr. Technol.* **2022**, *4*, 23–30,
1734 doi:10.1134/S251775162201005X.
- 1735 169. Falina, I.; Loza, N.; Loza, S.; Titskaya, E.; Romanyuk, N. Permselectivity of Cation Exchange Membranes Modified by
1736 Polyaniline. *Membranes (Basel)*. **2021**, *11*, 227, doi:10.3390/membranes11030227.
- 1737 170. Zhang, B.; Gao, H.; Xiao, C.; Tong, X.; Chen, Y. The trade-off between membrane permselectivity and conductivity: A
1738 percolation simulation of mass transport. *J. Memb. Sci.* **2020**, *597*, 117751, doi:10.1016/j.memsci.2019.117751.
- 1739 171. Salmeron-Sanchez, I.; Asenjo-Pascual, J.; Avilés-Moreno, J.R.; Ocón, P. Microstructural description of ion exchange
1740 membranes: The effect of PPy-based modification. *J. Memb. Sci.* **2022**, *659*, 120771, doi:10.1016/j.memsci.2022.120771.
- 1741 172. Pismenskaya, N.D.; Nevakshenova, E.E.; Nikonenko, V. V. Using a Single Set of Structural and Kinetic Parameters of the
1742 Microheterogeneous Model to Describe the Sorption and Kinetic Properties of Ion-Exchange Membranes. *Pet. Chem.* **2018**,
1743 *58*, 465–473, doi:10.1134/S0965544118060087.
- 1744 173. Falina, I. V.; Kononenko, N.A.; Demina, O.A.; Titskaya, E. V.; Loza, S.A. Estimation of Ion-Exchange Equilibrium Constant
1745 Using Membrane Conductivity Data. *Colloid J.* **2021**, *83*, 379–386, doi:10.1134/S1061933X21030054.
- 1746 174. Golubenko, D.V.; Karavanova, Y.A.; Melnikov, S.S.; Achoh, A.R.; Pourcelly, G.; Yaroslavtsev, A.B. An approach to increase
1747 the permselectivity and mono-valent ion selectivity of cation-exchange membranes by introduction of amorphous
1748 zirconium phosphate nanoparticles. *J. Memb. Sci.* **2018**, *563*, 777–784, doi:10.1016/j.memsci.2018.06.024.
- 1749 175. Melnikov, S.; Kolot, D.; Nosova, E.; Zabolotskiy, V. Peculiarities of transport-structural parameters of ion-exchange
1750 membranes in solutions containing anions of carboxylic acids. *J. Memb. Sci.* **2018**, *557*, 1–12,
1751 doi:10.1016/j.memsci.2018.04.017.
- 1752 176. Le, X.T. Permselectivity and microstructure of anion exchange membranes. *J. Colloid Interface Sci.* **2008**, *325*, 215–222,
1753 doi:10.1016/j.jcis.2008.05.050.
- 1754 177. Kozmai, A.; Nikonenko, V.; Pismenskaya, N.; Dammak, L.; Baklouti, L.; Yutskevich, Y. Effect of anion exchange membrane
1755 capacity loss on pH and electric conductivity of saline solution during neutralization dialysis. *J. Memb. Sci.* **2020**, *595*,
1756 117573, doi:10.1016/j.memsci.2019.117573.
- 1757 178. Sarapulova, V. V.; Titorova, V.D.; Nikonenko, V. V.; Pismenskaya, N.D. Transport Characteristics of Homogeneous and
1758 Heterogeneous Ion-Exchange Membranes in Sodium Chloride, Calcium Chloride, and Sodium Sulfate Solutions. *Membr.*
1759 *Membr. Technol.* **2019**, *1*, 168–182, doi:10.1134/S2517751619030041.
- 1760 179. Perreault, V.; Sarapulova, V.; Tsygurina, K.; Pismenskaya, N.; Bazinet, L. Understanding of Adsorption and Desorption
1761 Mechanisms of Anthocyanins and Proanthocyanidins on Heterogeneous and Homogeneous Cation-Exchange Membranes.
1762 *Membranes (Basel)*. **2021**, *11*, 136, doi:10.3390/membranes11020136.
- 1763 180. Tuan, L.X.; Buess-Herman, C. Study of water content and microheterogeneity of CMS cation exchange membrane. *Chem.*
1764 *Phys. Lett.* **2007**, *434*, 49–55, doi:10.1016/j.cplett.2006.11.056.

- 1765 181. Zabolotsky, V.I.; Lebedev, K.A.; Nikonenko, V.V.; Shudrenko, A.A. Identification of a microheterogeneous model for a
1766 heterogeneous membrane. *Russ. J. Electrochem.* **1993**, *29*, 811–816.
- 1767 182. Wyllie, M.R.J.; Southwick, P.F. An Experimental Investigation of the S.P. and Resistivity Phenomena in Dirty Sands. *J. Pet.*
1768 *Technol.* **1954**, *6*, 44–57, doi:10.2118/302-g.
- 1769 183. Sauer, M.C.; Southwick, P.F.; Spiegler, K.S.; Wyllie, M.R.J. Electrical Conductance of Porous Plugs - Ion Exchange
1770 Resin-Solution Systems. *Ind. Eng. Chem.* **1955**, *47*, 2187–2193, doi:10.1021/ie50550a044.
- 1771 184. Spiegler, K.S.; Yoest, R.L.; Wyllie, M.R.J. Electrical potentials across porous plugs and membranes. Ion-exchange
1772 resin-solution systems. *Discuss. Faraday Soc.* **1956**, *21*, 174–185, doi:10.1039/DF9562100174.
- 1773 185. Nareńska, A.; Wódzki, R. Diffusion of electrolytes across inhomogeneous permselective membranes. *Die Angew. Makromol.*
1774 *Chemie* **1979**, *80*, 105–118, doi:10.1002/apmc.1979.050800107.
- 1775 186. Wódzki, R.; Nareńska, A. Composition and structure of cation permselective membranes II. Multilayer electrochemical
1776 model. *Die Angew. Makromol. Chemie* **1980**, *88*, 149–163, doi:10.1002/APMC.1980.050880112.
- 1777 187. Demina, O.A.; Kononenko, N.A.; Falina, I. V. New approach to the characterization of ion-exchange membranes using a set
1778 of model parameters. *Pet. Chem. 2014 547* **2014**, *54*, 515–525, doi:10.1134/S0965544114070032.
- 1779 188. Filippov, A.N.; Safronova, E.Y.; Yaroslavtsev, A.B. Theoretical and experimental investigation of diffusion permeability of
1780 hybrid MF-4SC membranes with silica nanoparticles. *J. Memb. Sci.* **2014**, *471*, 110–117, doi:10.1016/j.memsci.2014.08.008.
- 1781 189. Filippov, A.; Khanukaeva, D.; Afonin, D.; Skorikova, G.; Ivanov, E.; Vinokurov, V.; Lvov, Y. Transport Properties of Novel
1782 Hybrid Cation-Exchange Membranes on the Base of MF-4SC and Halloysite Nanotubes. *J. Mater. Sci. Chem. Eng.* **2015**, *03*,
1783 58–65, doi:10.4236/msce.2015.31009.
- 1784 190. Filippov, A.; Afonin, D.; Kononenko, N.; Lvov, Y.; Vinokurov, V. New approach to characterization of hybrid
1785 nanocomposites. *Colloids Surfaces A Physicochem. Eng. Asp.* **2017**, *521*, 251–259, doi:10.1016/j.colsurfa.2016.08.079.
- 1786 191. Happel, J.; Brenner, H. *Low Reynolds number hydrodynamics.*; 1973; ISBN 9789024728770.
- 1787 192. Deo, S.; Filippov, A.; Tiwari, A.; Vasin, S.; Starov, V. Hydrodynamic permeability of aggregates of porous particles with an
1788 impermeable core. *Adv. Colloid Interface Sci.* **2011**, *164*, 21–37, doi:10.1016/j.cis.2010.08.004.
- 1789 193. Filippov, A.N. A Cell Model of an Ion-Exchange Membrane. Hydrodynamic Permeability. *Colloid J.* **2018**, *80*, 716–727,
1790 doi:10.1134/S1061933X18060030.
- 1791 194. Vasin, S.I.; Filippov, A.N.; Starov, V.M. Hydrodynamic permeability of membranes built up by particles covered by porous
1792 shells: Cell models. *Adv. Colloid Interface Sci.* **2008**, *139*, 83–96, doi:10.1016/j.cis.2008.01.005.
- 1793 195. Filippov, A.N. A Cell Model of the Ion-Exchange Membrane. Electrical Conductivity and Electroosmotic Permeability.
1794 *Colloid J.* **2018**, *80*, 728–738, doi:10.1134/S1061933X18060042.
- 1795 196. Brinkman, H.C. A calculation of the viscous force exerted by a flowing fluid on a dense swarm of particles. *Flow, Turbul.*
1796 *Combust.* **1949**, *1*, 27, doi:10.1007/BF02120313.
- 1797 197. Filippov, A.N.; Shkirskaia, S.A. Approbation of the Cell Model of a Cation-Exchange Membrane on 1 : 1 Electrolytes.
1798 *Membr. Membr. Technol.* **2019**, *1*, 278–285, doi:10.1134/S2517751619050020.
- 1799 198. Filippov, A.N.; Kononenko, N.A.; Loza, N.V.; Kopitsyn, D.S.; Petrova, D.A. Modelling of transport properties of
1800 perfluorinated one- and bilayer membranes modified by polyaniline decorated clay nanotubes. *Electrochim. Acta* **2021**, *389*,
1801 138768, doi:10.1016/j.electacta.2021.138768.
- 1802 199. Yadav, P.K.; Tiwari, A.; Singh, P. Hydrodynamic permeability of a membrane built up by spheroidal particles covered by
1803 porous layer. *Acta Mech.* **2018**, *229*, 1869–1892, doi:10.1007/s00707-017-2054-6.
- 1804 200. Yadav, P.K.; Deo, S.; Singh, S.P.; Filippov, A. Effect of magnetic field on the hydrodynamic permeability of a membrane
1805 built up by porous spherical particles. *Colloid J.* **2017**, *79*, 160–171, doi:10.1134/S1061933X1606020X.
- 1806 201. Tang, C.; Yaroshchuk, A.; Bruening, M.L. Flow through negatively charged, nanoporous membranes separates Li+and

- 1807 K+ due to induced electromigration. *Chem. Commun.* **2020**, *56*, 10954–10957, doi:10.1039/d0cc03143g.
- 1808 202. Kislyi, A.G.; Butylskii, D.Y.; Mareev, S.A.; Nikonenko, V. V. Model of Competitive Ion Transfer in an
1809 Electro-Baromembrane System with Track-Etched Membrane. *Membr. Membr. Technol.* **2021**, *3*, 131–138,
1810 doi:10.1134/S2517751621020062.
- 1811 203. Wijmans, J.G.; Baker, R.W. The solution-diffusion model: a review. *J. Memb. Sci.* **1995**, *107*, 1–21.
- 1812 204. García-Morales, V.; Cervera, J.; Manzanares, J.A. Pore entrance effects on the electrical potential distribution in charged
1813 porous membranes and ion channels. *J. Electroanal. Chem.* **2007**, *599*, 203–208, doi:10.1016/j.jelechem.2005.12.025.
- 1814 205. Sparreboom, W.; van den Berg, A.; Eijkel, J.C.T. Principles and applications of nanofluidic transport. *Nat. Nanotechnol.* **2009**,
1815 *4*, 713–720, doi:10.1038/nnano.2009.332.
- 1816 206. Bazant, M.Z.; Squires, T.M. Induced-charge electrokinetic phenomena. *Curr. Opin. Colloid Interface Sci.* **2010**, *15*, 203–213,
1817 doi:10.1016/j.cocis.2010.01.003.
- 1818 207. Yaroshchuk, A.; Boiko, Y.; Makovetskiy, A. Ion-Rejection, Electrokinetic and Electrochemical Properties of a Nanoporous
1819 Track-Etched Membrane and Their Interpretation by Means of Space Charge Model. *Langmuir* **2009**, *25*, 9605–9614,
1820 doi:10.1021/la900737q.
- 1821 208. Szymczyk, A.; Zhu, H.; Balanec, B. Ion Rejection Properties of Nanopores with Bipolar Fixed Charge Distributions. *J. Phys.*
1822 *Chem. B* **2010**, *114*, 10143–10150, doi:10.1021/jp1025575.
- 1823 209. Peters, P.B.; van Roij, R.; Bazant, M.Z.; Biesheuvel, P.M. Analysis of electrolyte transport through charged nanopores. *Phys.*
1824 *Rev. E* **2016**, *93*, 053108, doi:10.1103/PhysRevE.93.053108.
- 1825 210. Moya, A.A.; Nikonenko, V.V. A COMPARATIVE THEORETICAL STUDY OF POTENTIAL DISTRIBUTION AND
1826 CONDUCTIVITY IN CATION- AND ANION-EXCHANGE NANOPOROUS MEMBRANES FILLED WITH TERNARY
1827 ELECTROLYTES. *Electrochim. Acta* **2015**, *180*, 929–938, doi:10.1016/j.electacta.2015.09.025.
- 1828 211. Ryzhkov, I.I.; Lebedev, D.V.; Solodovnichenko, V.S.; Shiverskiy, A.V.; Simunin, M.M. Induced-Charge Enhancement of the
1829 Diffusion Potential in Membranes with Polarizable Nanopores. *Phys. Rev. Lett.* **2017**, *119*, 226001,
1830 doi:10.1103/PhysRevLett.119.226001.
- 1831 212. Catalano, J.; Hamelers, H.V.M.; Bonten, A.; Biesheuvel, P.M. Revisiting Morrison and Osterle 1965: The efficiency of
1832 membrane-based electrokinetic energy conversion. *J. Phys. Condens. Matter* **2016**, *28*, 324001,
1833 doi:10.1088/0953-8984/28/32/324001.
- 1834 213. Szymczyk, A.; Zhu, H.; Balanec, B. Pressure-Driven Ionic Transport through Nanochannels with Inhomogeneous Charge
1835 Distributions. *Langmuir* **2010**, *26*, 1214–1220, doi:10.1021/la902355x.
- 1836 214. Balanec, B.; Ghoufi, A.; Szymczyk, A. Nanofiltration performance of conical and hourglass nanopores. *J. Memb. Sci.* **2018**,
1837 *552*, 336–340, doi:10.1016/j.memsci.2018.02.026.
- 1838 215. Chen, Y.-T.; Hsu, J.-P. Pressure-driven power generation and ion separation using a non-uniformly charged nanopore. *J.*
1839 *Colloid Interface Sci.* **2022**, *607*, 1120–1130, doi:10.1016/j.jcis.2021.09.055.
- 1840 216. Liu, Z.; Liu, X.; Wang, Y.; Yang, D.; Li, C. Ion current rectification in asymmetric charged bilayer nanochannels. *Electrochim.*
1841 *Acta* **2022**, *403*, 139706, doi:10.1016/j.electacta.2021.139706.
- 1842 217. Wu, C.-T.; Hsu, J.-P. Electrokinetic behavior of bullet-shaped nanopores modified by functional groups: Influence of finite
1843 thickness of modified layer. *J. Colloid Interface Sci.* **2021**, *582*, 741–751, doi:10.1016/j.jcis.2020.08.022.
- 1844 218. Han, W.; Chen, X. A review: applications of ion transport in micro-nanofluidic systems based on ion concentration
1845 polarization. *J. Chem. Technol. Biotechnol.* **2020**, *95*, 1622–1631, doi:10.1002/jctb.6288.
- 1846 219. Hsu, J.-P.; Su, T.-C.; Lin, C.-Y.; Tseng, S. Power generation from a pH-regulated nanochannel through reverse
1847 electrodialysis: Effects of nanochannel shape and non-uniform H⁺ distribution. *Electrochim. Acta* **2019**, *294*, 84–92,
1848 doi:10.1016/j.electacta.2018.10.074.

- 1849 220. Ryzhkov, I.I.; Lebedev, D. V.; Solodovnichenko, V.S.; Minakov, A. V.; Simunin, M.M. On the origin of membrane potential
1850 in membranes with polarizable nanopores. *J. Memb. Sci.* **2018**, *549*, 616–630, doi:10.1016/j.memsci.2017.11.073.
- 1851 221. Ryzhkov, I.I.; Minakov, A. V. Theoretical study of electrolyte transport in nanofiltration membranes with constant surface
1852 potential/charge density. *J. Memb. Sci.* **2016**, *520*, 515–628, doi:10.1016/j.memsci.2016.08.004.
- 1853 222. Ryzhkov, I.I.; Shchurkina, M.A.; Mikhлина, E. V.; Simunin, M.M.; Nemtsev, I. V. Switchable ionic selectivity of membranes
1854 with electrically conductive surface: Theory and experiment. *Electrochim. Acta* **2021**, *375*, doi:10.1016/j.electacta.2021.137970.
- 1855 223. Ryzhkov, I.I.; Vyatkin, A.S.; Mikhлина, E. V. Modelling of Conductive Nanoporous Membranes with Switchable Ionic
1856 Selectivity. *Membr. Membr. Technol.* **2020**, *2*, 10–19, doi:10.1134/S2517751620010072.
- 1857 224. Bocquet, L.; Charlaix, E. Nanofluidics, from bulk to interfaces. *Chem. Soc. Rev.* **2010**, *39*, 1073–1095, doi:10.1039/b909366b.
- 1858 225. Guzmán-García, A.G.; Pintauro, P.N.; Verbrugge, M.W.; Hill, R.F. Development of a space-charge transport model for
1859 ion-exchange membranes. *AIChE J.* **1990**, *36*, 1061–1074, doi:10.1002/aic.690360713.
- 1860 226. Eikerling, M.; Kornyshev, A.A. Proton transfer in a single pore of a polymer electrolyte membrane. *J. Electroanal. Chem.*
1861 **2001**, *502*, 1–14, doi:10.1016/S0022-0728(00)00368-5.
- 1862 227. Biesheuvel, P.M.; Bazant, M.Z. Analysis of ionic conductance of carbon nanotubes. *Phys. Rev. E* **2016**, *94*, 050601,
1863 doi:10.1103/PhysRevE.94.050601.
- 1864 228. Zangle, T.A.; Mani, A.; Santiago, J.G. Theory and experiments of concentration polarization and ion focusing at
1865 microchannel and nanochannel interfaces. *Chem. Soc. Rev.* **2010**, *39*, 1014, doi:10.1039/b902074h.
- 1866 229. Melnikov, D. V.; Hulings, Z.K.; Gracheva, M.E. Electro-osmotic flow through nanopores in thin and ultrathin membranes.
1867 *Phys. Rev. E* **2017**, *95*, 1–8, doi:10.1103/PhysRevE.95.063105.
- 1868 230. Mansouri, A.; Scheuerman, C.; Bhattacharjee, S.; Kwok, D.Y.; Kostiuk, L.W. Transient streaming potential in a finite length
1869 microchannel. *J. Colloid Interface Sci.* **2005**, *292*, 567–580, doi:10.1016/j.jcis.2005.05.094.
- 1870 231. Yang, Y.; Pintauro, P.N. Multicomponent space-charge transport model for ion-exchange membranes. *AIChE J.* **2000**, *46*,
1871 1177–1190, doi:10.1002/aic.690460610.
- 1872 232. Hörtzel, A.; Tallarek, U. Ionic conductance of nanopores in microscale analysis systems: Where microfluidics meets
1873 nanofluidics. *J. Sep. Sci.* **2007**, *30*, 1398–1419, doi:10.1002/jssc.200600427.
- 1874 233. Schoch, R.B.; Han, J.; Renaud, P. Transport phenomena in nanofluidics. *Rev. Mod. Phys.* **2008**, *80*, 839–883,
1875 doi:10.1103/RevModPhys.80.839.
- 1876 234. Bazant, M.Z.; Kilic, M.S.; Storey, B.D.; Ajdari, A. Towards an understanding of induced-charge electrokinetics at large
1877 applied voltages in concentrated solutions. *Adv. Colloid Interface Sci.* **2009**, *152*, 48–88, doi:10.1016/j.cis.2009.10.001.
- 1878 235. Cwirko, E.H.; Carbonell, R.G. Interpretation of transport coefficients in Nafion using a parallel pore model. *J. Memb. Sci.*
1879 **1992**, *67*, 227–247, doi:10.1016/0376-7388(92)80027-H.
- 1880 236. Szymczyk, A.; Fievet, P.; Aoubiza, B.; Simon, C.; Pagetti, J. An application of the space charge model to the electrolyte
1881 conductivity inside a charged microporous membrane. *J. Memb. Sci.* **1999**, *161*, 275–285, doi:10.1016/S0376-7388(99)00118-0.
- 1882 237. Narębska, A.; Koter, S.; Kujawski, W. Ions and water transport across charged nafion membranes. Irreversible
1883 thermodynamics approach. *Desalination* **1984**, *51*, 3–17, doi:10.1111/j.1467-9353.2006.00281.x.
- 1884 238. Zhu, Z.; Wang, D.; Tian, Y.; Jiang, L. Ion/Molecule Transportation in Nanopores and Nanochannels: From Critical
1885 Principles to Diverse Functions. *J. Am. Chem. Soc.* **2019**, *141*, 8658–8669.
- 1886 239. Kurupath, V.P.; Kannam, S.K.; Hartkamp, R.; Sathian, S.P. Highly efficient water desalination through hourglass shaped
1887 carbon nanopores. *Desalination* **2021**, *505*, 114978, doi:10.1016/j.desal.2021.114978.
- 1888 240. Chen, Y.; Liu, Y.; Xu, Y.; Guo, X.; Cao, Y.; Ming, W. Review: Modeling and Simulation of Membrane Electrode Material
1889 Structure for Proton Exchange Membrane Fuel Cells. *Coatings* **2022**, *12*, 1145, doi:10.3390/coatings12081145.
- 1890 241. Zhao, J.; Li, X.; Shum, C.; McPhee, J. A Review of physics-based and data-driven models for real-time control of polymer

- 1891 electrolyte membrane fuel cells. *Energy AI* **2021**, *6*, 100114, doi:10.1016/j.egyai.2021.100114.
- 1892 242. Zhang, G.; Jiao, K. Multi-phase models for water and thermal management of proton exchange membrane fuel cell: A
1893 review. *J. Power Sources* **2018**, *391*, 120–133, doi:10.1016/j.jpowsour.2018.04.071.
- 1894 243. Olivier, P.; Bourasseau, C.; Bouamama, P.B. Low-temperature electrolysis system modelling: A review. *Renew. Sustain.*
1895 *Energy Rev.* **2017**, *78*, 280–300, doi:10.1016/j.rser.2017.03.099.
- 1896 244. Jahnke, T.; Futter, G.; Latz, A.; Malkow, T.; Papakonstantinou, G.; Tsotridis, G.; Schott, P.; Gérard, M.; Quinaud, M.;
1897 Quiroga, M.; et al. Performance and degradation of Proton Exchange Membrane Fuel Cells: State of the art in modeling
1898 from atomistic to system scale. *J. Power Sources* **2016**, *304*, 207–233, doi:10.1016/j.jpowsour.2015.11.041.
- 1899 245. Chen, Q.; Wang, Y.; Yang, F.; Xu, H. Two-dimensional multi-physics modeling of porous transport layer in polymer
1900 electrolyte membrane electrolyzer for water splitting. *Int. J. Hydrogen Energy* **2020**, *45*, 32984–32994,
1901 doi:10.1016/j.ijhydene.2020.09.148.
- 1902 246. Manso, A.P.; Marzo, F.F.; Barranco, J.; Garikano, X.; Garmendia Mujika, M. Influence of geometric parameters of the flow
1903 fields on the performance of a PEM fuel cell. A review. *Int. J. Hydrogen Energy* **2012**, *37*, 15256–15287,
1904 doi:10.1016/j.ijhydene.2012.07.076.
- 1905 247. Yang, Z.; Du, Q.; Jia, Z.; Yang, C.; Jiao, K. Effects of operating conditions on water and heat management by a transient
1906 multi-dimensional PEMFC system model. *Energy* **2019**, *183*, 462–476, doi:10.1016/j.energy.2019.06.148.
- 1907 248. Zhang, G.; Xie, X.; Xie, B.; Du, Q.; Jiao, K. Large-scale multi-phase simulation of proton exchange membrane fuel cell. *Int. J.*
1908 *Heat Mass Transf.* **2019**, *130*, 555–563, doi:10.1016/j.ijheatmasstransfer.2018.10.122.
- 1909 249. Zhang, H.; Rahman, M.A.; Mojica, F.; Sui, P.; Chuang, P.A. A comprehensive two-phase proton exchange membrane fuel
1910 cell model coupled with anisotropic properties and mechanical deformation of the gas diffusion layer. *Electrochim. Acta*
1911 **2021**, *382*, 138273, doi:10.1016/j.electacta.2021.138273.
- 1912 250. Zhao, J.; Li, X. Oxygen transport in polymer electrolyte membrane fuel cells based on measured electrode pore structure
1913 and mass transport properties. *Energy Convers. Manag.* **2019**, *186*, 570–585, doi:10.1016/j.enconman.2019.02.042.
- 1914 251. Yin, C.; Gao, Y.; Li, T.; Xie, G.; Li, K.; Tang, H. Study of internal multi-parameter distributions of proton exchange
1915 membrane fuel cell with segmented cell device and coupled three-dimensional model. *Renew. Energy* **2020**, *147*, 650–662,
1916 doi:10.1016/j.renene.2019.09.026.
- 1917 252. Yin, Y.; Wang, X.; Shanguan, X.; Zhang, J.; Qin, Y. Numerical investigation on the characteristics of mass transport and
1918 performance of PEMFC with baffle plates installed in the flow channel. *Int. J. Hydrogen Energy* **2018**, *43*, 8048–8062,
1919 doi:10.1016/j.ijhydene.2018.03.037.
- 1920 253. Tsukamoto, T.; Aoki, T.; Kanesaka, H.; Taniguchi, T.; Takayama, T.; Motegi, H.; Takayama, R.; Tanaka, S.; Komiyama, K.;
1921 Yoneda, M. Three-dimensional numerical simulation of full-scale proton exchange membrane fuel cells at high current
1922 densities. *J. Power Sources* **2021**, *488*, 229412, doi:10.1016/j.jpowsour.2020.229412.
- 1923 254. Schiffer, L.; Shirsath, A.V.; Raël, S.; Bonnet, C.; Lopicque, F.; Bessler, W.G. Electrochemical Pressure Impedance
1924 Spectroscopy for Polymer Electrolyte Membrane Fuel Cells: A Combined Modeling and Experimental Analysis. *J.*
1925 *Electrochem. Soc.* **2022**, *169*, 034503, doi:10.1149/1945-7111/ac55cd.
- 1926 255. Bagherighajari, F.; Ramiar, A.; Abdollahzadehsangroudi, M.; Páscoa, J.C.; Oliveira, P.J. Numerical simulation of the
1927 polymer electrolyte membrane fuel cells with intermediate blocked interdigitated flow fields. *Int. J. Energy Res.* **2022**, *46*,
1928 15309–15331, doi:10.1002/er.8233.
- 1929 256. Springer, T.E.; Zawodzinski, T.A.; Gottesfeld, S. Polymer Electrolyte Fuel Cell Model. *J. Electrochem. Soc.* **1991**, *138*,
1930 2334–2342, doi:10.1149/1.2085971.
- 1931 257. Weber, A.Z.; Newman, J. Transport in Polymer-Electrolyte Membranes. *J. Electrochem. Soc.* **2004**, *151*, A311,
1932 doi:10.1149/1.1639157.

- 1933 258. Zawodzinski, T.A.; Neeman, M.; Sillerud, L.O.; Gottesfeld, S. Determination of water diffusion coefficients in
1934 perfluorosulfonate ionomeric membranes. *J. Phys. Chem.* **1991**, *95*, 6040–6044, doi:10.1021/j100168a060.
- 1935 259. Barnoon, P.; Toghraie, D.; Mehmandoust, B.; Fazilati, M.A.; Eftekhari, S.A. Numerical modeling of species transport and
1936 functional characteristics of a proton exchange membrane fuel cell using an agglomerate model with a multi-phase model.
1937 *Energy Reports* **2022**, *8*, 11343–11362, doi:10.1016/j.egyr.2022.08.238.
- 1938 260. Tian, P.; Liu, X.; Luo, K.; Li, H.; Wang, Y. Deep learning from three-dimensional multiphysics simulation in operational
1939 optimization and control of polymer electrolyte membrane fuel cell for maximum power. *Appl. Energy* **2021**, *288*, 116632,
1940 doi:10.1016/j.apenergy.2021.116632.
- 1941 261. Ortiz-Imedio, R.; Gomez-Coma, L.; Fallanza, M.; Ortiz, A.; Ibañez, R.; Ortiz, I. Comparative performance of Salinity
1942 Gradient Power-Reverse Electrodialysis under different operating conditions. *Desalination* **2019**, *457*, 8–21,
1943 doi:10.1016/j.desal.2019.01.005.
- 1944 262. Tristán, C.; Pérez, G.; Fallanza, M.; Ortiz, A.; Ibañez, R.; Ortiz, I. A comprehensive study on the effects of operation
1945 variables on reverse electrodialysis performance. *Desalination* **2020**, *482*, 114389, doi:10.1016/j.desal.2020.114389.
- 1946 263. Tedesco, M.; Cipollina, A.; Tamburini, A.; van Baak, W.; Micale, G. Modelling the Reverse ElectroDialysis process with
1947 seawater and concentrated brines. *Desalin. Water Treat.* **2012**, *49*, 404–424, doi:10.1080/19443994.2012.699355.
- 1948 264. Gurreri, L.; Battaglia, G.; Tamburini, A.; Cipollina, A.; Micale, G.; Ciofalo, M. Multi-physical modelling of reverse
1949 electrodialysis. *Desalination* **2017**, *423*, 52–64, doi:10.1016/j.desal.2017.09.006.
- 1950 265. Moya, A.A. Numerical simulation of ionic transport processes through bilayer ion-exchange membranes in reverse
1951 electrodialysis stacks. *J. Memb. Sci.* **2017**, *524*, 400–408, doi:10.1016/j.memsci.2016.11.051.
- 1952 266. Moya, A.A. A Nernst-Planck analysis on the contributions of the ionic transport in permeable ion-exchange membranes to
1953 the open circuit voltage and the membrane resistance in reverse electrodialysis stacks. *Electrochim. Acta* **2017**, *238*, 134–141,
1954 doi:10.1016/j.electacta.2017.04.022.
- 1955 267. Moya, A.A. Uphill transport in improved reverse electrodialysis by removal of divalent cations in the dilute solution: A
1956 Nernst-Planck based study. *J. Memb. Sci.* **2020**, *598*, 117784, doi:10.1016/j.memsci.2019.117784.
- 1957 268. Leveque, M.A. Transmission de chaleur par convection. *Les lois la Transm.* **1928**, *13*, 204.
- 1958 269. Tedesco, M.; Hamelers, H.V.M.; Biesheuvel, P.M. Nernst-Planck transport theory for (reverse) electrodialysis: III. Optimal
1959 membrane thickness for enhanced process performance. *J. Memb. Sci.* **2018**, *565*, 480–487, doi:10.1016/j.memsci.2018.07.090.
- 1960 270. La Cerva, M.L.; Liberto, M. Di; Gurreri, L.; Tamburini, A.; Cipollina, A.; Micale, G.; Ciofalo, M. Coupling CFD with a
1961 one-dimensional model to predict the performance of reverse electrodialysis stacks. *J. Memb. Sci.* **2017**, *541*, 595–610,
1962 doi:10.1016/j.memsci.2017.07.030.
- 1963 271. Fan, H.; Yin, N. Elucidating conductivity-permselectivity tradeoffs in electrodialysis and reverse electrodialysis by
1964 structure-property analysis of ion-exchange membranes. *J. Memb. Sci.* **2019**, *573*, 668–681, doi:10.1016/j.memsci.2018.11.045.
- 1965 272. Mackie, J.S.; Meares, P. The diffusion of electrolytes in a cation-exchange resin membrane I. Theoretical. *Proc. R. Soc. London.*
1966 *Ser. A. Math. Phys. Sci.* **1955**, *232*, 498–509, doi:10.1098/rspa.1955.0234.
- 1967 273. Jin, D.; Xi, R.; Xu, S.; Wang, P.; Wu, X. Numerical simulation of salinity gradient power generation using reverse
1968 electrodialysis. *Desalination* **2021**, *512*, 115132, doi:10.1016/j.desal.2021.115132.
- 1969 274. Tedesco, M.; Mazzola, P.; Tamburini, A.; Micale, G.; Bogle, I.D.L.; Papapetrou, M.; Cipollina, A. Analysis and simulation of
1970 scale-up potentials in reverse electrodialysis. *Desalin. Water Treat.* **2015**, *55*, 3391–3403, doi:10.1080/19443994.2014.947781.
- 1971 275. Chen, M.; Mei, Y.; Yu, Y.; Zeng, R.J.; Zhang, F.; Zhou, S.; Tang, C.Y. An internal-integrated RED/ED system for
1972 energy-saving seawater desalination: A model study. *Energy* **2019**, *170*, 139–148, doi:10.1016/j.energy.2018.12.111.
- 1973 276. Saleem, M.W.; Jande, Y.A.C.; Kim, W.S. Performance optimization of integrated electrochemical capacitive deionization
1974 and reverse electrodialysis model through a series pass desorption process. *J. Electroanal. Chem.* **2017**, *795*, 41–50,

- 1975 doi:10.1016/j.jelechem.2017.04.025.
- 1976 277. Kim, M.; Kim, S.; Choi, J.; Kim, H.; Jeong, N.; Kwak, R. Numerical analysis of real-scale reverse electro dialysis with
1977 microscale structures and electrode segmentation. *Chem. Eng. J.* **2022**, *446*, 137357, doi:10.1016/j.cej.2022.137357.
- 1978 278. Pawlowski, S.; Geraldès, V.; Crespo, J.G.; Velizarov, S. Computational fluid dynamics (CFD) assisted analysis of profiled
1979 membranes performance in reverse electro dialysis. *J. Memb. Sci.* **2016**, *502*, 179–190, doi:10.1016/j.memsci.2015.11.031.
- 1980 279. Dong, F.; Jin, D.; Xu, S.; Xu, L.; Wu, X.; Wang, P.; Leng, Q.; Xi, R. Numerical simulation of flow and mass transfer in
1981 profiled membrane channels for reverse electro dialysis. *Chem. Eng. Res. Des.* **2020**, *157*, 77–91,
1982 doi:10.1016/j.cherd.2020.02.025.
- 1983 280. Jalili, Z.; Pharoah, J.; Stokke Burheim, O.; Einarsrud, K. Temperature and Velocity Effects on Mass and Momentum
1984 Transport in Spacer-Filled Channels for Reverse Electro dialysis: A Numerical Study. *Energies* **2018**, *11*, 2028,
1985 doi:10.3390/en11082028.
- 1986 281. Moya, A.A. A numerical comparison of optimal load and internal resistances in ion-exchange membrane systems under
1987 reverse electro dialysis conditions. *Desalination* **2016**, *392*, 25–33, doi:10.1016/j.desal.2016.04.016.
- 1988 282. He, Z.; Gao, X.; Zhang, Y.; Wang, Y.; Wang, J. Revised spacer design to improve hydrodynamics and anti-fouling behavior
1989 in reverse electro dialysis processes. *Desalin. Water Treat.* **2016**, *57*, 28176–28186, doi:10.1080/19443994.2016.1186569.
1990